How Does ATP Regulate Erythrocyte Glucose Transport?

A Dissertation Presented

By

Jeffry M Leitch

Submitted to the Faculty of the

University of Massachusetts
Graduate School of Biomedical Sciences , Worcester

in partial fulfillment of the requirements for the degree of

DOCTOR OF PHILOSOPHY

June 5th, 2007

Biochemistry and Molecular Pharmacology

HOW DOES ATP REGULATE ERYTHROCYTE GLUCOSE TRANSPORT?

A Dissertation Presented

By

Jeffry M. Leitch

Approved as to style and content by:

Dr. William Royer, Chair of Committee

Dr. Osman Bilsel, Member of Committee

Dr. William Kobertz, Member of Committee

Dr. Paul Pilch, Member of Committee

Dr. Ann Rittenhouse, Member of Committee

Dr. Anthony Carruthers, Thesis Advisor

Dr. Anthony Carruthers
Dean of the Graduate School of Biomedical Sciences

Department of Biochemistry & Molecular Pharmacology

June 5th, 2007

COPYRIGHT NOTICE

Parts of this dissertation have appeared in:

Leitch, J. M. and Carruthers, A. (2007) ATP-dependent sugar transport complexity in human erythrocytes. Am J Physiol Cell Physiol. 292, C974-C986.

Leitch, J. M. and Carruthers A. (2007) Preferential transport of α- or β-sugar anomrs does not account for GLUT1 mediated, ATP induced sugar exchange complexities in human erythrocytes. J Gen Physiol. *submitted.*

Leitch, J. M. and Carruthers A. (2007) Using counterflow transport to probe ATP induced complexities in human erythrocyte sugar transport. J Gen Physiol. *submitted.*

ABSTRACT

Human erythrocyte glucose sugar transport displays a complexity that is not explained by available models. Sugar transport was examined in resealed red cell ghosts under equilibrium exchange conditions (intracellular [sugar] = extracellular [sugar]). Exchange 3-O-methylglucose (3MG) import and export are monophasic in the absence of cytoplasmic ATP but are biphasic when ATP is present. Biphasic exchange is observed as the rapid filling of a large compartment (66% cell volume) followed by the slow filling of the remaining cytoplasmic space. Two models for biphasic sugar transport are presented in which 3MG must overcome a sugar-specific, physical (diffusional) or chemical (anomerization) barrier to equilibrate with cell water. The anomerization model was rejected through several lines of direct experimental investigation. 1) The sizes of the fast and slow phases of sugar transport do not correlate with the equilibrium anomer distributions of all GLUT1 sugar substrates. 2) Increasing the rate of anomerization by addition of exogenous intracellular mutarotase has no effect on biphasic transport kinetics. 3) Direct measurement of initial rates of sugar uptake or exchange demonstrates that GLUT1 shows no anomer preference. The physical barrier model was further refined by the use of the counterflow condition (intracellular [sugar] >> extracellular [sugar]). The presence of a physical barrier alone was unable to explain the complex counterflow time courses observed. As a result, the model was modified to include the action of a specific sugar export that is compartmentalized from rapidly equilibrating, GLUT1-mediated uptake and exit.

ACKNOWLEDGMENTS

I would like to express my gratitude and thanks to my thesis advisor, Dr. Anthony Carruthers. Without his drive to understand sugar transport and his understanding of the complexities involved, this thesis would never have been started, let alone finished. I would like to thank members of the Biochemistry and Molecular Pharmacology department who have always showed an interest in this research and have contributed many suggestions and ideas. I would especially like to thank my thesis committee; Drs. William Royer, William Kobertz, Osman Bilsel, and Ann Rittenhouse, who have helped guide me through the process of becoming a scientist.

I would like to thank my family, for without their support I would not be where I am today. I would like to especially thank my parents, Mike and Robin Leitch, for always encouraging me and allowing a curious kid to grow into a curious adult. I would like to thank my in-laws, Phil and Mary LaMont for their support throughout my thesis work. Finally, I would like to thank Sharon Virginia LaMont Leitch, without whom I know grad school would not have been nearly as enjoyable. Her support didn't just make this possible, she made it fun.

TABLE OF CONTENTS

LIST OF FIGURES

LIST OF TABLES

LIST OF ABBREVIATIONS

2DG 2-deoxy-D-glucose

2-NBDG . . . . . 2-(N-(7nitrobenz-2-oxa-1,3-diazol-4-yl)-D-glucosamine

3FDG 3-fluoro-3-deoxy-D-glucose

3MG 3-O-methyl-D-glucose

C-Ab . . . . . .GLUT1 c-terminal antibody

CCB . . . . . cytochalasin B

CCD . . . . . cytochalasin D

CCE . . . . . cytochalasin E

CPMs . . . . . counts per minute

δ-Ab . . . . . exofacial antibody specific to tetrameric GLUT1

DNP 2,4-dinitrophenol

DTT . . . . . dithiothreitol

e1 . . . . . inward facing substrate binding site for a carrier protein

e2 . . . . . outward facing substrate binding site for a carrier protein

EDTA . . . . . ethylenediaminetetraacetic acid

EGTA . . . . . ethylene glycol-bis(2-aminoethylether)-N,N,N`,N`-tetracetic acid

ENT1 . . . . . equilibrative nucleoside transport isoform 1

FACS . . . . . fluorescence activated cell sorting

GLUT1 . . . . . equilibrative glucose transporter isoform 1

GLUTs . . . . . family of equilibrative glucose transporters

GlpT . . . . . *E. coli* glycerol-3-phosphate transporter

HPLC . . . . . high performance liquid chromatography

LacY . . . . . *E. coli* lactose permease

MFS . . . . . major facilitator superfamily

OxlT . . . . . *E. coli* oxalic acid transporter

PCA . . . . . perchloric acid

pCMBS . . . . . p-chloromercuiphenylsulfonic acid

PAGE . . . . . polyacrylamide gel electrophoresis

SDS . . . . . sodium dodecylsulfate

CHAPTER I

LITERATURE REVIEW OF HUMAN ERYTHROCYTE SUGAR TRANSPORT

Why study carrier mediated trans-phospholipid bilayer diffusion?

All cells are enveloped by a hydrophobic phospholipid bilayer which permits non-stokesian diffusion of small hydrophobic molecules and prevents the free diffusion of hydrophilic metabolites and ions. As a result, cells require specific mechanisms to facilitate the import or export of selected molecules (1). Cells accomplish solute transport by using amphiphilic bilayer-spanning integral membrane proteins. These proteins are categorized in three main classes based on structure, function, and selectivity (Figure 1.1) (2). The first and least selective class comprises the pores which form a hydrophilic membrane-spanning hole allowing sufficiently small molecules to transit; the only selectivity being conferred by the size of the hydrophilic passage (3). The second class of proteins comprises the channels. These proteins are mainly involved in the selective movement of specific ions down an electrochemical concentration gradient into or out of the cell. Channels are usually gated so that they are not open at all times (4, 5). The channel mechanism allows for a high transmembrane flux of ions upon channel opening. The third and most substrate diverse class of transport proteins is the carriers. The carriers are mainly responsible for the specific diffusion of metabolites, including carbohydrates, nucleosides and nucleotides, amino acids, cations, anions, amines, and other molecules (2). As these carri-

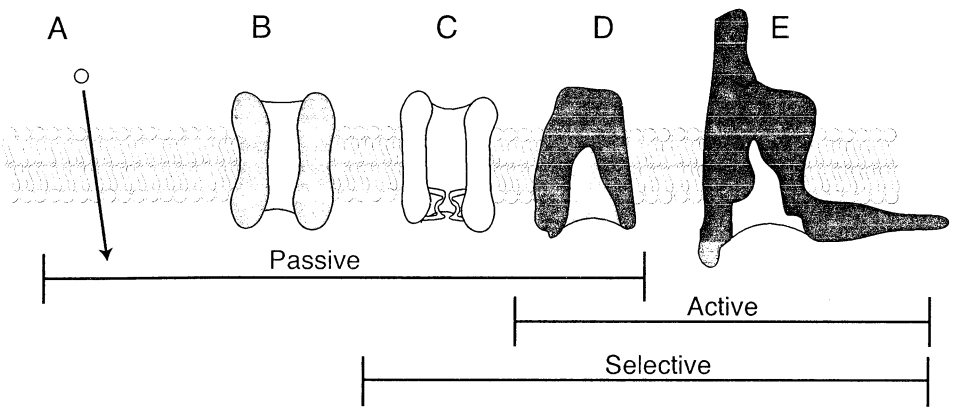

Figure 1.1. Mechanisms of Transbilayer Diffusion.

Shown left to right: **A**. Protein independent, Non-Stokesian diffusion - Small hydrophobic molecules partition into the non-polar environment of the lipid bilayer and freely diffuse into and out of cells or cellular compartments. **B.** Pore Facilitated Diffusion - Proteinatious membrane pores in the lipid bilayer form an aqueous pathway that allows the stokesian diffusion of water soluble molecules. Selectivity is based solely on size, which may be regulated. Pore cavities can range in size from several Å (alphatoxin) to tens of nanometers (nuclear pore complex). **C**. Channel Facilitated Diffusion - Channels are similar to pores in that they form an aqueous cavity within the membrane, but are much more selective and usually only allow the diffusion of one ion type. Gating (opening and closing of the channel) is normally regulated. **D.** Carrier Mediated Diffusion - Carriers usually present one binding site at either the one or the other membrane surface. Interconversion between the two conformations results in solute diffusion. **E.** Carriers can catalyze passive diffusion or can transfer solutes against a concentration gradient by coupling solute transfer to the energetically downhill transfer of a second transported species or to ATP hydrolysis.

ers provide the cellular metabolic machinery with essential substrates, it is easy to see why carriers are necessary for life.

The carriers are proposed to exist in at least two distinct conformations and undergo reversible conformational change upon substrate binding that leads to substrate movement across the lipid bilayer (6, 7). While coupling transport to a significant protein conformational change is energetically costly and thus decreases the next flux of solutes, such a mechanism allows for greater specificity. This unique feature of carriers not only facilitates the transfer of substrates down a concentration gradient (passive diffusion), but also permits net solute transfer against a concentration gradient (active transport) by coupling solute transport to a second favorable substrate gradient (symport and antiport) or to ATP hydrolysis (8, 9).

It is estimated that there are nearly 800 genes in the human genome encoding proteins responsible for the movement of molecules across cell membranes (10). Abnormalities in membrane diffusion processes or regulation of those processes are associated with many diseases, including diabetes (11), cystic fibrosis (12), long QT syndrome (13, 14), Menkes (15) and Wilsons (16-18) diseases, depression, and bacterial antibiotic resistance (19, 20). Understanding the mechanism of carrier function may lead to the development of novel therapies for treating human diseases. Mutations in the erythrocyte, and endothelial glucose transport protein, GLUT1, result in GLUT1 deficiency syndrome which is characterized by infantile seizure, development delays, microcephaly, and if untreated, early death (21, 22). As GLUT1 is responsible for the movement of sugar across the

blood-brain barrier, a decrease in the transport efficiency of GLUT1 results in normal physiological blood sugar concentrations, but low cerebrospinal fluid glucose which is incompatible with normal rates of neuronal glucose utilization.

Sugar metabolism and homeostasis

Glucose is the preferred substrate for ATP production in most cells. However, glucose is highly polar and does not readily diffuse across cell membranes. Specific glucose transporters have evolved in order to ensure intracellular glucose availability for energy consumption. In humans, equilibrative sugar transport is catalyzed by a family of integral membrane proteins called glucose transporters (GLUTs) (23). There are 13 accepted members which are expressed in a tissue specific manner and catalyze the diffusion of a variety of sugar substrates (24).

Class I members (GLUT1-4) are primarily responsible for the transbilayer facilitated diffusion of glucose. GLUT1 is found in most tissues where it functions as a basal glucose transporter, but is highly expressed in the endothelial and cardiovascular systems where it functions to deliver glucose across blood-tissue barriers (25). GLUT2 is expressed in liver and pancreatic β-cells (25) and GLUT2 polymorphism may contribute to Type II diabetes susceptibility (26-28). GLUT2 may also function as a high affinity glucosamine transporter (29). GLUT3 is found in brain tissue, but appears to be restricted to neuronal cells and is not found in the blood-brain barrier (30-32). GLUT4 is the insulin responsive glucose transporter and is found in adipose and skeletal muscle tissue (25, 33).

Class II (GLUT 5, 7, 9, 11) function as fructose transporters. GLUT5 was first described in the small intestine where it is responsible for the uptake of dietary fructose (34). It is also found in other tissues including erythrocytes where it may function as a general basal fructose transporter (35). While most GLUTs are found at the plasma membrane, GLUT7 is found in the endoplasmic reticulum and is responsible for transport of sugar into the lumen (36). GLUT9 is a fructose transporter found in liver and kidney (37). GLUT11 is found predominately in skeletal muscle and heart (38, 39).

Class III members (GLUT 6, 8, 10, 12 and the H^+/myoinositol transporter) have just recently been described. GLUT8, found in blastocysts, is responsible for sugar uptake before implantation and is necessary for embryo development (40). GLUT10 is a high-affinity glucose transporter and is perhaps involved in type-II (insulin insensitive) diabetes as it is expressed at high levels in pancreas and liver (41, 42). GLUT12 is found in insulin sensitive tissues and cancer cells (43).

GLUT1 is a member of the major facilitator superfamily

The human glucose transporters belong to a large family of permeases. The major facilitator superfamily (MFS) proteins comprise transporters capable of uniport, symport, and antiport and are found in all organisms including bacteria and higher eukaryotes (44). MFS members are responsible for the diffusion of a diverse set of substrates including but not limited to simple sugars, oligosaccharides, inositols, drugs, amino acids, nucleosides, organophosphate esters, Krebs cycle metabolites, and a large variety of organic and

inorganic anions and cations (45). Gene sequencing and hydropathy analysis suggests that MFS proteins share a common topology, tertiary structure, and translocation mechanism (46, 47). MFS proteins are characteristically 400 to 600 amino acid residues in length and contain twelve to fourteen hydrophobic putative transmembrane α-helices with cytosolic N- and C-termi.

Recently, the crystal structures of several bacterial MFS proteins have been solved by X-ray diffraction (48, 49) or by electron diffraction (50-52). The structures of the lactose permease (LacY), glycerol-3-phosphate transporter (GlpT), and oxalic acid transporter(OxlT) represent the inward facing carrier conformation. These proteins adopt a heart shape with the N-terminal and C-terminal halves forming the two lobes (Figure 1.2). These structures have twelve transmembrane helices arranged around a hydrophilic cavity (47). Helices 1-6 are pseudosymmetrically related to helices 7-12 with a large cytoplasmic loop connecting the two halves. It appears that helices 3, 6, 9, and 12 form anchor points within the membrane, while helices 2, 5, 8, 11 line the cavity. Helices 1, 4, 7, and 10 are the least perpendicular to the membrane and form the substrate cavity. Movements of these four helices may be involved in the translocation pathway by generating the periplasm facing conformation (53, 54). The structure of a MFS closely related transporter, the melibiose symporter, shows a very similar tertiary shape, however the resolution is too poor to accurately determine helical arrangement (52). The apparent pseudosymmetry in primary structure and tertiary shape suggesting that alternative helical packing may occur and that more MFS transporter structures must be solved before arriving at

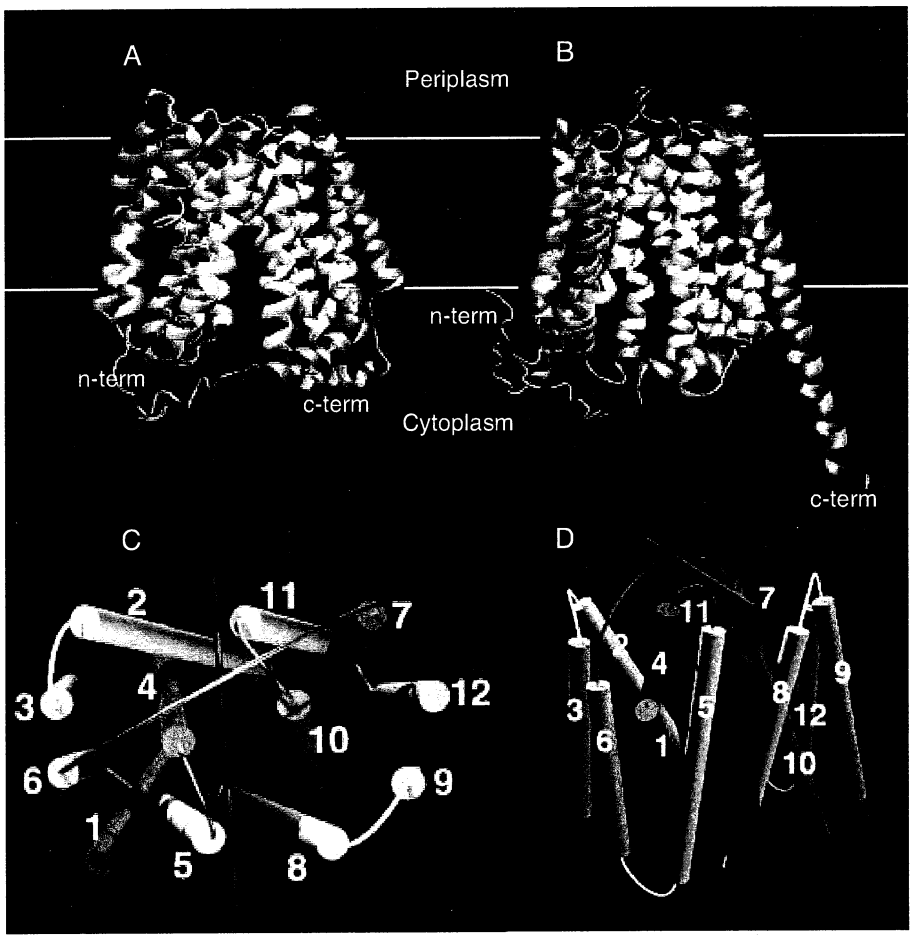

Figure 1.2. Structure of MFS Transporters.

A. X-ray crystal structure of the *E. coli* lactose permease. **B.** X-ray crystal structure of the *E. coli* glycerol-3-phosphate transporter. **C.** View of the helical arrangement of *E. coli* oxylate transporter from the cytoplasm. **D.** View of the helical arrangement of the oxylate transporter as seen parallel to the membrane with the cyoplasmic surface on top. The "mirror" in both C and D illustrate the 2-fold pseudosymmetry. In all four representations, transmembrane helices 1, 4, 7, and 10 are pink, helices 2, 5, 8, and 11 are yellow, and helices 3, 6, 9, and 12 are green. Figure panels C and D are reproduced with kind permission from S. Subramaniam (50).

a consensus structure.

All human glucose transporters belong to the MFS and display a similar putative topography to that of LacY, GlpT, and OxlT (see Figure 1.7 for sequence alignments of human GLUT1, LacY and GlpT). Figure 1.3 shows the probable topology of GLUT1, which is consistent with other MFS proteins, as obtained through hydropathy analysis (55), asparagine-linked scanning glycosylation (56), cysteine scanning mutagenesis (57-63), and limited protein digestion (64). GLUT1 has 12 transmembrane alpha helices, an asparagine-linked glycosylation site at N-45, a large cytoplasmic loop between helices 6 and 7, and cytosolic N- and C-termini. Cysteine scanning mutagenesis has ascertained that regions of transmembrane helices 1 (65), 2 (66), 5 (63), 7 (58, 66), 8 (67), 10 (68), 11 (62) are accessible to water soluble pCMBS, while no regions of transmembrane helix 3 (61) is accessible. Helix 4 (60) and Helix 12 (59) demonstrate pCMBS accessibility in-consistencies with the MFS structural paradigm.

GLUT1 and the simple carrier transport mechanism and kinetics

The MFS members, including the human GLUTs are thought to have a similar translocation mechanism. Widdas first proposed a mechanism for the passive, facilitated diffusion of molecules across a lipid bilayer described as the simple carrier (1) which was further and mathematically described by Lieb and Stein (6). They proposed that carriers function by displaying one of two dynamically interconverting conformations, one which displays a substrate binding site at one side of the membrane and the other displaying a

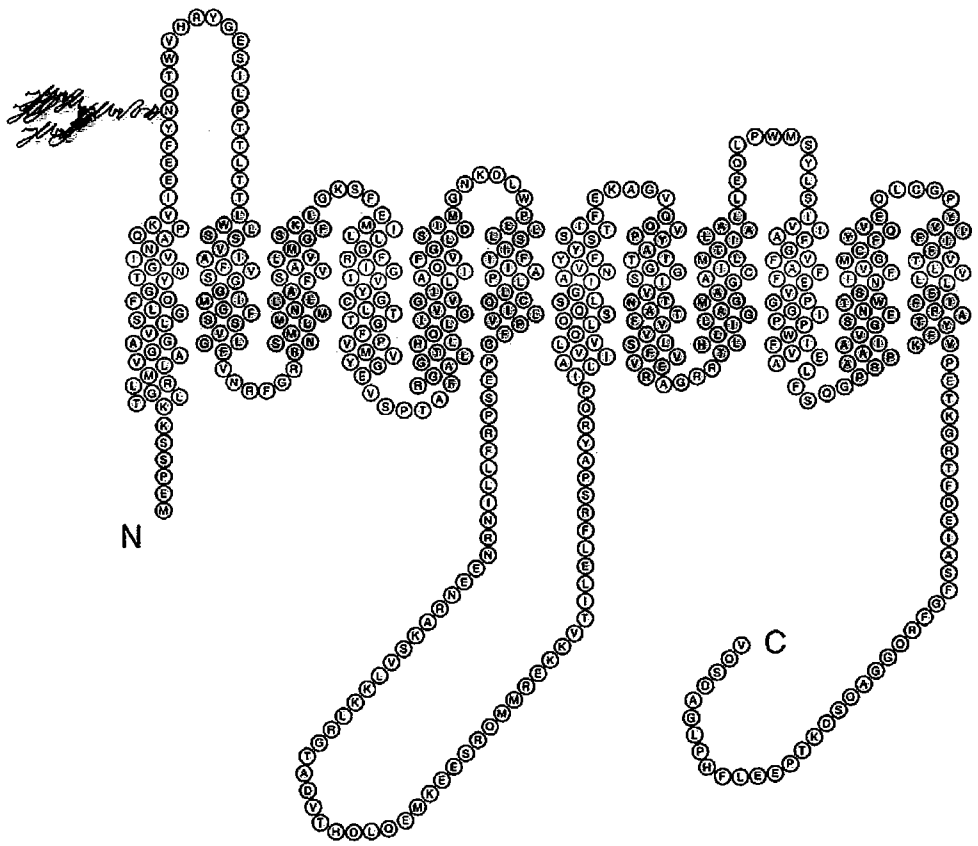

Figure 1.3. Putative Topology of GLUT1.

The human GLUT1 primary structure is shown as a topology model which includes 12 transmembrane helices, cytosolic N- and C-termini, an N-linked glycosylation site at N45, and a large cytosolic loop between transmembrane helix 6 and 7. The helices are color coded based on the known MFS structures and on predicted water accessibility where structural helices not involved in the translocation mechanism (3, 6, 9, 12) are green, pore lining helices (2, 5, 8, 11) are blue, and helices involved in translocation (1, 4, 7, 10) are pink.

binding site on the opposite side. This model allows for the independent movement of substrate from one side of the membrane to the other. For example, with pores or channels, if the concentration of substrate was saturating on one side (side 1) of the membrane, unidirectional movement of substrate in the opposite direction (from side 2 to side 1 of the membrane) is inhibited. This occurs because channels and pores have binding sites that are simultaneously accessible to both sides of the membrane and the transport pathway is too narrow to permit solutes to pass in opposite directions. However, this behavior is not observed for many carrier-mediated systems. In fact for some systems the presence of saturating substrate at one side of the membrane can increase the flux of substrate in the opposite direction (2). This indicates either that the translocation pathway only has access to one side of the membrane at a time or that the bound substrates can be transported simultaneously in opposite directions. Figure 1.4 shows the proposed mechanism and King-Altman diagram for a simple carrier. The simple carrier kinetic model can be solved and simplified to the form:

$$v_{12}=\frac{KS_1+S_1S_2}{K^2R_{00}+KR_{12}S_1+KR_{21}S_2+KR_{ee}S_1S_2} \qquad \text{Eq. 1.1}$$

where v_{12} is the unidirectional rate of diffusion from side 1 to side 2, K is the intrinsic dissociation constant under the hypothetical situation when there is no substrate at either side of the membrane, and the R terms are the reciprocal of V_{max} where $1/R_{12}$ is V_{max} for transport from side 1 to side 2, $1/R_{21}$ is the V_{max} for the reverse reaction, $1/R_{ee}$ is the V_{max} when substrate is present at equal concentrations at both sides, and $1/R_{00}$ is the maximal rate of interconversion of the non-substrate bound carrier (relaxation in Figure 1.4) (2).

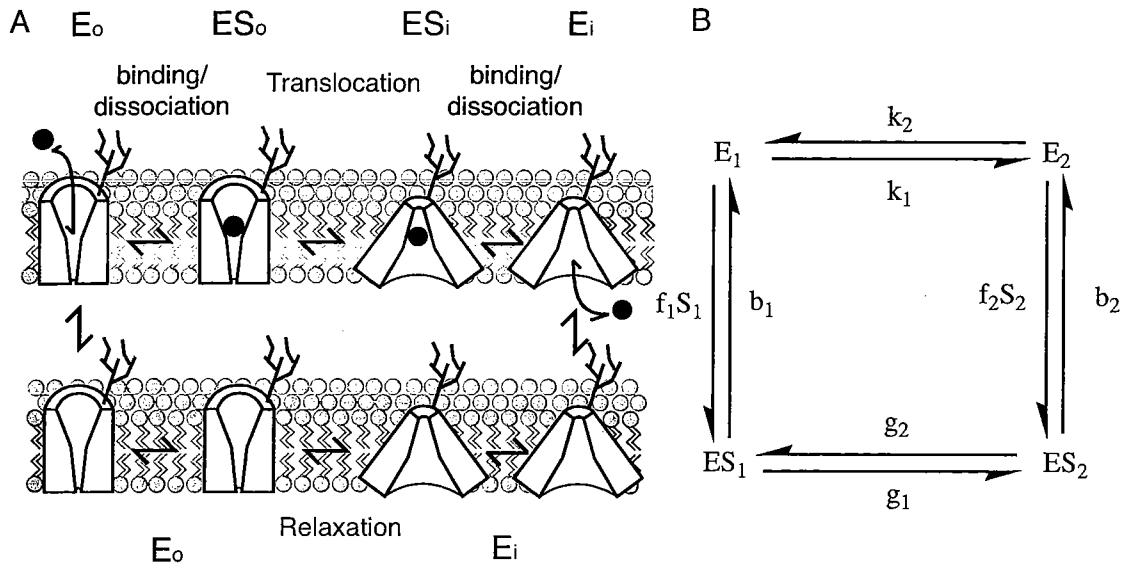

Figure 1.4. The Simple Carrier Mechanism.

A. Schematic diagram of the simple carrier translocation mechanism. The carrier displays one binding site which alternates between the two sides of the membrane. Substrate binding and a subsequent conformational change to the alternative binding site moves the substrate across the membrane. Regeneration of the first binding site in the absence of substrate is necessary for a second round of transport to occur. **B.** King-Altman diagram of the simple carrier mechanism with associated binding and rate constants. From equation 1.1; $R_{12} = 1/k_2 + 1/g_1$; $R_{21} = 1/k_1 + 1/g_2$; $R_{ee} = 1/g_1 + 1/g_2$; $R_{00} = 1/k_1 + 1/k_2$; and $K = b_2k_2/f_2$.

The model allows that the measured K_m and V_{max} under different transport conditions - zero-trans (where the substrate concentration on one side of the membrane is zero), equilibrium exchange (where the concentration is identical on both sides of the membrane and unidirectional transport is measured), infinite-cis (saturating concentration on one side, varied concentration on the other, and net transport is measured), or infinite-trans (saturating concentration of substrate on one side, varied on the other, and unidirectional transport against the gradient is measured) - as long as the same values for basic observable parameters are found. This is indeed the case for many carrier systems including the human equilibrative nucleoside transporter (ENT1) found in human erythrocytes (69-72), and the human hydrophobic amino acid transporter (73, 74).

Human GLUT1, arguably the most extensively studied transport system, does not behave as a simple carrier. Transport complexity is especially obvious in zero-trans exit and infinite-cis entry conditions (75). In the zero-trans exit condition, cells are loaded with various starting sugar concentrations and the initial rate of exit is measured (76, 77) or the complete time course of exit is analyzed by using an integrated Michaelis-Menten equation (76, 78-80). Initial rate measurements (76, 77) routinely provide estimates of $K_{m(app)}$ for sugar exit that are 2- to 3-times lower than those obtained by analysis of the complete time-course of sugar exit (76, 78-80). In the infinite-cis sugar uptake experiment, the external sugar level is saturating and the concentration of intracellular sugar that reduces net sugar uptake by one-half is measured. $K_{m(app)}$ for infinite-cis entry is routinely 5- to 10-fold lower than the value predicted by the simple carrier model for sugar

transport (79, 81-83). Not all glucose transporters show kinetic discrepancies with the simple carrier model however. Human GLUT4, the insulin sensitive glucose transporter in adipocytes and skeletal muscle, behaves as a simple carrier (84).

GLUT1 oligomeric structure and implications on transport kinetics

Since the simple carrier is inadequate to explain the transport anomalies seen with human erythrocyte glucose transport, alternative models must be considered. Several structural and ligand binding studies suggest that the human erythrocyte transporter (GLUT1) is a tetramer or higher-order oligomer. The cholic acid solubilized carrier exists in two forms which are consistent with a homodimer and homotetramer (85). Cryoelectron microscopy of detergent solubilized GLUT1 and freeze fracture microscopy of GLUT1 proteoliposomes are also consistent with tetramer formation (86). The homodimer is produced when GLUT1 is purified in the presence of the reducing agent dithiotheritol (DTT) while the homotetramer is produced in the absence of reductant. DTT reduces two specific cysteines (C347 and C421) which are not thought to form an intermolecular disulfide, but may form an intramolecular disulfide, mixed disulfides, or other oxidized species (87). Recent work by Kara Levine shows that the last three transmembrane helices and perhaps only transmembrane helix 9 is sufficient for GLUT3-GLUT1 chimera proteins to associate with GLUT1 (unpublished results). The oxidation of these cysteines is not the only determinate of oligomerization as GLUT1-GLUT4 chimeras which contain the first 199 amino acids of GLUT1 are able to associate with wt-GLUT1

to form hetero-oligomers (88) and alanine mutation at position 338 may disrupt oligomerization and transport (89). Other detergents appear to promote either dimer or tetramer formation in the absence of reductant (86, 90). The non-ionic detergent n-octyl-β-D-glucoside especially stabilizes the tetramer while the related detergent, n-dodecyl-β-D-maltoside, is destabilizing.

It is interesting to note that inhibitor binding stoichiometry is also dependent on the oligomeric state. In the absence of DTT, purified GLUT1 binds 0.5 moles of cytochalasin B (CCB) per mole of GLUT1, but following reduction, the GLUT1:CCB binding stoichiometry becomes 1:1 (91). Stopped-flow and equilibrium analysis of cytochalasin B binding to purified GLUT1 proteoliposomes indicate that there are cooperative interactions between inhibitors that bind on the inside exit site and substrates that bind at the outside sugar uptake sites (92-94). Other ligand binding studies show that human GLUT1 displays multiple exit sites as cytochalasin B binding shows positive cooperativity where the binding of one inhibitor increases the apparent affinity for a second inhibitor (90), and GLUT1 displays multiple sugar uptake sites as low concentrations of extracellular impermeable inhibitors accelerate zero-trans sugar uptake (95).

These observations support the hypothesis that GLUT1 operates as a fixed- or two-site carrier (Figure 1.5) as first proposed by Baker and Widdas (96-98). Here, the carrier simultaneously presents substrate binding sites on both sides of the membrane and exchange transport is mediated by two substrates moving through the translocation pathway in opposite directions. Because the two substrates may pass by each other in the

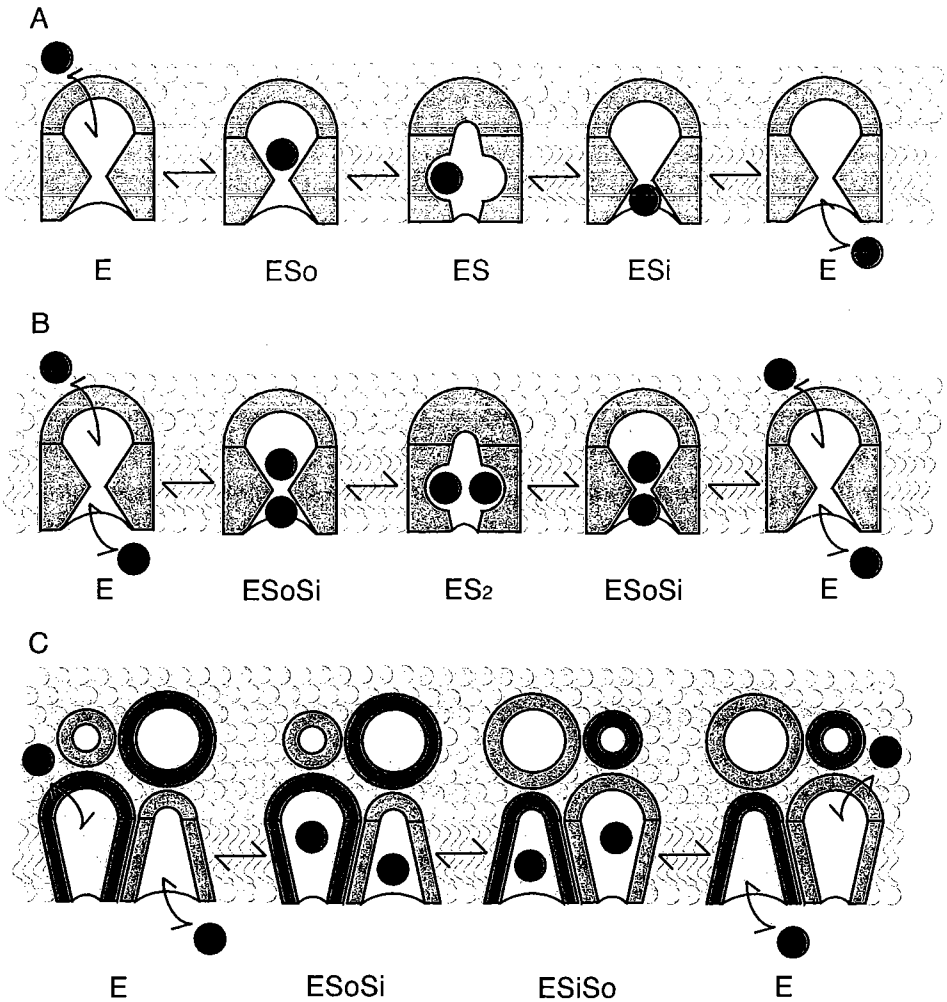

Figure 1.5. The Fixed-Site Carrier Mechanism.

A. Two-site carrier first envisioned by Baker and Widdas where a single carrier displays binding sites on both sides of the membrane simultaneously. **B.** Carrier as in A mediating exchange transport which allows substrates to bypass one another in the translocation pathway. **C.** Two-site carrier described by Carruthers depicting exchange transport. Here the carrier is a homotetramer with each subunit forming a translocation pathway and allosteric interactions between subunits require that two subunits display an exofacial binding site and the other two subunits display endofacial binding sites.

translocation pathway, the mechanism still allows for movement through the carrier that is opposite of net transport and therefore meets the requirement for a carrier mediated mechanism (*vide supra*). Interestingly, assuming that a fixed-site carrier is an oligomer of identical simple carriers whose substrate binding sites are arranged in an antiparalllel fashion and where the isomerization of one subunit promotes the isomerization of the others, further relaxes restraints imposed by the simple carrier. This model allows for deviation from Michalis-Menten kinetics at low substrate concentrations under equilibrium exchange conditions (99).

GLUT1-mediated glucose transport in rat and rabbit erythrocytes seems to be compatible with a fixed-site carrier model (100-102). Sequence homology between human and rat GLUT1 is 98.4% identity (55, 103, 104). Six common residues in rabbit and rat GLUT1 diverge from human GLUT1 sequence but all six substitutions show positive scores on the point accepted mutation similarity scale (105). However, glucose transport in human erythrocytes is incompatible with the fixed-site carrier (79, 99, 106).

Unstirred layer effects on human erythrocyte glucose transport

If sequence divergence does not explain the failure of the fixed-site carrier model to explain human erythrocyte glucose transport while the fixed-site carrier is adequate for rat erythrocyte glucose transport, then human red cell transport complexity must come from factors extrinsic to the GLUT1 translocation pathway. The sugar transport capacity of human red cells is 220- to 10,000-fold greater than that of rat basal adipocytes (84), rat

red cells (100) and avian erythrocytes (107). Naftalin and Holman (97) have discussed several ways by which this could give rise to transport complexity.

Transport measurements in human red cells are technically challenging even at low temperatures owing to the very high GLUT1 density of human red cells and the high catalytic turnover of GLUT1 (77). Significant backflux of imported sugar during the course of a transport determination would lead to underestimation of net import. However, complex kinetics are still observed using rapid measurement devices where little backflux would occur (108, 109).

If net cellular sugar import were comprised of two steps - transport followed by intracellular diffusion/distribution - the diffusional step could become rate-limiting if the transport step were sufficiently rapid. Evidence for non-uniform intracellular distribution of sugars has been obtained in both human and rat erythrocytes (79, 100, 110-112).

According to the diffusional barrier hypothesis, human red cell net sugar import comprises rapid transport (owing to high cellular GLUT1 content) and slow intracellular diffusion/distribution. The overall result is one where net sugar import is rate-limited by intracellular diffusion/distribution not by transport. Measurements of sugar uptake in rat or rabbit erythrocytes, however, largely reflect low capacity GLUT1-mediated transport and thus provide a more accurate description of the intrinsic properties of GLUT1. With the addition of an unstirred layer, the discrepancies between predicted and experimental $K_{m(app)}$ for infinte-cis sugar uptake and the difference between $K_{m(app)}$ for zero-trans exit integrated rate and initial rate analyses may be resolved. The unstirred layer causes an

underestimation of net sugar import as the concentration of intracellular sugar available to the transporter is underestimated. A more detailed analysis of red cell 3–O–methylglucose uptake reveals that net influx is a biexponential process characterized by rapid filling of a small compartment and slow filling of a larger compartment and is seen as direct evidence for a diffusion barrier (113).

Naftalin and Holman first proposed that the diffusional barrier may result from high-capacity sugar binding by bulk hemoglobin (97). Hemoglobin is known to be modified by non-specific (114-116) and by specific glycation reactions (117, 118). There is also evidence that glycation is highly reversible and may occur on a time scale compatible with an apparent unstirred layer effect (119, 120). Much of the glucose transport complexity is lost when human red cells are ghosted (hypotonically lysed) and resealed with an artificial cytosol. However hemoglobin is not the only cytosolic factor removed by ghosting and artificial cytosol containing low molecular weight (under 10KD) red cell cytoplasmic factors mimics transport in intact red cells (80).

Nucleotide regulation of human GLUT1

Several studies have shown that human GLUT1 is a nucleotide binding protein, and ATP binding changes GLUT1-mediated sugar transport properties. ATP depleted red cell cytosol, when resealed into human erythrocyte ghosts, is unable to retain transport complexity (121, 122). GLUT1 binding of ATP directly affects substrate and inhibitor binding. GLUT1 intrinsic tryptophan fluorescence is quenched by D-glucose, with two

apparent K_d's (high and low affinity), by cytochalisin B, and by ATP (123-125). ATP binding alters $K_{d(app)}$ for all glucose induced quenching, lowering the high affinity sugar K_d and increasing the low affinity sugar K_d. ATP binding is cooperative as measured by fluorescence quenching (90, 126). AMP and ADP bind to the transporter, but with less affinity, and only ATP affects transport properties (127). There is some controversy regarding GLUT1 regulation by ATP (128, 129), but the overwhelming evidence suggest that ATP does regulate GLUT1.

The nucleotide binding domain of GLUT1 has yet to be fully characterized. GLUT1 contains a Walker A ATP binding motif II (residues 225-229) and motif III (residues 421-423) (130). Alanine scanning mutagenesis determined that mutations in both these domains alter transport, but the effect on ATP regulation remains unknown (131). GLUT1 also contains a consensus Walker B ATP binding motif between residues 326-344 (132). Alanine mutagenesis at positions 338-344 disrupts transport but seems to have little effect on ATP photo-label incorporation (89) and alanine mutagenesis of residues Glu329 and/or Arg333/344 results in doubled ATP photo-label incorporation but loss of ATP regulation of transport (89, 133). GLUT1 residues 301-364 form one element responsible for ATP binding as identified by N-terminal sequencing of azido-ATP photo-labeled GLUT1 proteolytic fragments (134).

Other data show that ATP binding induces structural changes in GLUT1. GLUT1-ATP interactions disrupt C-terminal antibody (C Ab) binding to GLUT1 (135, DeZutter, unpublished results). Several cytosolic lysine residues in the C-terminus (K477) and in

loop 6 (K256 and K257) are specifically protected by ATP from trypsin cleavage and covalent modification (Blodgett, unpublished results). Resealing of C-Ab into ghosts abolishes ATP regulation of sugar transport suggesting that movement of the C-terminus is necessary for the ATP effect (Levine, unpublished results). GLUT1 is a high-affinity (μM) sugar binding protein capable of binding two moles of sugar per mole of GLUT1 in the presence of ATP (112).

These data suggest the following model for ATP regulation of GLUT1 mediated sugar transport in human erythrocytes (Figure 1.6). The GLUT1 tetramer is able to bind at least two molecules of ATP (the exact stoichiometry is unknown) which alters GLUT1 catalytic function. The large cytosolic loop between helices 6 and 7 and the C-terminus are hypothesized to interact with each other after ATP binding to form a high-affinity sugar binding site. After formation of the high-affinity binding site, recently transported sugar first binds to the site before slowly diffusing into bulk cell water. This produces the biexponential uptake kinetics seen at limiting substrate concentrations (*vide supra*). As human red cell GLUT1 concentration is ~20 μM, sugar binding to GLUT1 easily explains the observed 30 μM sugar binding sites (113). This model accounts for the kinetics first described by an unstirred layer, and for the increased sugar binding capacity of GLUT1 after ATP binding. In the absence of ATP, the sugar binding site does not form and sugar is able to freely diffuse between the exit site and cytosol. Low intracellular pH eliminates the putative salt bridge between E329 and R333/334 and alleviates ATP regulation while increasing ATP binding capacity.

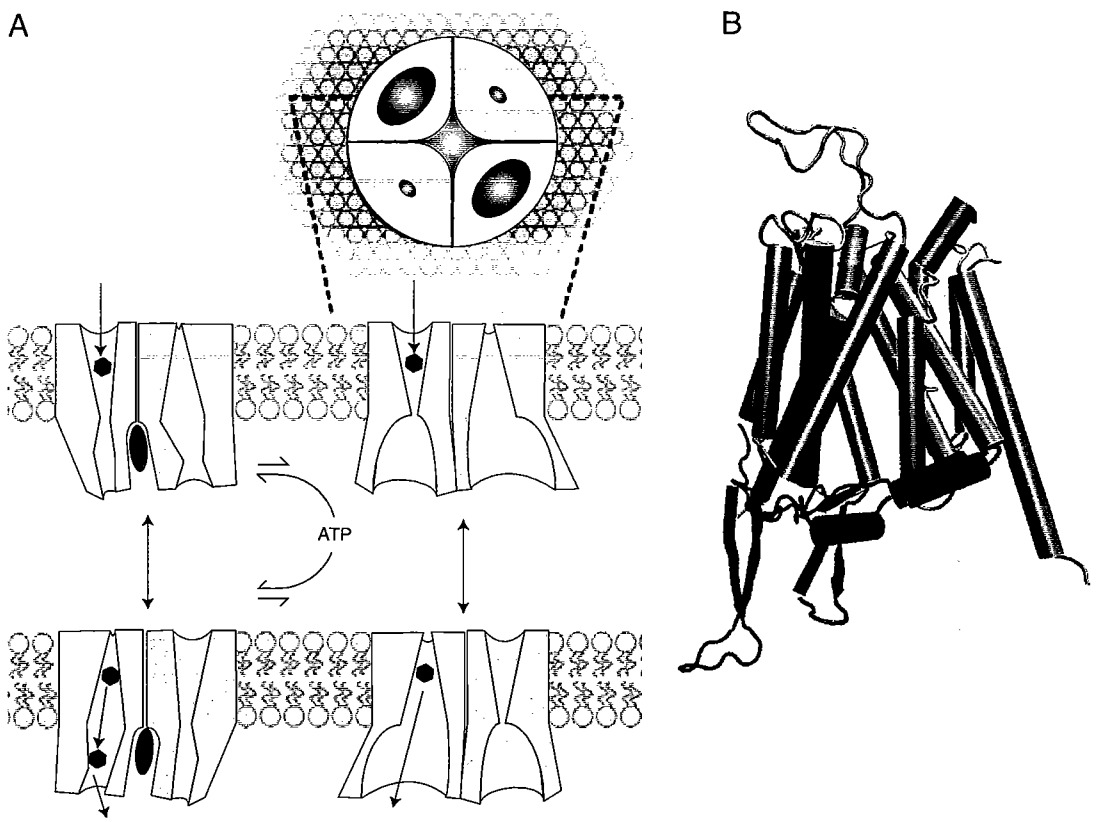

Figure 1.6. Proposed Mechanism of ATP Regulation of GLUT1.

A. Diagrammatic representation of the ATP cage hypothesis. In the absence of cytosolic ATP (right) the GLUT1 tetramer is able to freely exchange sugar with interstitium and cytosol. Upon ATP binding (left), a conformational change in the cytoplasmic C-terminus and loop 6 create an additional high affinity sugar binding/occlusion site. Uptake proceeds as transport through GLUT1 into the occlusion site where sugar binds. Bound sugar then dissociates and either slowly diffuses into bulk cytosol or rebinds to the exit site. **B.** GLUT1 homology models based on LacY and GlpT. Cytosolic loop 6 is found in two energy minimized structures, one where the loop is extended away from the exit site (blue) and one where it is doubled back and partially blocking the exit site (red).

Molecular modeling of GLUT1 sequence onto the structures of other MFS proteins may give us insights into the proposed structural rearrangements. Multiple alignments of GLUT1 to GlpT and LacY were generated using PDB-Blast, 3D-Jigsaw (136), EsyPred3D (137), GRDB, FFAS03 (138, 139), Sam-T99 (140), SUPERFAMILY (141), INBGU, FUGUE2 (142), 3D-PSSM (136), mGenTHREADER (143, 144), psipred (145, 146), profsec (147), and 3D-Jury using the Polish Bioinformatics Meta Server. The alignments generated by FFAS03 contain minimal gaps and predicted transmembrane helices are in sync (Figure 1.7). After submission to Swiss-Model (148), predicted GLUT1 structures were obtained. These structures are of a monomeric GLUT1 carrier as the LacY and GlpT structures are monomeric. However, residues involved in substrate binding, some GLUT1 deficiency mutations, and cytochalasin B photolabeling map to the structural cavity suggesting that the structure model may be representative of a single GLUT1 subunit. It is interesting to note that GLUT1 has an extension in the cytoplasmic loop 6 compared to both GlpT and LacY and that the loop is not fully resolved in GlpT. As such, the GLUT1 loop 6 is modeled in using energy minimization. The LacY based structure depicts the loop extended away from the transporter while in GlpT based structure the loop is folded up and into the exit site. Is is interesting to speculate that these two structural states relate to the ATP free and bound states (Figure 1.6).

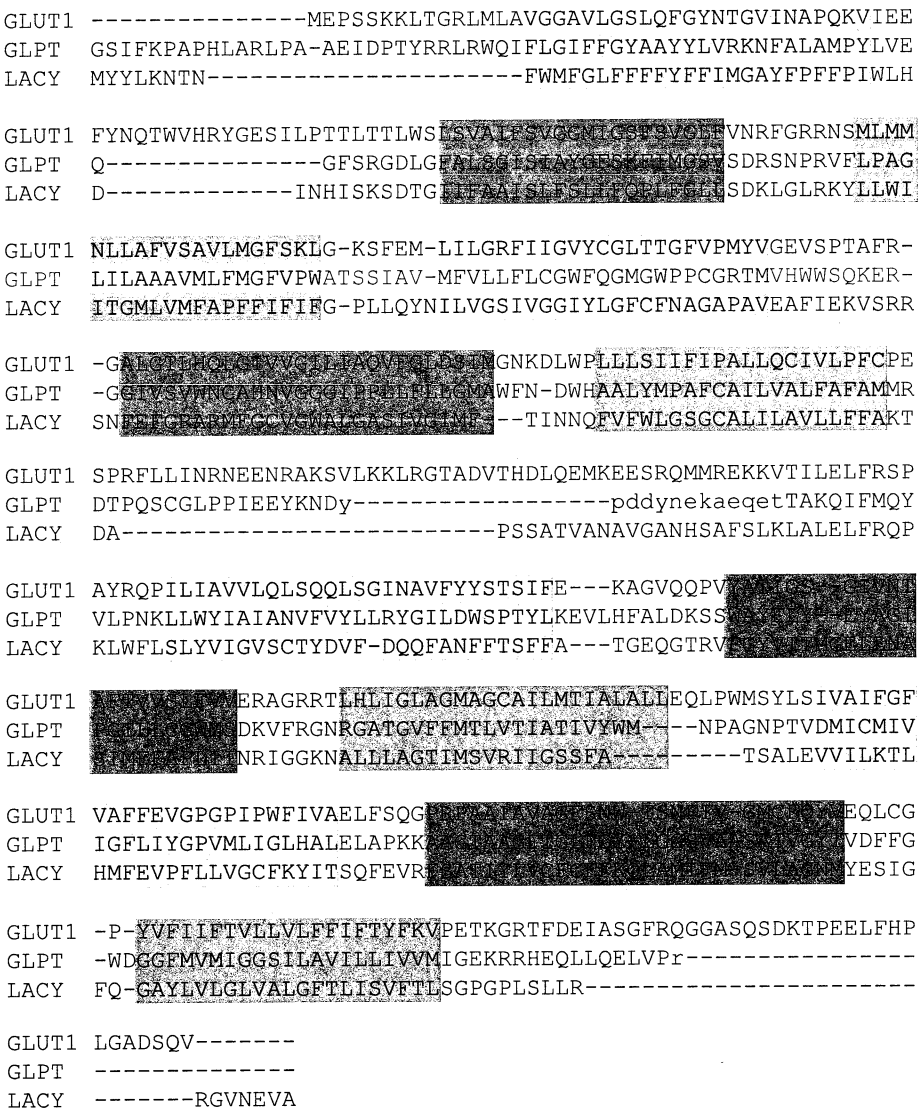

Figure 1.7. Sequence Alignments of GLUT1, GlpT, and LacY.

The sequence alignment of GLUT1 to the two crystalized MFS proteins is shown. Predicted transmembrane helices for GLUT1 and actual transmembrane helices for GlpT and LacY are shown in colored boxes. Helices 1, 4, 7, and 10 are pink, 2, 5, 8, and 11 are blue, and 3, 6, 9, and 12 are green. Gaps are indicated by "-" and amino acids not resolved in the crystal structure (GlpT) are shown in lower case.

Physiological significance of human GLUT1 regulation

What advantage is obtained from glucose transport regulation in erythrocytes where transport capacity vastly exceeds metabolic demand? Perhaps the benefit is not realized by the transporting cell but rather, by cells to which glucose is subsequently transferred.

Skeletal muscle plasma water space is relatively small (1.8% of total muscle water (149)). As a result, efficient extraction of plasma water glucose is necessary to meet the metabolic demand. Demand for serum glucose is increased during exercise- or insulin-stimulation of skeletal muscle glucose transport and metabolism which lower plasma glucose levels even further (150). The capillary endothelium of muscle is extensively fenestrated which facilitates the rapid depletion of serum nutrients by diffusion from blood to skeletal muscle plasma water (151). When serum glucose levels fall due to net transfer to muscle plasma water and muscle cells, red cell cytoplasmic glucose (45% of total blood glucose) becomes a significant additional source of glucose. The very high GLUT1 content of higher primate and odontocete erythrocytes may contribute to total glucose transfer from blood to other tissues (152). Human erythrocytes are capable of achieving 50% equilibration with serum glucose within 1.2 sec at 37 °C and thus can exchange upwards of 82 to 98% of intracellular glucose with blood serum in the 2 to 4 seconds required for an erythrocyte to transit the muscle capillary bed (153, 154). Regulation of erythrocyte glucose transport therefore permits controlled expansion/contraction of the blood glucose available for exchange with the interstitium of glycolytically active tissues.

Remaining questions

While the ATP cage hypothesis addresses most of the kinetic anomalies and structural data known on GLUT1; several key questions remain. How is it that human erythrocyte sugar transport displays kinetic discrepancies with a two-site carrier in the presence of ATP when rat GLUT1 does not? While it has not been studied, it seems unlikely that rat and rabbit GLUT1 would not bind and be regulated by ATP when there is such high sequence identity. It is equally unlikely that rat and rabbit erythrocytes are ATP depleted under the conditions analyzed. Parental (hamster) and exogenous (human) GLUT1-mediated sugar transport are insensitive to cellular ATP-depletion in CHO cells (126, 133) while ATP-sensitive, human GLUT1-mediated sugar transport is observed in transfected HEK cells (126, 133) and in Clone 9 cells (155). This suggests that cellular environment influences GLUT1 phenotype.

The ATP cage hypothesis is also unclear on the mechanism for peripheral tissue glucose homeostasis. If a role of erythrocytes is to increase or decrease the amount of blood glucose available to metabolizing tissue as signaled by intracellular ATP, then how does red cell intracellular ATP concentrations respond to peripheral tissue metabolic demands? The cage hypothesis suggests that the ATP-replete state would demonstrate slow glucose exchange between erythrocyte cytosol and blood plasma while the ATP-depleted state would exhibit fast glucose exchange. Erythrocyte intracellular ATP levels will rise or lower depending on the metabolic demand of the red cell, but how would erythrocyte ATP levels be sensitive to the metabolic demand of the peripheral tissue?

Is human red cell sugar transport complexity an artifact of measurement? Human red cell membrane GLUT1 content approaches 10% total protein by mass (112) resulting in extremely rapid sugar transport rates at all temperatures studied (109). Measurements of transport are, therefore, complicated by the necessity for rapid sampling procedures (77, 109) but may be simplified by use of the equilibrium exchange condition (156).

The thesis presented here attempts to ascertain if the red cell sugar transport complexity is real, and if so, how does ATP regulate glucose exchange in human erythrocytes?

CHAPTER II

ATP-DEPENDENT SUGAR TRANSPORT COMPLEXITY IN HUMAN ERYTHROCYTES

Abstract

Human erythrocyte glucose sugar transport was examined in resealed red cell ghosts under equilibrium exchange conditions (intracellular [sugar] = extracellular [sugar]). Exchange 3-O-methylglucose (3MG) import and export are monophasic in the absence of cytoplasmic ATP but are biphasic when ATP is present. Biphasic exchange is observed as the rapid filling of a large compartment (66% cell volume) followed by the slow filling of the remaining cytoplasmic space. Biphasic exchange at 20 mM 3MG eliminates the possibility that the rapid exchange phase represents ATP-dependent 3MG binding to the glucose transport protein (GLUT1; cellular [GLUT1] $\leq$ 20 μM). Immunofluorescence activated cell sorting analysis shows that biphasic exchange does not result from heterogeneity in cell size or GLUT1 content. Nucleoside transporter mediated uridine exchange proceeds as rapidly as 3MG exchange but is monoexponential regardless of cytoplasmic ATP concentrations (157). This eliminates cellular heterogeneity or an ATP-dependent, nonspecific intracellular diffusion barrier as causes of biphasic exchange. Red cell ghost 3MG and uridine equilibrium volumes (130 fL) are unaffected by ATP. GLUT1 intrinsic activity is unchanged during rapid and slow phases of 3MG ex-

change. Two models for biphasic sugar transport are presented in which 3MG must overcome a sugar-specific, physical (diffusional) or chemical (isomerization) barrier to equilibrate with cell water. These results suggest that biphasic 3MG transport results from ATP-dependent, differential transport of 3MG anomers, ß-3MG is preferred 19-fold over α-3MG.

Introduction

A family of integral membrane proteins called glucose transporters (GLUTs) (23) mediates equilibrative sugar transport in mammalian cells. The glucose transport protein, GLUT1, catalyzes sugar transport in cells of the reticulo-endothelial system (55, 103) and presents an interesting experimental puzzle. The steady-state kinetics of GLUT1-mediated sugar transport in rabbit (102), rat (100, 110) and avian (158, 159) erythrocytes and in basal (insulin-starved) rat adipocytes (84) are consistent with classical models for carrier-mediated solute transport (6, 96). GLUT1-mediated sugar transport in human red cells, however, displays a kinetic complexity that has proven difficult to reconcile with models for carrier mediated transport (76, 77, 79, 81, 106, 160).

Transport complexity is especially obvious in zero-trans exit and infinite-cis entry conditions (75). In the zero-trans exit condition, cells are loaded with various starting sugar concentrations and the initial rate of exit is measured (76, 77) or the complete time course of exit is analyzed by using an integrated Michaelis-Menten equation (76, 78-80). Initial rate measurements (76, 77) routinely provide estimates of $K_{m(app)}$ for sugar exit that

are 2- to 3-times lower than those obtained by analysis of the complete time course of sugar exit (76, 78-80). In the infinite-cis sugar uptake experiment, the external sugar level is saturating and the concentration of intracellular sugar that reduces net sugar uptake by one-half is measured. $K_{m(app)}$ for infinite-cis entry is routinely 5- to 10-fold lower than the value predicted by classical carrier models for sugar transport (79, 81-83).

Why is it that human red cell sugar transport displays kinetic complexity while GLUT1-mediated sugar transport in rabbit, rat and avian erythrocytes and in rat adipocytes is consistent with sugar transport models? Human, rat and rabbit GLUT1 share 98.4% identity (55, 103, 104). Six common residues in rabbit and rat GLUT1 diverge from human GLUT1 sequence but all six substitutions show positive scores on the point accepted mutation similarity scale (105), suggesting that each substitution is unlikely to affect structure or function. If sequence divergence is not the cause of transport complexity, GLUT1 phenotypic variation must result from differences in cellular environment, GLUT1 expression levels or artifacts of measurement.

The sugar transport capacity of human red cells is 220- to 10,000-fold greater than that of rat basal adipocytes (84), rat red cells (100) and avian erythrocytes (107). Naftalin and Holman (97) have discussed several ways by which this could give rise to transport complexity. 1) Transport measurements in human red cells are technically challenging, even at low temperatures, owing to the very high GLUT1 density of human red cells and the high catalytic turnover of GLUT1 (77). Significant backflux of imported sugar during the course of a transport determination would lead to underestimation of net import. 2) If

net cellular sugar import were comprised of two steps - transport followed by intracellular diffusion/distribution - the diffusional step could become rate-limiting if the transport step were sufficiently rapid. Evidence for non-uniform intracellular distribution of sugars has been obtained in both human and rat erythrocytes (79, 100, 110-112).

According to the diffusional barrier hypothesis, human red cell net sugar import is comprised of rapid transport (owing to high cellular GLUT1 content) and slow intracellular diffusion/distribution. The overall result is one where net sugar import is rate-limited by intracellular diffusion/distribution and not by transport. Measurements of sugar uptake in rat or rabbit erythrocytes, however, largely reflect low capacity GLUT1-mediated transport and thus may provide a more accurate description of the intrinsic properties of GLUT1.

This hypothesis infers that GLUT1-mediated sugar transport is inherently simple but that operational complexity is caused by factors extrinsic to the transport system. Transport complexity is lost in cytosol-depleted human red cell ghosts (80, 121, 161, 162) but is preserved if ATP is included in artificial cytosol during red cell resealing (121, 124). Does this mean that human GLUT1 is uniquely ATP-sensitive? Human GLUT1 is an ATP-binding protein (126, 127) and contains three sequence motifs that form the ATP-binding pocket of human adenylate kinase (132). One of these domains (GLUT1 residues 332-338) has been identified by peptide mapping, by micro-sequencing of proteolyzed, azidoATP-photolabelled human GLUT1 (134) and by scanning alanine mutagenesis (133) as a domain critically involved in nucleotide-GLUT1 interaction. This domain is

unchanged in rabbit and rat GLUT1 sequence where there is no *a priori* reason to assume that it does not serve a similar function. It is not known, however, whether rabbit or rat red cell sugar transport are modulated by altered intracellular ATP. Parental (hamster) and exogenous (human) GLUT1-mediated sugar transport are insensitive to cellular ATP-depletion in CHO cells (126, 133) while ATP-sensitive, human GLUT1-mediated sugar transport is observed in transfected HEK cells (126, 133) and in Clone 9 cells (155). This suggests that cellular environment influences GLUT1 phenotype.

These observations stimulate two questions. 1) Is human red cell sugar transport complexity an artifact of measurement? 2) If complexity is real, do human erythrocytes, Clone 9 and HEK cells uniquely express cellular factors that partner in ATP-modulation of sugar transport? We address the former question in the present study. Human red cell membrane GLUT1 content approaches 10% total protein by mass (112) resulting in extremely rapid sugar transport rates at all temperatures studied (109). Measurements of transport are, therefore, complicated by the necessity for rapid sampling procedures (77, 109) but may be simplified by use of the equilibrium exchange condition (163). In equilibrium exchange, intracellular [sugar] = extracellular [sugar], no net transport occurs and unidirectional sugar fluxes are measured by addition of radio-tracer sugar either to the external or internal media. In principle, radio-tracer fluxes under these conditions are first order and thus mono-exponential in a uniform population of cells. The use of this condition will allow investigation of whether sugar transport in red cells reflects the properties

of transmembrane sugar flux alone or whether steps subsequent to transmembrane flux also contribute to overall transport behavior.

Materials and Methods

Materials: ^{3}H-3-O-methylglucose, ^{14}C-3-O-methylglucose, ^{3}H-uridine, and ^{14}C-uridine were purchased from Sigma Chemicals. Rabbit antisera raised against a synthetic carboxyl–terminal peptide of GLUT1 (C-Ab) were obtained from East Acres Biologicals. Sheep antisera raised against tetrameric GLUT1 (δ-Ab) were prepared as described previously (164). Fluorescein-conjugated goat anti-rabbit Ab was purchased from Molecular Probes. Fluorescein-conjugated goat anti-sheep Ab was purchased from Calbiochem. Human blood was purchased from Biological Specialties Cooperation. Other reagents were purchased from Sigma Chemicals.

Solutions: Kaline consisted of 150 mM KCl, 5 mM $MgCl_2$, 5 mM EGTA, 5mM HEPES, pH 7.4. Lysis buffer contained 10 mM Tris-HCl, 2mM EDTA, pH 8.0. Stripping solution contained 2 mM EDTA, 15.4 mM NaOH, pH 12. Sugar-stop solution consisted of ice-cold Kaline containing 20 μM CCB and 200 μM phloretin. Uridine-stop solution consisted of ice-cold Kaline containing 50 μM S-nitrothioinosine.

Red Cells: Red cells were isolated by washing whole human blood in 4 or more volumes of ice-cold Kaline and centrifuging at 10,000 x g for 15 minutes at 4 °C. Serum and buffy coat were removed by aspiration and the wash, centrifugation, aspiration cycle repeated until the buffy coat was no longer visible. Cells were resuspended in 4 volumes

of sugar free or sugar containing Kaline and incubated for 1 hour at 37 °C to deplete or load intracellular sugar.

Red Cell Ghosts: Ghosts were hypotonically lysed by re-suspending washed red cells in 10 volumes of ice-cold lysis buffer for 10 minutes. Membranes were harvested by centrifugation at 27,000 x g for 20 minutes. Ghosts were repeatedly washed with lysis buffer and centrifuged until the membranes appeared light pink (about 3 cycles). Ghosts were then washed with 10 volumes ice-cold Kaline and collected by centrifugation at 27,000 x g. Harvested membranes were resealed by incubation in 4 volumes of Kaline ± 4 mM ATP (37 °C) for 1 hour and collected by centrifugation at 27,000 x g for 15 minutes at 4 °C. Resealed ghosts were stored on ice until used.

Net 3-O-methylglucose uptake: Sugar-depleted cells or ghosts were incubated in 20 volumes of ice-cold Kaline containing 100 μM unlabeled 3MG and 0.5 μCi/mL labeled 3MG. Uptake was allowed to proceed for intervals as short at 6 seconds to intervals as long as 3 hours. Uptake was arrested by addition of ice-cold stop buffer and ghosts were centrifuged at 14,000 x g for 1 minute. The supernatant was removed by aspiration and ghosts were washed with 20 volumes of sugar stop buffer, re-centrifuged and supernatant aspirated. The ghost pellet was extracted with 500 μL of 3% perchloric acid, centrifuged, and samples of the clear supernatant were counted in duplicate. Zero time points were collected by the addition of sugar stop solution to ghosts followed by uptake media. Samples were then immediately processed. Radioactivity associated with cells at zero time was subtracted from all non-zero time points. Equilibrium time points were col-

lected using an overnight incubation. All time points were normalized to the equilibrium time point. All solutions and tubes used in the assay were pre-incubated on ice for 30 minutes prior to the start of the experiment. Triplicate samples were processed for each time point.

Initial rate, zero-trans 3-O-methyl-glucose uptake - time dependence: Sugar-depleted cells or ghosts were allowed to rest in 20 volumes of ice-cold Kaline for intervals as short as 30 seconds or as long as 3 hours. Thirty seconds prior to the end of the rest interval, a small volume of 3MG and 0.5 μCi/mL tracer 3MG were added to the suspension to a final [3MG] of 100 μM. Uptake was stopped by addition of sugar stop solution and cells or ghosts were processed as above. A zero time point was obtained as described above. An equilibrium time point was obtained by allowing ghosts to uptake unlabeled and labeled 3MG overnight at 4 ˚C. Uptake rates were expressed as μmol/(min.L cell water) by subtracting the zero time point and normalizing to the equilibrium time point.

3-O-methylglucose equilibrium exchange, uptake and exit: Ghosts were resealed in the presence of 0.1, 2.5, 10 or 20 mM unlabeled 3MG and trace amount (0.5 μCi/mL) of ^{14}C-3MG, centrifuged, and the supernatant was aspirated. Ghosts were then incubated in 20 volumes of ice-cold Kaline containing the same concentration of 3MG and 0.5 μCi/mL ^{3}H-3MG. Exchange was allowed to proceed for time intervals as short as 6 seconds to intervals as long as 10 hours. Exchange was then stopped by the addition of ice-cold sugar stop and ghosts were treated as above with zero-trans uptake.

Uridine equilibrium exchange, uptake and exit: Experiments were performed as with 3MG equilibrium exchange except that the transport substrate was uridine and uridine stop was used to stop the reaction and to wash the ghosts.

GLUT1 Immunofluorescence microscopy and FACS analysis: For C-Ab immunofluorecence staining, 50 μL of non-fixed unsealed ghosts were washed once in ice-cold Kaline, centrifuged at 4 °C, and the supernatant aspirated. 1:500 dilution of C-Ab was added to the pellet and the suspension was incubated at 4 °C for 2 hours, centrifuged and supernatant aspirated. Ghosts were washed with ice-cold Kaline. Secondary antibody (1:500 dilution) was added to the pellet and the suspension was incubated at 4 °C for 1 hour, centrifuged and supernatant removed by aspiration. Ghosts were washed 5 times with ice-cold Kaline and brought to a final volume of 500 μL. For δ-Ab staining, re-sealed ghosts are incubated with a 1:500 dilution of δ-Ab at 37 °C for 1 hour, and then processed as above. For microscopy, 10 μL of the suspension was added to a poly-lysine coated cover slip and adhered by low speed centrifugation. Cover slips were washed 5 times with 10 mL of ice-cold Kaline. Fluorescence microscopy was performed on an Olympus BX-51 fluorescence microscope. For FACS analysis, 50 μL of the immunofluorescence stained ghosts were mixed with ~1 mL of FACS buffer in a FACS sample tube. FACS analysis was performed using a Becton Dickinson FACS Scan sampled for 10,000 counts and analyzed with Cell Quest 3.3.

Ghost accessible volumes: Ghosts were prepared and resealed with and without intracellular ATP. After resealing, 2.5 mM 3MG or uridine and tracer ^{3}H-3MG or ^{3}H-

uridine and ^{14}C-sucrose were added to the ghosts and the radio-tracers were allowed to equilibrate with cell water. The samples were centrifuged at 14000 x g for 1 minute and known volumes of supernatant and pellet were sampled and counted for both isotopes. Ghosts were counted on a hemocytometer. Tracer accessible volume (V_{acc}) was calculated as:

$$V_{acc} = \frac{\left(1 - \frac{^{14}C_p}{^{14}C_s}\right)\frac{^{3}H_p V_s}{^{3}H_s}}{\text{Cell Number}} \qquad \text{Eq. 2.1}$$

where ^{14}C and ^{3}H refer to the respective dpms, V is the sample volume, and S and P refer to supernatant and pellet. In this manner, the extracellular volume of the pellet is subtracted by measuring the sucrose space. Alternatively, ghosts were resealed with 2.5 mM 3MG and 2.5 mM uridine plus ^{3}H-3MG and ^{14}C-uridine or ^{14}C-3MG and ^{3}H-uridine radio-tracers. At 0 and 15 hours post resealing, ghosts were sedimented by centrifugation and the supernatant was sampled. The ghost pellets were washed twice with 20 μM CCB, 200 μM phloretin, and 50 μM S-nitrothioinosine in ice-cold Kaline. Known volumes of supernatant and pellet were counted for 3MG and uridine and pellet to supernatant ratios were computed.

Red cell and ghost electron microscopy: Scanning Electron Microscopy (SEM) of red cells and ghosts was carried out as previously described (165)(166). Red blood cells and ghosted cells were fixed by immersion in 2.5% (v/v) glutaraldehyde in 0.5 M sodium phosphate buffer (pH 7.2) for 1 hr at room temperature. Fixed samples were then washed three times in the same buffer. Following the third wash the cells were post fixed

for 1 hr in 1% osmium tetroxide (w/v) in the phosphate buffer, washed 3X in buffer and left overnight at 4° C. The next morning, the samples were dehydrated through a graded series of ethanol to 100% and then the bottoms of the tubes were excised, placed in porous sample holders and Critical Point Dried in liquid CO_2. After drying, tubes were emptied onto aluminum SEM stubs coated with adhesive carbon tape. The edges were then painted with silver conductive paste and the SEM stubs were sputter coated with Au/Pd (80/20). The specimens were then examined using an ETEC autoscan scanning electron microscope at 20 kV accelerating voltage.

Curve fitting procedures: Where appropriate, data sets were analyzed by nonlinear regression using the software packages KaleidaGraphTM 4.0 (Synergy Software, Reading, PA) or Igor-Pro (version 5, Wavemetrics, Lake Oswego, OR).

Results

The effect of ATP on 3-O-methylglucose equilibrium exchange transport: The effect of intracellular ATP on equilibrium exchange 3MG transport at 4 °C was monitored over the course of five hours by measuring the simultaneous uptake of tracer ^{3}H-3MG and exit of ^{14}C-3MG (Figure 2.1). Resealed ghosts lacking intracellular ATP show an exchange time course that follows a single, simple exponential rise or decay for uptake and exit respectively. This is expected for a passive transport process characterized by a single rate limiting step and occurring in a uniform population of cells. When ghosts are resealed with 4 mM intracellular ATP, however, the time course changes, becoming

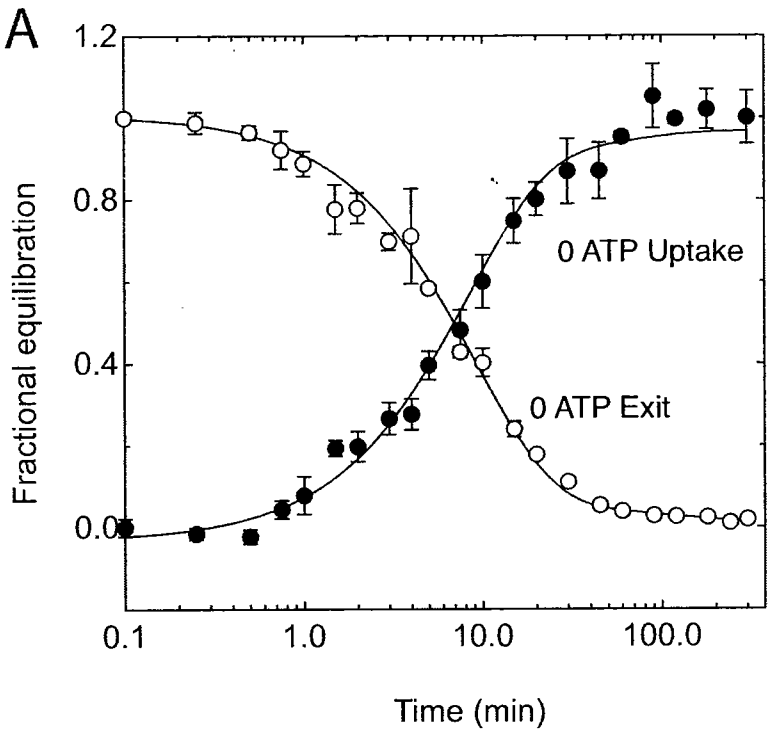
A
1.2
0.8
0.4
0.0
Fractional equilibration
0 ATP Uptake
0 ATP Exit
0.1
1.0
10.0
100.0
Time (min)

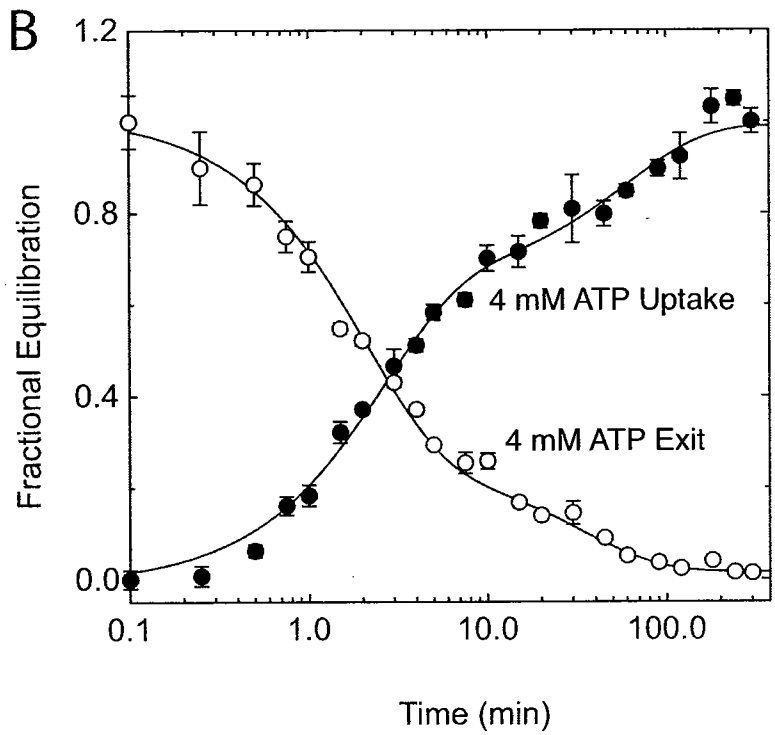
B
1.2
0.8
0.4
0.0
Fractional Equilibration
4 mM ATP Uptake
4 mM ATP Exit
0.1
1.0
10.0
100.0
Time (min)

Figure 2.1. Time Course of 3-O-methylglucose Equilibrium Exchange Uptake and Exit in Red Cell Ghosts Containing or Lacking Intracellular ATP.

Ordinate: fractional equilibration; Abscissa: time in minutes (note log scale). **A.** Exchange of 2.5 mM 3MG in red cell ghosts resealed without intracellular ATP. Uptake (•) follows a single exponential rise and exit (○) follows a single exponential decay. Curves drawn through the points are computed by nonlinear regression and take the forms: $(1-e^{-kt})$ for uptake and e^{-kt} for exit where k is the observed rate constant. The measured means ± SEM are: A (0 ATP) - uptake, k = 0.079 ± 0.004 min^{-1}; exit, k = 0.071 ± .004 min^{-1}. **B.** Exchange of 2.5 mM 3MG in red cell ghosts resealed with 4 mM intracellular ATP. Uptake (•) and exit (○) follow biexponential kinetics. Curves drawn through the points are computed by nonlinear regression of the form: $A(1-e^{-k_1t})+(1-A)(1-e^{-k_2t})$ for uptake and $A(e^{-k_1t})+(1-A)(e^{-k_2t})$ for exit where k_1 is the observed rate constant for the fast phase, k_2 is the slow phase rate constant, and A is the fractional component of total uptake or exit described by the fast phase. Values of k, A, k_1, and k_2 are shown in Table 2. 1.

biphasic for both unidirectional uptake and exit. The early phase of transport is accelerated 4-fold in the presence of ATP. After 10 minutes when one-half to two-thirds of unidirectional exchange is complete, the rate of transport declines by more than 10-fold to a rate approaching 2-fold slower than transport in the absence of ATP. Table 2.1 summarizes fit parameters for ghosts lacking and containing ATP. Equilibrium exchange time courses have been studied previously by this laboratory but biphasic transport was observed only at the lowest [3MG] employed (0.1 mM 3MG (113)) where biphasic exchange may be related to GLUT1 sugar binding. Those studies did not monitor transport beyond 5 minutes which explains why biphasic equilibrium exchange transport at higher [3MG] was not observed.

One explanation for biphasic transport in the presence of ATP is that a significant sub-population of ghosts spontaneously reseal before ATP is introduced so that the measurements sample a mixed population of ATP containing (fast) and ATP lacking (slow) ghosts. This simple hypothesis is refuted by the observation that the slow phase of 3MG transport in ATP-containing ghosts is more than twice as slow as transport in ATP-free ghosts.

Red cell ghosts present a relatively uniform population of cell sizes and GLUT1 contents: A mixed population of ghost cell sizes or GLUT1 content could account for biphasic 3MG exchange transport. As cell size decreases, the surface area : volume ratio increases thereby increasing the rate of GLUT1-mediated equilibration of radio-tracer sugar. Altered GLUT1 content (or activity) at the membrane surface also de-

Table 2.1. Effect of Substrate Concentration and ATP on Rate Constants and Components of 3MG Equilibrium Exchange

[3MG]	- ATP k_{obs}[a]		+ ATP fast k_{obs}[a]		+ ATP slow k_{obs}[a]		+ ATP fast component size[b]	
	Uptake	Exit	Uptake	Exit	Uptake	Exit	Uptake	Exit
100 µM	0.168 ± 0.010	0.132 ± 0.010	0.357 ± 0.043	0.671 ± 0.070	0.012 ± 0.004	0.040 ± 0.005	0.722 ± 0.039	0.575 ± 0.032
2.5 mM	0.090 ± 0.004	0.100 ± 0.004	0.372 ± 0.019	0.392 ± 0.007	0.015 ± 0.002	0.018 ± 0.005	0.651 ± 0.018	0.819 ± 0.005
10 mM	0.104 ± 0.004	0.109 ± .004	0.320 ± 0.013	0.287 ± .007	0.012 ± 0.001	0.026 ± 0.001	0.681 ± 0.014	0.768 ± 0.005
20 mM	0.098 ± 0.008	0.122 ± 0.006	0.386 ± 0.050	0.167 ± 0.012	0.025 ± 0.003	0.009 ± 0.001	0.468 ± 0.038	.708 ± 0.026

[a]All rate constants are first order and have units of min^{-1} and are shown as mean ± SEM.

[b]Fast component size represents the size (fraction of total 3MG accessible space) of the exchange transport component described by the fast rate constant and is shown as mean ± SEM. The size of the component described by the slow rate constant is 1 - fast fractional size.

termines the rate constant for radio-tracer equilibration.

GLUT1 content was assayed by immunofluorescence microscopy of fixed or living cells and by fluorescence activated cell sorting (FACS). Figures 2.2A-C show fluorescence micrographs of ghosts stained with antibodies directed to cytoplasmic (Figure 2.2A) or extracellular (Figure 2.2B, C) GLUT1 epitopes. The use of cytoplasmic-epitope directed antibodies (C-Ab) necessitates cell fixation/permeabilization. FACS analysis of GLUT1 staining by exofacial antibodies (δ-Ab) suggests a uniform population of cells ± ATP (Figure 2.2E). C-Ab staining of unsealed ghosts ± ATP produces similar results (data not shown). Cell size was quantified by FACS analysis of single cell light scattering. Ghosts show a single population of scattering intensities as detected at either low (data not shown) or high angles (Figure 2.2D) and scattering is independent of cytoplasmic ATP content (157).

The effect of ATP on ENT1 mediated uridine exchange transport: Previous models have rationalized sugar transport complexity by hypothesizing an unstirred layer beneath the red cell membrane (79, 97, 110). While predicted deviations from simple Michaelis-Menten kinetics at low [3MG] are observed for sugar exit in human and rat red cells (100, 112), direct evidence for this unstirred layer is not available.

ENT1-mediated uridine transport was examined in order to determine whether the putative unstirred layer is sugar transport specific. Figure 2.3 shows the time course of 2.5 mM uridine exchange in ghosts ± ATP. Although there are 100-fold fewer nucleoside

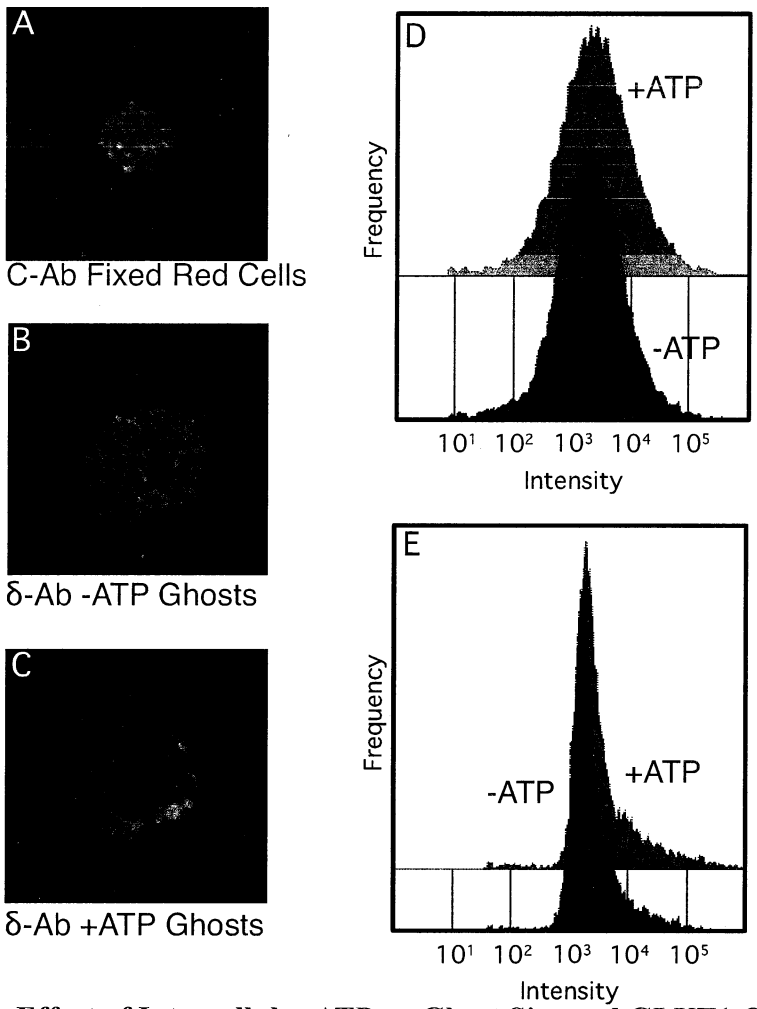

Figure 2.2. Effect of Intracellular ATP on Ghost Size and GLUT1 Content.

A. Immunofluorescence labeling and microscopy of fixed and permeabilized red blood cells stained with C-Ab. **B.** Living, non-fixed ghosts resealed without ATP and stained with δ-Ab. **C.** Living non-fixed ghosts resealed with 4 mM ATP stained with δ-Ab. **D.** FACS analysis (large angle light scattering) was used to assay ghost size in cells lacking (blue) or containing (red) intracellular ATP. **E.** GLUT1 content was measured by FACS analysis of δ-Ab staining. For D and E; Ordinate: number of cells; Abscissa: Intensity of signal (note log scale).

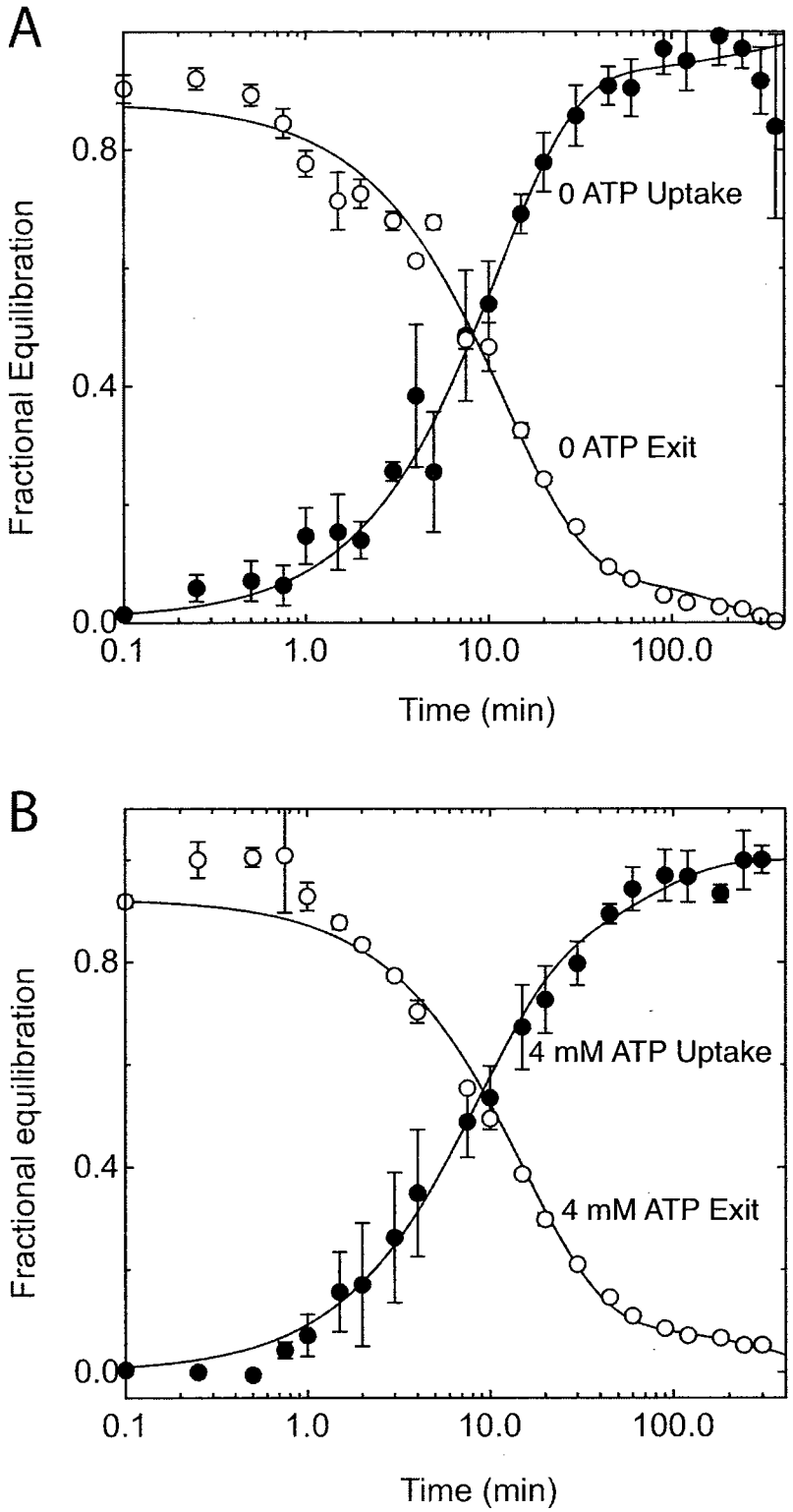
A
Fractional Equilibration
0.0
0.4
0.8
0.1
1.0
10.0
100.0
Time (min)
0 ATP Uptake
0 ATP Exit
B
Fractional equilibration
0.0
0.4
0.8
0.1
1.0
10.0
100.0
Time (min)
4 mM ATP Uptake
4 mM ATP Exit

Figure 2.3. Time Course of Uridine Equilibrium Exchange Uptake and Exit With and Without Intracellular ATP.

Ordinate: fractional equilibration; Abscissa: time in minutes (note log scale). **A.** Exchange of 2.5 mM Urd in red cell ghosts resealed without intracellular ATP. **B.** Exchange of 2.5 mM 3MG in red cell ghosts resealed with 4 mM intracellular ATP. Uptake (•) follows a single exponential rise and exit (○) follows a single exponential decay. Curves drawn through the points are computed by nonlinear regression and take the forms: $(1-e^{-kt})$ for uptake and e^{-kt} for exit where k is the observed rate constant. The measured means ± SEM are: **A.** (0 ATP) - uptake, $k = 0.079 \pm 0.004$ min^{-1}; exit, $k = 0.071 \pm .004$ min^{-1}; **B.** (4 mM ATP) - uptake, $k = 0.076 \pm 0.005$ min^{-1}; exit, $k = 0.065 \pm 0.005$ min^{-1}.

transporters per red cell than there are glucose transporters, K_m for uridine transport is approximately 100-times lower than $K_{m(app)}$ for GLUT1-mediated 3MG transport (167). The apparent rate-constant for transport of any species, k, is proportional to the ratio $V_{max}/K_{m(app)}$ (2), hence sugar and uridine transport proceed at similar rates. Uridine uptake and exit are monoexponential in ghosts regardless of cellular ATP content (Figure 2.3). If an intracellular unstirred layer/diffusional barrier does exist, it must be selective for GLUT1 substrates. Monophasic uridine exchange transport in ghosts lacking and containing ATP also argues against multiple cell sizes in resealed ghosts.

Effect of intracellular ATP on accessible sugar and uridine volumes: Table 2.2 summarizes two experiments in which the intracellular 3MG and uridine spaces of red cell ghosts were measured in the absence and presence of 4 mM intracellular ATP. 3MG and uridine spaces are identical and are unaffected by inclusion of 4 mM ATP during resealing. Differences between experiments may result from cell counting errors caused by low contrast of red cell ghosts in the hemocytometer. As transport experiments span several hours, the time-dependence of cell volumes was also investigated. The normalized internal to external ratios of [3MG] and [uridine] ± ATP at 0 and 15 hours are shown in Figure 2.4. There is no change in the accessible volume over that time.

Effect of preincubation time on initial rates and time courses of transport: ATP levels are reduced by approximately 50% during the 5 hours of an exchange time course experiment (data not shown). While AMP and ADP do not directly affect transport, they serve as competitive inhibitors of ATP binding to GLUT1 (127). It is possible,

Table 2.2. Effect of ATP on Substrate Accessible Internal Volume[a]

Substrate	0 ATP	+ ATP
3-O-methylglucose	134 ± 8[b], 100 ± 8[c]	129 ± 5[b], 81 ± 6[c]
Uridine	133 ± 13[b], 98 ± 9[c]	133 ± 7[b], 77 ± 4[c]

[a] Volume measured in fL and shown as mean ± SEM.

[b] Experiment 1

[c] Experiment 2

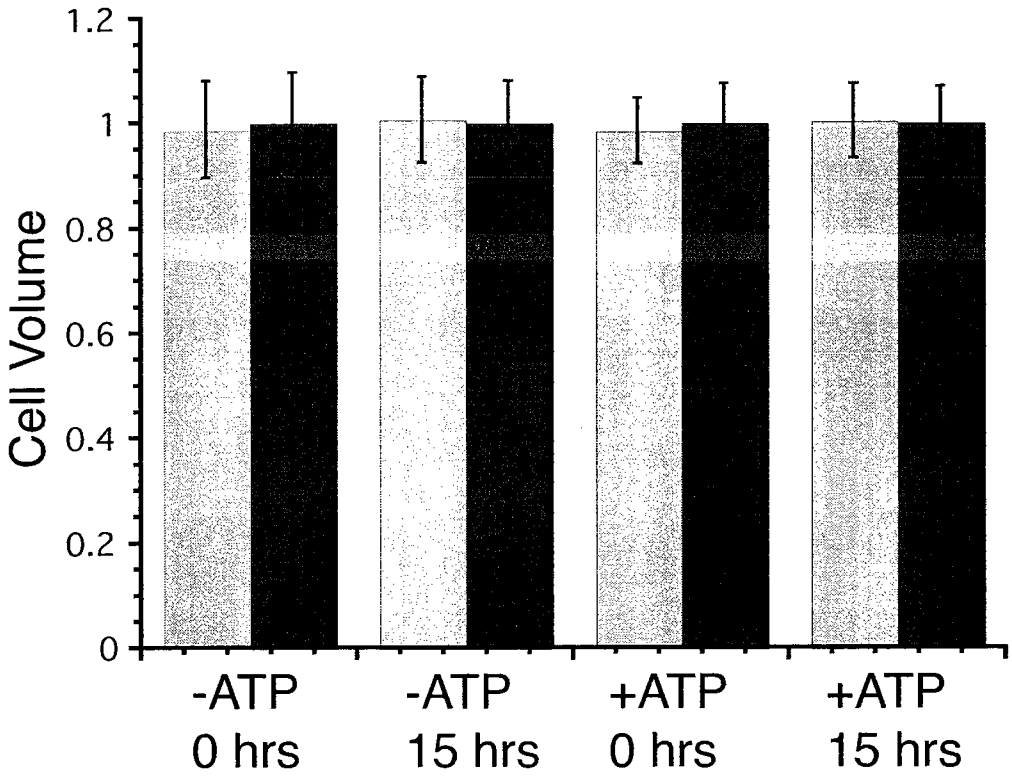

Figure 2.4. Accessible Internal Ghost Volumes.

Effect of time on accessible 3-O-methylglucose (▒) and uridine (▮) volumes of ghosts lacking or containing 4 mM ATP. Ordinate: accessible volume normalized to uridine; Abscissa: key indicating the time of measurement after resealing and cellular ATP content. Results are shown as mean ± SEM of triplicate measurements.

therefore, that nucleotide dependent changes in GLUT1 intrinsic activity occur during the time course of our measurements. To examine this possibility, both the time course of net 3MG uptake and the instantaneous rate of 3MG uptake were measured in ATP-free and ATP-containing ghosts before and after 5 hours of mock (sugar free) transport. Figure 2.5A shows that ATP-modulation of zero-trans uptake persists after 5 hours. No change in the instantaneous (initial) rate of zero-trans 3MG uptake is observed following 5 hours (Figure 2.5B). Biphasic exchange transport persists in ghosts that have previously exchanged 3MG for 15 hours prior to being assayed for radio-tracer exchange (Figure 2.5C). These data indicate that time-dependent changes in the intrinsic activity of GLUT1 do not account for biphasic sugar transport.

ATP modulation of red cell ghost morphology: Red cells and ghosts containing or lacking ATP were examined by scanning electron microscopy. Figure 2.6 shows the morphological changes induced by ATP depletion. Red cell membranes become spherical and highly crenated following ghosting in the absence of ATP. Ghost resealing in the presence of Mg·ATP reverses this effect.

Discussion

Human erythrocyte sugar transport displays a kinetic complexity that is not explained by available models for carrier-mediated facilitated diffusion (77, 79, 81, 106, 160, 168). In contrast, rat, rabbit and pigeon erythrocyte sugar transport are compatible with available transport models (100, 102, 110, 159). Sequence identity between rat or

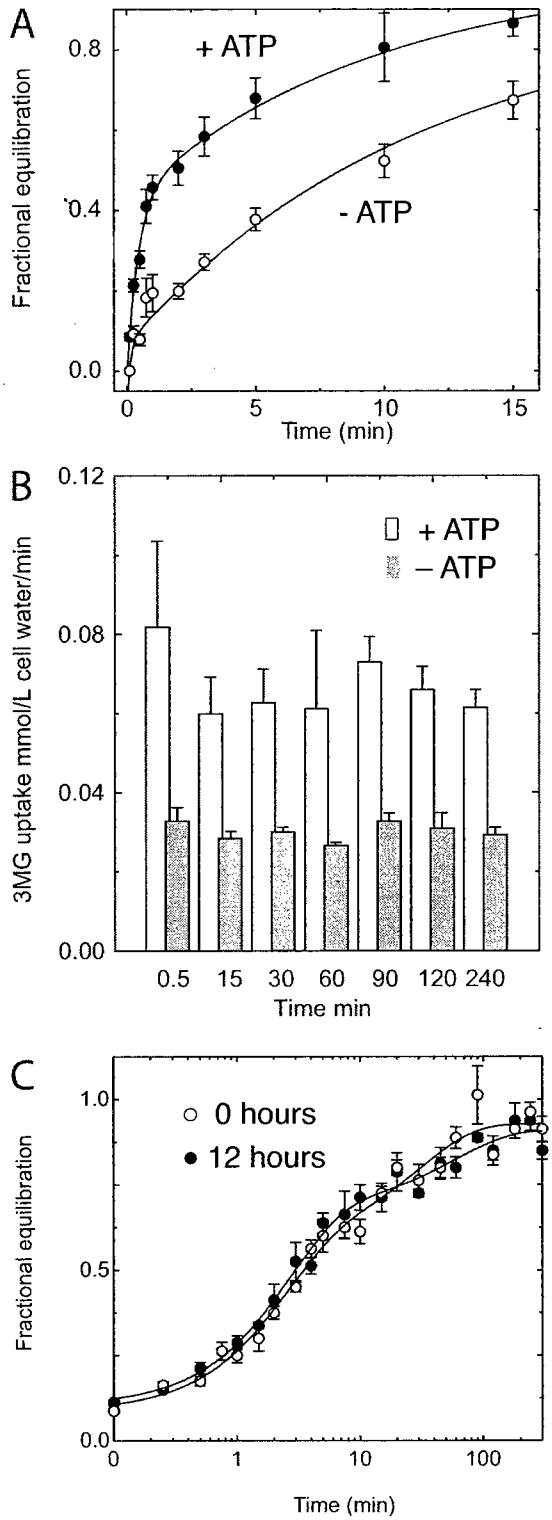
A
+ ATP
- ATP
Fractional equilibration
0.0
0.4
0.8
0
5
10
15
Time (min)
B
+ ATP
– ATP
3MG uptake mmol/L cell water/min
0.00
0.04
0.08
0.12
0.5
15
30
60
90
120
240
Time min
C
0 hours
12 hours
Fractional equilibration
0.0
0.5
1.0
0
1
10
100
Time (min)

Figure 2.5. Effect of Time on Initial Rate and Time Course of Transport.

A. Zero-trans uptake of 100 μM 3MG in red cell ghosts resealed with (•) and without (○) intracellular ATP and permitted to rest in 20 volumes of ice-cold Kaline for 5 hours. Ordinate: fractional equilibration; Abscissa: time in minutes. Curves drawn through the points were computed by nonlinear regression to assuming the biexponential form: $A(1-e^{-k_1 t})+(1-A)(1-e^{-k_2 t})$ where k_1 and k_2 are the observed rate constants for phase 1 and 2 respectively and A is the fractional component of total uptake described by phase 1. In the absence of ATP, $A = 0.12 \pm 0.03$, $k_1 = 2.6 \pm 1.5$ min $^{-1}$ and $k_2 = 0.06 \pm 0.01$ min^{-1}. In the presence of ATP, $A = 0.43 \pm 0.03$, $k_1 = 2.2 \pm 0.3$ min^{-1} and $k_2 = 0.10 \pm 0.01$ min^{-1}. **B.** Time dependence of initial rates of zero-trans uptake plus (□) and minus (▒) ATP. Ghosts were allowed to rest in Kaline for the specified time following which a small volume of 3MG to make a final concentration of 100 μM was added and the initial rate of transport was measured over a 30 second interval. Ordinate: uptake rate in mmol .min^{-1}.(L cell water)$^{-1}$; Abscissa: Time of pre-incubation prior to measurement of uptake rate. **C.** Time course of 2.5 mM 3MG equilibrium exchange in the presence of 4 mM intracellular ATP measured immediately after resealing (○) or following 12 hours of unlabeled 3MG equilibrium exchange (•). Curves were drawn by nonlinear regression assuming exchange is described as above. The results are: Control, $A = 0.72 \pm 0.03$, $k_1 = 0.372 \pm 0.054$ min^{-1}, and $k_2 = 0.017 \pm 0.007$ min^{-1}; 12 hours post control, $A = 0.59 \pm 0.07$, $k_1 = 0.411 \pm 0.116$ min^{-1}, and $k_2 = 0.032 \pm 0.013$ min^{-1}.

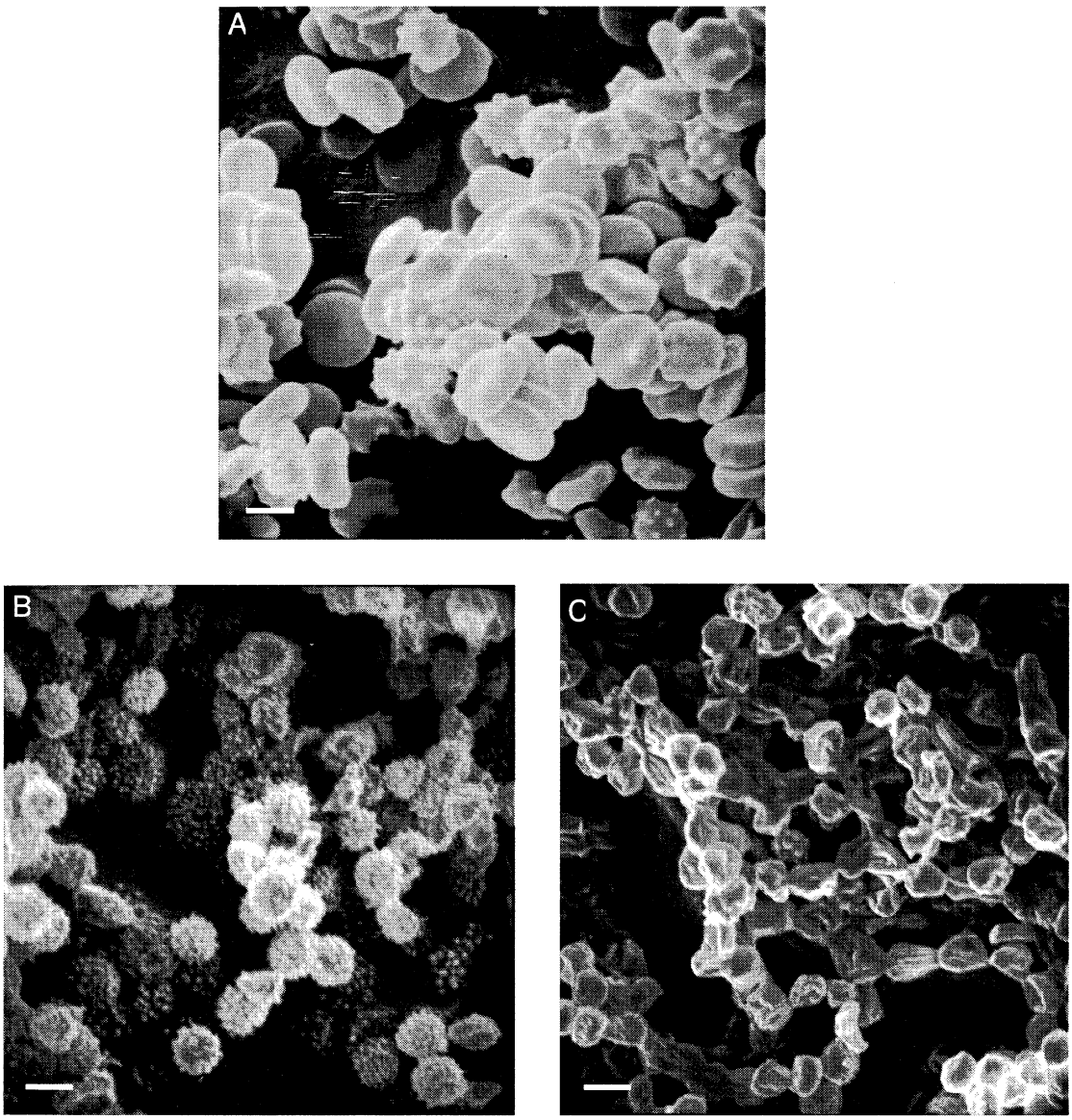

Figure 2.6. Effect of Intracellular ATP on Ghost Morphology.

Scanning electron microscopy of **A.** red blood cells, **B.** resealed ghosts lacking ATP, and **C.** resealed ghosts containing 4 mM intracellular ATP. The white bar in each frame is 5 μm.

rabbit GLUT1 and human GLUT1 is extremely high (> 98.9%) suggesting that transport complexity in human red cells is not caused by specific, human GLUT1 sequence changes. Using cellular sugar transport and cytochalasin B binding capacities as a point of comparison, rat, rabbit and pigeon red blood cells contain 500- to 10,000-fold fewer copies of GLUT1 than their human counterparts (100, 102, 159). It has been proposed, therefore, that human red cell sugar transport asymmetry is associated with very high cellular GLUT1 content and may, in fact, be an artifact resulting from the technical challenge of measuring extremely rapid sugar fluxes (79, 97, 99). Reversible red blood cell lysis ("ghosting") to remove non-membrane associated factors modifies the steady-state kinetics of human red blood cell sugar transport resulting in the loss of transport complexity (80, 121, 123, 124). Thus, cytosolic factors also play an important role in regulating transport function.

Naftalin and Holman (97) proposed that an unstirred layer at the cytosolic surface of the membrane would increase $K_{m(app)}$ for sugar exit because the concentration of sugar beneath the membrane falls more rapidly than total intracellular sugar. Naftalin initially proposed that nonspecific sugar association with hemoglobin accounted for this "unstirred layer" effect (79). However, the presence or absence of bulk hemoglobin has no affect on transport (121, 169). Rather, cytosolic ATP modulates red cell sugar transport symmetry (121). Evidence for an unstirred layer is available from three sources. Net 3MG uptake in human red blood cells display biphasic kinetics suggesting rapid equilibration with an unstirred layer and slower equilibration with bulk cytosol (113). Steady-

state sugar exit experiments in human red cells display a specific deviation from Michaelis-Menten kinetics at low intracellular [sugar] that is characteristic of an intracellular unstirred layer (6, 112). Counterflow experiments in rat red cells (radiolabeled sugar net uptake by cells in which cytoplasmic [sugar] > extracellular [sugar]) suggest a non-uniform distribution of unlabeled and labeled sugars within the cell (100, 110).

The unstirred layer hypothesis was later modified following the discovery of an ATP-dependent, GLUT1 high-affinity non-catalytic sugar binding site (112). GLUT1 sugar binding and occlusion (slow release of sugar from the GLUT1·sugar complex) were proposed to be responsible for biphasic sugar transport. At sub-saturating sugar concentrations (50 μM) where biphasic uptake is observed, the fast phase of transport was hypothesized to represent sugar movement through the GLUT1 translocation pathway plus its ensuing interaction with the high affinity site. Subsequent release of translocated sugar into cytosol is rate-limited by a diffusional barrier or cage formed by the GLUT1 C-terminus interacting with cytoplasmic loop-6. While delayed within the cage, the probability of sugar re-association with the exit site and translocation back to interstitium is high. The net effect is reduced net sugar import. This model predicts that the size of the fast component of transport in any cell is dependent on [GLUT1]. Transport complexity, however, should be independent of cellular [GLUT1] because both phenotypes are consequences of the intrinsic properties of GLUT1. The nominal "absence" of transport complexity in rat, rabbit and avian red cells refutes this hypothesis. Furthermore, sugar

translocation through the transport pore is now known to occur on the time-scale of milli-seconds rather than seconds (109).

To eliminate complexities inherent to zero-trans experiments, measurements of transport under equilibrium exchange conditions where no net change in [sugar] occurs are employed. Two previous studies have examined GLUT1-mediated sugar equilibrium exchange in detail. Weiser, Razin and Stein measured exchange uptake and exit in both cold-stored and fresh human red cells (163). They concluded that exchange kinetics were mono-phasic, but used early time points (< 30 sec) in their analysis and thereby missed the second slower phase. They also observed that cold-storage of red cells raises the K_m for transport by nearly two-fold. Previous studies by this laboratory demonstrate biphasic sugar exchange transport in intact red cells, but only at the lowest [3MG] tested (< 1 mM) (113). This led to the conclusion that biphasic transport was due to sugar binding in the cell. We now know that detection and analysis of the slower phase of transport at 4 °C requires measurements beyond 5 minutes and this prompted us to extend our analysis of equilibrium exchange transport to later time points.

When red cell ghosts are ATP-depleted, radio-tracer 3MG equilibrium exchange follows simple monophasic kinetics. Exchange in ATP loaded red cell ghosts shows biphasic exchange kinetics at all [3MG] tested. Neither fast nor slow phases of exchange transport can be attributed to sugar complexation by GLUT1 as [GLUT1] is 20 μM while [3MG] ranges from 0.1 to 20 mM. ATP-dependent deviation from monophasic exchange kinetics is not due to heterogeneity in ghost size, cellular GLUT1 content or GLUT1 ac-

tivity. Monophasic ENT1-mediated uridine exchange kinetics in the presence of intracellular ATP also argue against ATP dependent ghost heterogeneity.

Monophasic uridine exchange kinetics imply that biphasic 3MG exchange kinetics are either GLUT1 specific, sugar specific, or specific to both transporter and substrate. If a sugar-specific compartment exists in ATP loaded cells, then the 3MG space of ATP loaded cells should be greater than the uridine space. ATP removal should be without effect on the 3MG space but will increase the uridine space. This was not observed. If a specific sugar-binding compartment explains the ATP-dependent slow phase of exchange transport, then the 3MG space of ATP loaded cells should be greater than the uridine space while ATP depletion will reduce the 3MG space of the cell to that of the uridine space which remains unchanged. The observation that ATP has no affect on 3MG or uridine space refutes both hypotheses.

The possibility of a time-dependent change in the intrinsic kinetics of transport over the 5 hours of measurement is refuted by two observations: 1) instantaneous 3MG transport rates do not change with time and, 2) biphasic exchange of radiolabeled 3MG is recapitulated following 12 hours of exchange of unlabeled sugar. In sum, these results suggest two serial barriers to 3MG transport. The first barrier is translocation through GLUT1 while the nature of the second barrier is unknown. Two possibilities exist - the barrier is a physical barrier (e.g. permeability barrier or unstirred layer) or the barrier is a chemical barrier (e.g. sugar is reversibly converted to a second species).

The physical barrier hypothesis: A physical barrier model for ATP dependent, GLUT1-mediated biphasic 3MG equilibrium exchange is illustrated in Figure 2.7. In normal red cell discocytes, GLUT1 is anisotropically distributed in the plasma membrane. The cytosol, however, contains two diffusionally isolated compartments (e.g. see (170)). Cytosol adjacent to GLUT1-enriched membrane rafts (compartment 1) is accessible to newly imported sugars. Cytosol adjacent to GLUT1-depleted membrane (compartment 2) is inaccessible to newly imported sugars. Thus sugar transport rapidly fills compartment 1 while equilibration of compartment 2 requires diffusion across the barrier separating compartments 1 and 2. The uridine transporter ENT1, by contrast, is uniformly distributed across the membrane such that both 3MG compartments are accessible to imported uridine. Upon Mg^{2+}·ATP depletion-induced echinocytosis (171), red cell GLUT1 becomes uniformly distributed in the plasma membrane and/or the diffusion barrier between cytoplasmic compartments is lost making the entire cellular space directly accessible to transported 3MG.

Several predictions follow from this model: 1) artificial, non-ATP depleting spheroechinocyte formation will induce monophasic 3MG exchange kinetics, 2) high resolution GLUT1 membrane localization will be different from ENT1 localization, 3) slowing transport by use of inhibitors will inhibit the fast component of transport but not the slow phase.

The chemical barrier hypothesis: A chemical barrier describes sugar conversion to a second molecular species within the cell (Figure 2.8). A sugar could, for example, be

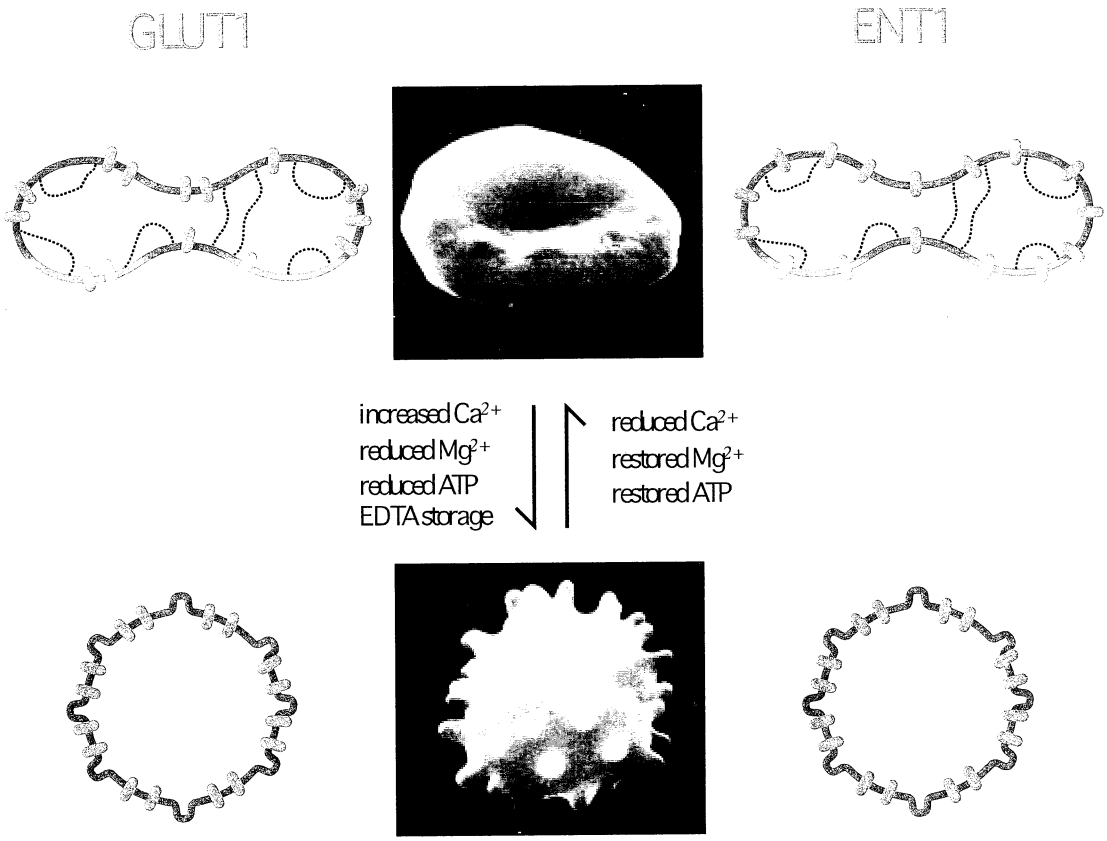

Figure 2.7. The Physical Barrier.

With sufficiently high intracellular [Mg^{2+}] and [ATP], red cells and ghosts are biconcave and GLUT1 is restricted to specific areas of the membrane. Cytoplasmic space that is adjacent to GLUT1-depleted plasma membrane is diffusionally isolated from cytoplasmic space adjacent to GLUT1-enriched membrane. ENT1/2 is isotropically distributed in the membrane so that Urd is transported into both cytoplasmic compartments simultaneously. ATP and/or Mg^{2+} depletion results in phosphatidylserine redistribution and echinocyte formation. GLUT1 surface distribution in spheroechinocytes is isotropic and/or diffusional isolation of cytoplasmic spaces is lost resulting in monophasic 3MG exchange.

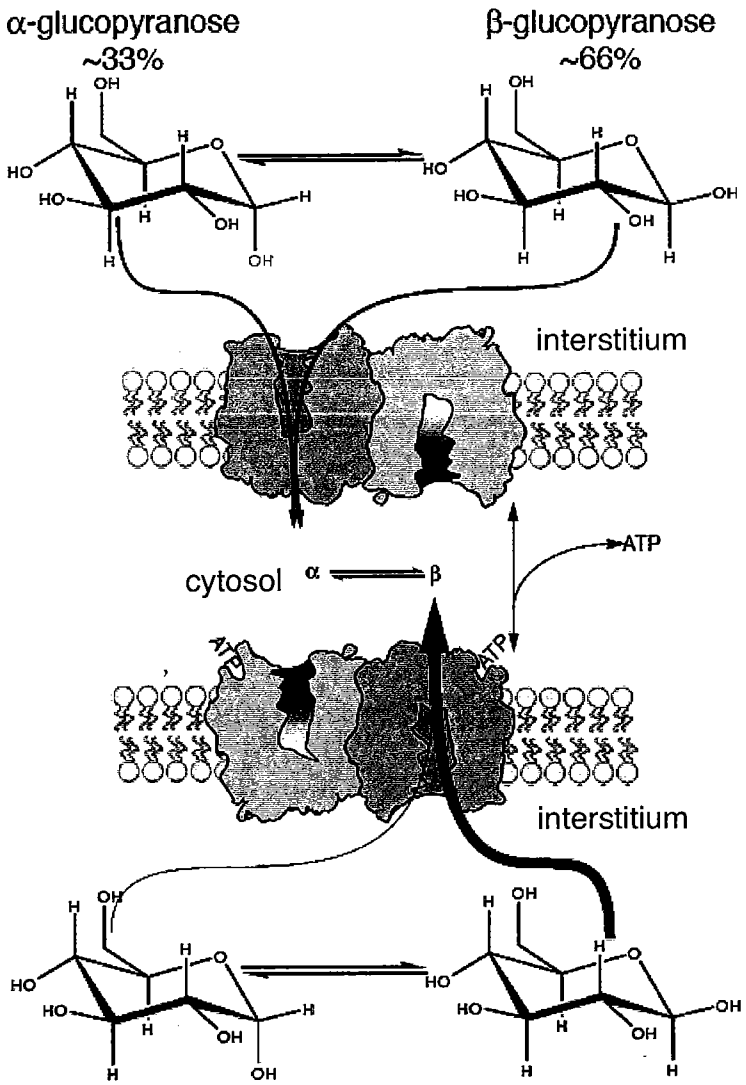

Figure 2.8. The Chemical Barrier.

Sugars undergo spontaneous anomerization between α- and β-forms in aqueous solution. Both α- and β-sugars are transported but β-sugar is transported with 27-fold higher capacity in the presence of cytoplasmic ATP. α- and β-sugars compete for uptake and exit. β-sugars equilibrate most rapidly across the membrane but mutarotation to α- sugar ensures that both α- and β-sugars are available in the cytoplasm.

metabolized, undergo anomerization, or become complexed to a binding partner. If metabolized, the transformed species must remain a substrate for bidirectional transport (by either GLUT1 or other transporters) otherwise the cytoplasmic distribution space available to sugar plus its metabolite would exceed the cell water volume. 3MG is, however, a nonmetabolizable sugar which is neither transformed following transport into or out of the cell (172, 173). We therefore reject the metabolism hypothesis. If transported sugar complexes with an intracellular binding partner, the cytoplasmic distribution space available to free and bound sugar would exceed the cell water volume. Since this is not observed, this permits rejection of the binding partner hypothesis.

Differential transport of sugar anomers could explain biphasic sugar transport. D-Glucose and 3MG anomerize slowly in aqueous solution between α- and β-anomers ($t_{1/2}$ = 10 min at 37 °C; equilibrium ratio of α- : β-anomer = 33:66; (174)). In α-D-glucose and α-3MG, the hydroxyl-group at carbon 1 is axial and oriented below the glucopyranose ring, while for the β-anomers, the OH-group is equatorial. Could the orientation of this hydroxyl group affect transporter affinity or capacity for substrate? Epimers of D-glucose (analogs in which the position of the hydroxyl group at specific locations around the glucopyranose ring is reversed) show strikingly different affinities for the red cell sugar transporter. Studies with D-galactose (a C-4 epimer of D-glucose), D-allose (C-3) or D-mannose (C-2)) indicate that that opposite hydroxyl configurations cause a 12-, infinite or 3-fold (respectively) increase in K_{iapp} (relative to D-glucose) for inhibition of sorbose uptake by red cells (175). Where it has been studied (e.g. D-galactose), this 12-

fold reduction in affinity is without effect on V_{max} for sugar transport (176). It would not be surprising, therefore, if α- or β-3MG were preferentially transported by GLUT1.

The equilibrium ratio of β-3MG to α-3MG at 4 - 20°C is 66:33 which is very close to the relative sizes of fast and slow 3MG compartments observed in ATP-loaded red cell ghosts (see Table 2.1). The consequences on transport include: underestimation of $K_{m(app)}$ and V_{max} for net sugar uptake; overestimation of $K_{m(app)}$ for sugar exit; underestimation of $K_{m(app)}$ exit into saturating sugar solutions.

If biphasic sugar transport is explained by differential transport of α- and β-anomers, several predictions follow: 1) β-3MG is the preferred GLUT1 substrate in the presence of ATP (ratio of fast to slow transport rates = 19:1; see Table 2.1). In the absence of ATP both anomers are transported efficiently, 2) equilibrium compartment sizes in ATP-containing cells are proportional to equilibrium anomer distributions, 3) acceleration of mutarotation to a rate several-fold faster than the slow rate of transport eliminates the slow phase of transport, 4) slowing transport by use of inhibitors will inhibit both the fast and slow phases of transport because both phases are carrier-mediated.

Tests of the barrier hypotheses: The physical and chemical barrier hypotheses predict mutually exclusive outcomes for test 4 - the impact of partial transport inhibition on the kinetics of biphasic sugar transport. The physical barrier hypothesis predicts that only the rapid phase of transport is inhibited by transport inhibitors because the slow phase is a GLUT1-independent event (diffusion). The chemical barrier hypothesis predicts inhibition of both phases because each represents GLUT1-mediated transport of

substrate. Previous results have shown that maltose and cytochalasin B are capable of inhibiting both phases under zero-trans net uptake experiments (109). It is therefore concluded that the the physical barrier hypothesis is untenable.

Refining the anomer (chemical barrier) hypothesis: The rate constant for subsaturating 3MG exchange transport is proportional to $V_{max}/K_{m(app)}$ (99). Reduced transport of α-3MG could thus be explained by reduced V_{max}, increased $K_{m(app)}$ or by a combination of both effects. Figure 2.9 illustrates a simulated exchange uptake of α- and β-3MG in which the available experimental data is fit. β-3MG is transported more rapidly than α-3MG but the sum of both processes describes total cellular exchange uptake. Exchange transport is assumed to follow simple Michaelis-Menton kinetics and uptake of radio-trace 3MG is described by:

$$\text{uptake} = v_{\alpha}^{oi} + v_{\beta}^{oi} - v_{\alpha}^{io} - v_{\beta}^{io} \qquad \text{Eq. 2.2}$$

where

$$v_{\alpha}^{oi} = \frac{V_{\alpha}\alpha Q_o}{K_{\alpha}\left(1+\frac{S_o\alpha}{K_{\alpha}}+\frac{S_o\beta}{K_{\beta}}+\frac{Q_o\beta}{K_{\beta}}\right)+\alpha Q_o}$$

$$v_{\beta}^{oi} = \frac{V_{\beta}\beta Q_o}{K_{\beta}\left(1+\frac{S_o\beta}{K_{\beta}}+\frac{S_o\alpha}{K_{\alpha}}+\frac{Q_o\alpha}{K_{\alpha}}\right)+\beta Q_o}$$

$$v_{\alpha}^{io} = \frac{V_{\alpha}\alpha Q_i}{K_{\alpha}\left(1+\frac{S_i\alpha}{K_{\alpha}}+\frac{S_i\beta}{K_{\beta}}+\frac{Q_i\beta}{K_{\beta}}\right)+\alpha Q_i}$$

$$v_{\beta}^{io} = \frac{V_{\beta}\beta Q_i}{K_{\beta}\left(1+\frac{S_i\beta}{K_{\beta}}+\frac{S_i\alpha}{K_{\alpha}}+\frac{Q_i\alpha}{K_{\alpha}}\right)+\beta Q_i}$$

where v_{α}^{oi} and v_{β}^{oi} are unidirectional uptake of radiolabeled α- and β-3MG (Q), v_{α}^{io} and v_{β}^{io} are unidirectional exit of radiolabeled α- and β-3MG, V_β is V_{max} and $K\beta$ is K_m for exchange transport of β-3MG, V_α and K_α are V_{max} and K_m for α-3MG exchange, S_i and S_o are the intracellular and extracellular concentrations of total unlabeled 3MG, Q_i and Q_o are the intracellular and extracellular concentrations of total radiolabeled 3MG. α is the fraction of S or Q that exists as α-3MG, and β is the fraction of S or Q that exists as β-3MG. Total (radiolabeled α- and β-3MG) exchange uptake data at 2.5 mM 3MG and 10 μM ^{3}H-3MG were simulated by fourth-order Runge-Kutta numerical integration. V_{max} and $K_{m(app)}$ parameters for α- and β-3MG were varied by an interactive least-squares procedure until the deviation between observed and predicted uptake reach a minimum. The result suggests that β-3MG (V_{max} = 1.48 mmol min^{-1} L cell water^{-1} and $K_{m(app)}$ = 4.7 mM) is a more efficient substrate for exchange transport than α-3MG (V_{max} = 0.53 mmol min^{-1} L cell water^{-1} and $K_{m(app)}$ = 37.1 mM). Figure 2.9 also shows the observed kinetics of α-3MG mutarotation at 4°C as measured by circular dichroism. 3MG mutarotation is significantly slower than exchange uptake of α-3MG as required by the anomer (chemical-barrier) model for sugar transport. The complete 3MG exchange data set (Table 2.1) has been reanalyzed by this procedure and the results are summarized in Table 2.3. V_β, K_β, V_α, and K_α are independent of 3MG concentration and direction of

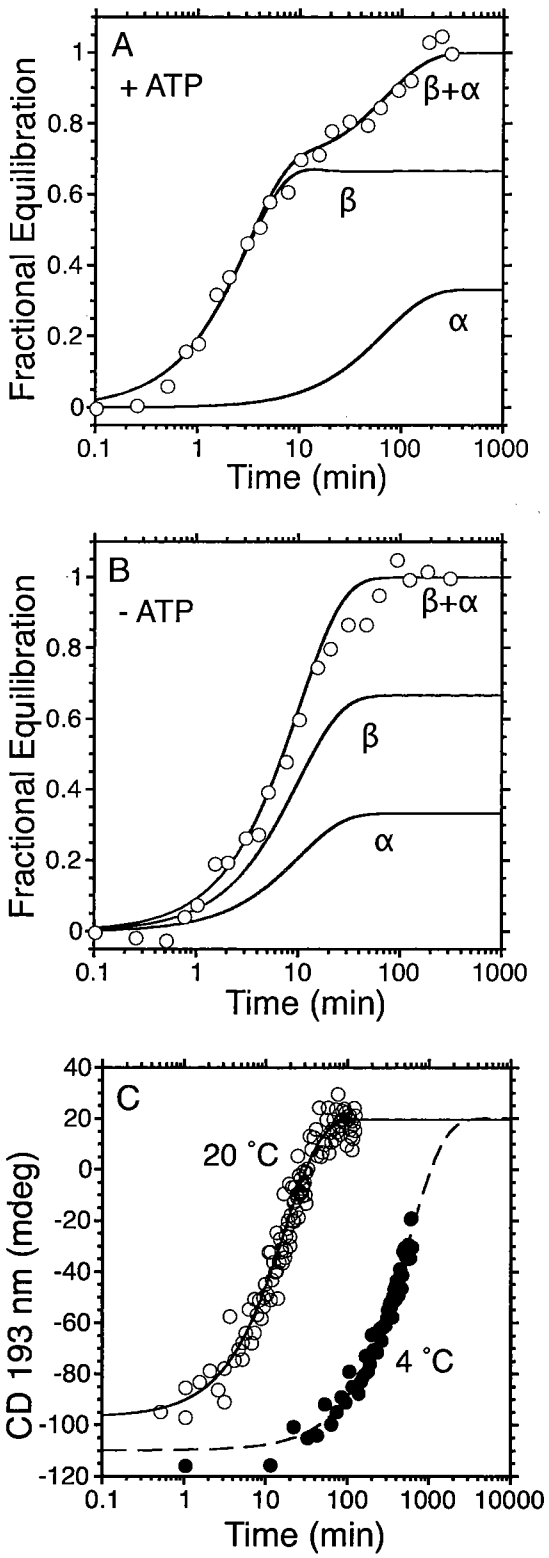
A
+ ATP
β+α
β
α
Fractional Equilibration
Time (min)
B
- ATP
β+α
β
α
Fractional Equilibration
Time (min)
C
20 °C
4 °C
CD 193 nm (mdeg)
Time (min)

Figure 2.9. Simulated Time Course of α- and β-3MG Equilibrium Exchange Transport.

A. Simulated time course of 2.5 mM 3MG exchange uptake in the presence of 4 mM ATP. Ordinate: fractional equilibration; abscissa: time in minutes (note log scale). Measured exchange uptake (○) is simulated using Eq. 2.2. β-3MG uptake (—) seen the presence of competing α-3MG uptake (—), and total 3MG (α- + β-3MG) (—) as the observable 3MG uptake and have the following paramaters; $K_{m(app)}$ = 37 mM and V_{max} = 0.53 mmol min^{-1} L cell $water^{-1}$ for α-3MG, and $K_{m(app)}$ = 4.7 mM and V_{max} = 1.48 mmol min^{-1} L cell $water^{-1}$ for β-3MG. **B.** Simulated time course of 2.5 mM 3MG exchange uptake in the absence ATP. Measured exchange uptake (○) is simulated using Eq. 2.2. β-3MG uptake (—) seen the presence of competing α-3MG uptake (—), and total 3MG (α- + β-3MG) (—) as the observable 3MG uptake and have the following paramaters; $K_{m(app)}$ = 35 mM and V_{max} = 3.35 mmol min^{-1} L cell $water^{-1}$ for both α-3MG and β-3MG. From this analysis, Eq. 2.2 and be reduced to Eq. 2.3. **C.** The time course of α-3MG anomerization at 20 °C (○) and at 4 °C (•). Ordinate: CD at 193 nm (mdeg); abscissa: time in minutes (note log scale) The curves drawn through the points are single exponentials computed by non-linear regression and are characterized by first order rate constants of 0.058 ± 0.002 min^{-1} and 0.0019 ± 0.0000 for 20 °C and 4 °C respectively.

Table 2.3. Kinetics of α- and β-3MG Transport

Parameter		Condition	
Exchange	Zero-trans inhibition	0 ATP	4 mM ATP
K_α			27.5 ± 2.44
K_β			3.74 ± 0.21
V_α			1.28 ± 0.11
V_β			3.20 ± 0.25
k_α			0.05 ± 0.00
k_β			0.86 ± 0.06
K		34.9 ± 1.62	
V		5.21 ± 0.31	
k		0.15 ± 0.01	
	K_α		5.29 ± 0.49
	K_β		0.77 ± 0.13

Values are means ± SEM. The time course of exchange uptake and exit at 0.1, 2.5, 10, and 20 mM 3MG analyzed according to Eq. 2.2 (+ATP) or Eq. 2.3 (-ATP) by an iterative least squares procedure to obtain K_α, K_β ($K_{m(app)}$ for α- and β-3MG), V_α, V_β (V_{max} for α- and β-3MG) for 4 mM ATP, and K and V (K_m and V_{max}) for 0 ATP. The first order rate constants, k_α, k_β, and k, are $V_{max}/K_{m(app)}$. 3MG inhibition of the initial rate of radiolabeled 3MG uptake by ATP-containing ghosts was measured by equilibrated (35:65) or initially dissolved (80:20) α:β 3MG solutions to obtain K_α and K_β ($K_{i(app)}$) for α- and β-3MG inhibition of zero-trans 3MG uptake.

radiotracer movement (uptake or exit). V_β is 2.5 fold greater than V_α and K_α is 7.4 fold greater than K_β. This shows that the major impact of reorientation of the anomeric hydroxyl group to the α-configuration is a sevenfold loss in affinity for sugar binding.

In the absence of intracellular ATP, radiolabeled 3MG exchange transport is consistent with a single transport process described by:

$$\text{uptake} = v^{oi} - v^{io} \qquad \text{Eq. 2.3}$$

where

$$v^{oi} = \frac{VQ_o}{K\left(1+\frac{S_o}{K}\right)+Q_o} \qquad v^{io} = \frac{VQ_i}{K\left(1+\frac{S_i}{K}\right)+Q_i}$$

where V and K are V_{max} and $K_{m(app)}$ for 3MG exchange transport. Analysis of exchange transport in the absence of ATP (Table 2.3) indicates that $K_{m(app)}$ and V_{max} are 35 mM and 5.2 mmol min^{-1} L cell $water^{-1}$ respectively. This indicates that ATP depletion results in the loss of high affinity β-3MG binding. The ATP-GLUT1 interaction is therefore a primary determinant of high-affinity β-3MG exchange transport.

Few previous studies have examined the transport of α- and β-D-glucose in red cells (177-179). Unlike liver which contains significant mutarotase activity (180), the human red cell and red cell ghosts are devoid of mutarotase (178). Even so, 3MG is not a substrate for porcine kidney mutarotase *in vitro* and not expected to be a substrate for human mutarotase and 4 mM ATP is without effect on mutarotase accelerated anomerization of D-glucose (*vide infra*). The observation of high-affinity β-3MG exchange in the

presence of ATP is therefore not explained by a mutarotase inhibition by ATP. For a discussion on the affect of mutarotase on exchange transport, please see Chapter 3.

When freshly dissolved, α- and β-D-glucose are relatively equipotent in their inhibition of the the initial rate of radiolabeled D-glucose uptake from an equilibrium mixture of ^{14}C-α-D-glucose and ^{14}C-ß-D-glucose (178). This suggests that differences in rate constants for transport of α- and β-anomers reflect differential capacity for transport rather than differences in binding affinity. This is reexamined for zero-trans ^{14}C-3MG uptake in red cell ghosts containing or lacking 4 mM ATP. Proton NMR of freshly dissolved, unlabeled α-3MG and of an equilibrium solution of 3MG indicates that "α-3MG" is in fact 80% α-anomer and 20% β-anomer. The equilibrium solution contains a 35:65 ratio of α:β anomers of 3MG. These sugars were used as inhibitors of ^{14}C-3MG at 4 °C. ^{14}C-3MG is, of course, an equilibrium mixture of ^{14}C-α- and ^{14}C-β-3MG. Uptake was measured at 100 μM ^{14}C-3MG with increasing amounts of unlabeled 3MG (0 to 10 mM). Figure 2.10 shows that "α-3MG" and equilibrium 3MG inhibit unidirectional ^{14}C-3MG uptake half-maximally at 1-2 mM. For the analysis, the mechanism is assumed to be a fixed-site carrier capable of the simultaneous uptake of two substrate molecules, the binding of one inhibitor and one substrate, or the binding of two inhibitor molecules and follows the form:

$$v = \frac{\frac{[S]}{K_m}V + 2\frac{[S]^2}{\theta K_m^{\,2}}V + 2\frac{[S][I]}{\theta K_m K_I}V}{1 + \frac{[S]}{K_m} + \frac{[S]^2}{\theta K_m^{\,2}} + \frac{[S][I]}{\theta K_m K_I} + \frac{[I]}{K_I} + \frac{[I]^2}{\theta K_I^{\,2}}} \qquad \text{Eq. 2.4}$$

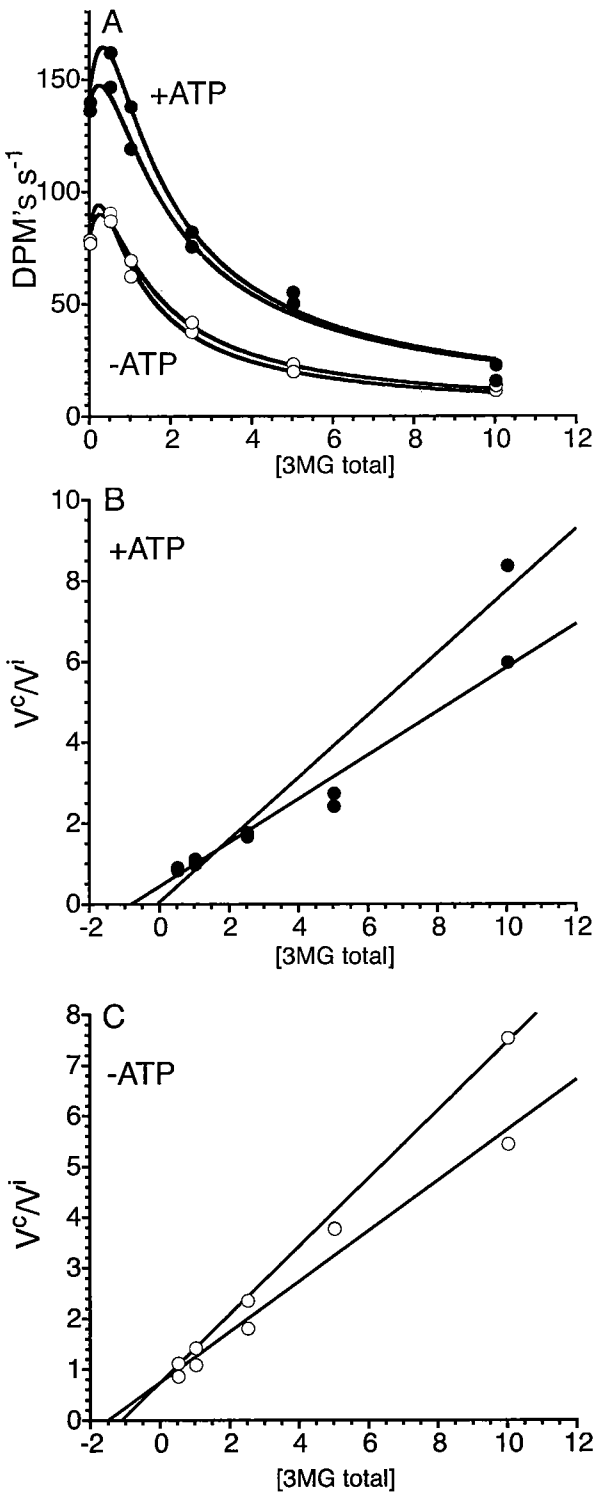
A
+ATP
-ATP
DPM's s-1
150
100
50
0
0
2
4
6
8
10
12
[3MG total]
B
+ATP
Vc/Vi
10
8
6
4
2
0
-2
0
2
4
6
8
10
12
[3MG total]
C
-ATP
Vc/Vi
8
7
6
5
4
3
2
1
0
-2
0
2
4
6
8
10
12
[3MG total]

Figure 2.10. Inhibition of Initial Rates of Net-uptake by 66:33 β:α-3MG and 20:80 β:α-3MG.

A. Inhibition of the initial rate of 100 μM ^{14}C-3MG net uptake by an equilibrated 3MG solution (66:33 β:α) in the presence (•) and absence of ATP (○) or a freshly dissolved 3MG solution (20:80 β:α) in the presence (•) and absence of ATP (○). Curves drawn through points are computed by non-linear regression to Eq. 2.4. For all conditions, the $K_{I(app)}$ is 1 mM. **B.** Transformation of + ATP data from A by plotting the ratio of the un-inhibited rate to the inhibited rate versus inhibitor concentration. **C.** Transformation of - ATP data from A by plotting the ratio of the uninhibited rate to the inhibited rate versus inhibitor concentration.

where v is the observed rate, [S] is the concentration of radiolabel, [I] is the concentration of total cold 3MG, V is the Michalis-Menten V_{max} and K_m is the Michalis-Menten constant for uptake of radiolabel, K_I is the inhibition constant, and θ is the coopertivity factor. This allows for the stimulation of radiolabel uptake seen at low concentrations of inhibitor and the inhibition of uptake at higher concentrations. This confirms our earlier findings with α- and β-D-glucose (178) and suggests only small differences in the affinity of GLUT1 for α- and β-3MG.

However, an alternative analysis of the data give contrasting results. The data in Figure 2.10 fall on a line when expressed as the ratio of the observed rate in the absence of unlabeled 3MG to the rate in the presence of unlabeled 3MG vs. the concentration of unlabeled 3MG. The slope of the inhibition data employing equilibrium 3MG is significantly greater than the slope of the α-3MG inhibition data. With this type of analysis, the slope is given by:

$$\frac{\beta}{K_\beta} + \frac{\alpha}{K_\alpha} \qquad \text{Eq. 2.5}$$

where α and β are the fractional amounts of α- and β-3MG present in the uptake medium and K_α and K_β are $K_{m(app)}$ for uptake of α- and β-3MG respectively. Using the measured slopes and the known ratios of α:β anomers present in solution, K_α and K_β are calculated as 3.97 ± 0.67 and 1.05 ± 0.02 mM respectively (Table 2.3). These parameters are unchanged by intracellular ATP. Recognizing that $K_{m(app)}$ for zero-trans sugar transport is typically much lower than $K_{m(app)}$ for exchange transport but that the

exchange:zero-trans $K_{m(app)}$ ratio is preserved for different substrates (e.g. compare D-glucose and D-galactose; (181)).

Physiological significance: A preference for α-D-glucose in transport and/or metabolism has been reported for liver (180, 182, 183), pancreatic beta cells (184-188), muscle (189) adipose (190) and yeast cells (191). Cardiac muscle hexokinase displays high affinity but low capacity for α-D-glucose and low affinity but high capacity for β-D-glucose (192). Brain, retina, erythrocytes and lens cells appear to prefer β-D-glucose or show no preference (177, 178, 183, 193-196). β-D-Glucose is more potent than α-D-Glucose in inhibiting vagally-mediated secretion of gastric acid (197). These observations illustrate the physiological significance of differential transport and utilization of glucose anomers and suggest that cells expressing GLUT1 or GLUT3 may prefer the β-anomer while cells expressing GLUT2 or GLUT4 may prefer the α-anomer.

Significance to previous transport studies: How might these findings affect interpretation of red cell glucose transport determinations? Transport measurements are normally obtained by initial rate analysis over intervals of 1 minute or less. If initial rates of transport are derived largely from uptake of β-sugar, they are related to (and must be corrected for) the amount of β-sugar present in solution during the measurement. Thus $K_{m(app)}$ may be overestimated by 1.5-fold. Furthermore, computed rates and K_{mapp} must be corrected for competitive inhibition by the omnipresent, lower affinity α-sugar. This result could also explain (see (198) and (199) for detailed expositions) how integrated rate

equation analysis of time course data results in overestimation of K_{mapp} for transport because all time courses are artificially extended owing to slower transport of α-sugar.

Conclusion

ATP-containing human red blood cell ghosts exhibit biphasic equilibrium exchange 3MG transport at sugar concentrations ranging from 1 to 20 mM. This observation is inconsistent with previous models for ATP-modulation of GLUT1 activity. A new hypothesis proposes that ATP-GLUT1 interactions promote preferential transport of β-3MG and that extended time courses of sugar transport in human red cells reveal deviations from simple kinetics owing to low capacity α-3MG transport and continuous ß-3MG and α-3MG mutarotation. In the absence of ATP, both anomers may be transported equally well or differences in the kinetics of ß-3MG and α-3MG become too small to measure with existing methodologies. Differential transport of 3MG anomers (and thus transport complexity) is only observable in cells where rate constants for 3MG transport are greater than those for 3MG mutarotation.

Chapter III

PREFERENTIAL TRANSPORT OF α- AND β-SUGAR ANOMERS DOES NOT EXPLAIN GLUT1 MEDIATED ATP INDUCED BIPHASIC SUGAR EXCHANGE

Abstract:

Sugar uptake in human erythrocytes displays biphasic kinetics. Import is consistent with the rapid filling of a large cytoplasmic component followed by the slower filling of a smaller component. This behavior has been attributed to the preferential transport of β-sugar by GLUT1. The present study examines several predictions of the anomer transport hypothesis and reports significant disagreement between expected and observed behavior. The sizes of the fast and slow phases of transport do not correspond to the equilibrium anomer distributions of other GLUT1 sugar substrates. Increasing the rate of anomerization by addition of intracellular mutarotase has no effect on biphasic transport kinetics. Direct measurement of initial rates of sugar uptake or exchange demonstrates that GLUT1 shows no anomer preference. These findings refute the hypothesis proposed in Chapter II that biphasic erythrocyte transport results from differential transport of sugar anomers.

Introduction:

Human cellular membrane D-glucose transport is mediated by a family of integral membrane proteins called D-glucose transporters. GLUT1 was the first member of this family to be isolated and cloned and is found primarily in the cardiovascular system and where it is especially concentrated in erythrocytes (200). Possibly because transport in human erythrocytes has been so extensively studied, it has been observed that steady state red cell D-glucose transport is inconsistent with available carrier models (7, 76, 80, 106). Rat, rabbit and avian erythrocytes are characterized by a much lower D-glucose transport content (100, 107) and sugar transport in these cells is consistent with the carrier models proposed by Stein and Lieb (201). Further investigation of GLUT1 mediated sugar transport in human erythrocytes has demonstrated that ATP directly modulates D-glucose transport (121, 124, 135, 202). The mechanism of ATP regulation of GLUT1 is not well understood. A previous hypothesis formulated that ATP binding induces a conformational change in the carrier causing sugar occlusion or binding within cytoplasmic GLUT1 domains (109, 112). Chapter 2 has shown that equilibrium exchange transport data collected at sugar concentrations of 20 mM is incompatible with this hypothesis and we have therefore proposed that ATP binding converts GLUT1 from a carrier with no specific preference for sugar anomers into a carrier that has a reduced K_m and increased V_{max} for β-D-glucose transport and an increased K_m and reduced V_{max} for α-D-glucose transport (Fig-

ure 2.8). Anomerization is slowed by D_2O and acidic pH (182, 203) - agents also known to modify steady-state sugar transport kinetics (110) (126) (204).

GLUT1 anomeric specificity has been previously studied, but with inconsistent conclusions. D-glucose metabolism in human erythrocytes displays a preference for β-D-glucose at physiological sugar concentrations (205, 206), but at subsaturating concentrations α-D-glucose utilization is more rapid (207). However, D-glucose transport is not rate limiting for metabolism in human erythrocytes and specificity in anomer metabolism does not translate into specificity in anomer transport and may in fact represent the specificity of hexokinase (183). In rat erythrocytes where transport capacity is 100 fold less, both α-D-glucose (206) and β-D-glucose (208) have been suggested to be the preferred glycolytic substrate.

Faust first examined differential transport of α- and β-D-glucose in the red cell and found that β-D-glucose penetrates nearly three times faster than α-D-glucose (177). Naftalin and Holman interpreted this result to indicate that β-D-glucose binds with higher affinity than the α-anomer (97). Carruthers and Melchior later looked at human GLUT1 infinite-cis entry in erythrocytes for both α- and β-D-glucose and found no difference in the rate of uptake (178). Examination of the ability of α- or β-D-glucose competition with radiolabeled sugar for zero-trans uptake demostrates identical $K_{i(app)}$ for α- or β-D-glucose. It now appears that this assay is not the most discriminating test for anomeric specificity (*vide supra*). Miwa et. al. repeated the infinite-cis uptake experiment and saw

that β-D-glucose is imported 1.5 times faster than α-D-glucose (179). Kuchel et. al. examined equilibrium exchange exit of D-1-^{13}C-D-glucose and observed that α- is exported nearly twice as fast as β-D-glucose (209). Potts and Kuchel studied the exchange of 3-deoxy-3-fluoro-D-glucose (3FDG) using a spin transfer technique and found that exchange of the β-anomer was significantly faster than α-D-glucose exchange (210). However, a second study using a slightly different technique demonstrated that α-3FDG transport is characterized by a lower Km(app) than β-3FDG and consequently displays a higher flux (211). Others have repeated 3FDG exchange as well as 2-,4-, and 6-deoxy-6-fluoro-D-glucose transport measurements and have found that the α-anomer has a higher permeability than the β-anomer (212). Unfortunately, the anomeric preference for 1-position fluoroanalogs is unknown as only β-1-deoxy-1-fluoroglucose is transported (213). However, $K_{i(app)}$ for the β-isomer is 15 mM whereas the $K_{i(app)}$ for the α-isomer is much higher at 78 mM (175). Appleman and Lienhard examined the ability of both D-glucose anomers to accelerate the interconversion GLUT1 between the external binding conformation and the internal binding conformation and found that α-D-glucose was 37% more effective as measured by exofacial and endofacial inhibitor binding kinetics (214). Janoshazi and Solomon looked at GLUT1 tryptophan quenching by α- and β-D-glucose and while the initial binding was too fast to measure, it appears that subsequent GLUT1 conformational changes have different activation energies for the two sugar anomoers; specifically β-D-glucose is favored at higher temperatures while α-D-glucose

is preferred at lower temperatures (215). The literature therefore presents multiple demonstrations of anomeric specificity in human red cell sugar transport, but there is little consensus as to the preferred substrate. It is therefore necessary to test the anomer hypothesis by multiple independent methods. The results of the present study demonstrate that GLUT1 displays no anomeric specificity and differential transport of sugar anomers does not account for biphasic exchange kinetics.

Materials and Methods:

Materials: ^{3}H-3-O-methylglucose was purchased from Sigma Chemicals. Human blood was purchased from Biological Specialties Cooperation. Procine Kidney Mutarotase was purchased from Calzyme Laboratories Inc. Other reagents were purchased from Sigma Chemicals.

Solutions: Kaline consisted of 150 mM KCl, 5 mM MgCl, 5 mM EGTA, 5mM HEPES, pH 7.4. Lysis buffer contained 10 mM Tris-HCl, 2mM EDTA, pH 8.0. Sugar-stop solution consisted of ice-cold Kaline containing 20 μM CCB and 200 μM phloretin.

Red Cells: Red cells were isolated by washing whole human blood in 4 or more volumes of ice-cold Kaline and centrifuging at 10,000 x g for 15 minutes at 4 °C. Serum and buffy coat were removed by aspiration and the wash, centrifugation, aspiration cycle repeated until the buffy coat was no longer visible. Cells were resuspended in 4 volumes of sugar free or sugar containing Kaline and incubated for 1 hour at 37 °C to deplete or load intracellular sugar.

Red Cell Ghosts: Ghosts were hypotonically lysed by re-suspending washed red cells in 10 volumes of ice-cold lysis buffer for 10 minutes. Membranes were harvested by centrifugation at 27,000 x g for 20 minutes. Ghosts were repeatedly washed with lysis buffer and centrifuged until the membranes appeared light pink (about 3 cycles). Ghosts were then washed with 10 volumes ice-cold Kaline and collected by centrifugation at 27,000 x g. Harvested membranes were resealed by incubation in 4 volumes of Kaline ± 4 mM ATP (37 °C) for 1 hour and collected by centrifugation at 27,000 x g for 15 minutes at 4 °C. Resealed ghosts were stored on ice until used.

Net sugar uptake: Sugar-depleted cells or ghosts were incubated in 20 volumes of ice-cold Kaline containing 100 μM unlabeled sugar and 0.5 μCi/mL labeled sugar. Uptake was allowed to proceed for intervals as short as 6 seconds to intervals as long as 3 hours. Uptake was arrested by addition of ice-cold stop buffer and ghosts were centrifuged at 14,000 x g for 1 minute. The supernatant was removed by aspiration and ghosts were washed with 20 volumes of sugar stop buffer, re-centrifuged and supernatant aspirated. The ghost pellet was extracted with 500 μL of 3% perchloric acid, centrifuged, and samples of the clear supernatant were counted in duplicate. Zero time points were collected by the addition of sugar stop solution to ghosts followed by uptake media. Samples were then immediately processed. Radioactivity associated with cells at zero time was subtracted from all non-zero time points. Equilibrium time points were collected using an overnight incubation. All time points were normalized to the equilibrium time point. All

solutions and tubes used in the assay were pre-incubated on ice for 30 minutes prior to the start of the experiment. Triplicate samples were processed for each time point.

Sugar equilibrium exchange uptake: Ghosts were resealed in the presence of 1 mM unlabeled sugar(s), centrifuged, and the supernatant was aspirated. Ghosts were then incubated in 20 volumes of ice-cold Kaline containing the same concentration of unlabeled sugar(s) and 0.5 μCi/mL label(s). Exchange was allowed to proceed for time intervals as short as 6 seconds to intervals as long as 10 hours. Exchange was then stopped by the addition of ice-cold sugar stop and ghosts were treated as above with zero-trans uptake.

Proton NMR: Data were collected at 24 °C on a 400 MHz Oxford NMR.

Sugar anomerization rates: Anomerization was measured by optical rotation with a Rudolph Autopol II. Briefly, 10 or 100 mM initially dissolved sugar in temperature equilibrated Kaline ± 4 mM ATP was placed into a 10 mL, 10 cm path-length thermojacketed cell and optical rotation was measured over time. For mutarotase experiments, an appropriate amount of 1000 U/mL mutarotase in Kaline was placed into the thermojacketed cell and allowed to equilibrate prior to the addition of freshly dissolved 10 mM D-glucose in Kaline.

HPLC analysis of sugar anomers: Sugar anomers were chromagraphically separated on a Bio-Rad HPX-87C column as previously described (216). The column was equilibrated on ice with diH_2O as the mobile phase. Unlabeled sugars were detected by

using a Waters Model 410 Differential Refractometer and radioactively labeled sugars by a Packard 505TR Flow Scintillation Analyzer.

HPLC analysis of red cell nucleotides: The cytosolic nucleotides of 50 μL of packed red cells were extracted with 50 μL of 3% PCA and precipitated lipids and protein removed by centrifugation. The acidic supernatant was neutralized by addition of a sodium bicarbonate solution and filtered through a 0.45 μm spin filter. The filtered solution was then injected onto a Higgins Analytical C18 column with a mobile phase of 15 mM ammonium acetate, pH 6.0 and linear gradient of 0 to 10% methanol and a flow rate of 1 ml/min. Nucleotides were detected by a Walters 484 Tunable Absorbance Detector set at 260 nm.

Results

Inhibition of 3MG exchange by α- and β-methyl-D-glucosides: Methyl-D-glucosides are not transportable substrates for GLUT1 and seem to bind only at the GLUT1 cytosolic binding site. The anomeric barrier hypothesis for ATP regulation of GLUT1 suggests that β-sugars are the preferred substrate for the ATP-bound GLUT1 complex. If this is the case, then β-methyl-D-glucoside should be a more potent inhibitor of GLUT1 mediated transport than the α-epimer. Figure 3.1 shows the dose response for methylglycoside inhibition of 2.5 mM 3MG exchange transport initial rates. While both α- and β-methyl-D-glucoside inhibit transport by 50%, $K_{i(app)}$'s for inhibition are not as expected. The α-epimer is the more potent inhibitor with a $K_{i(app)}$ of 0.6 mM and 12 mM

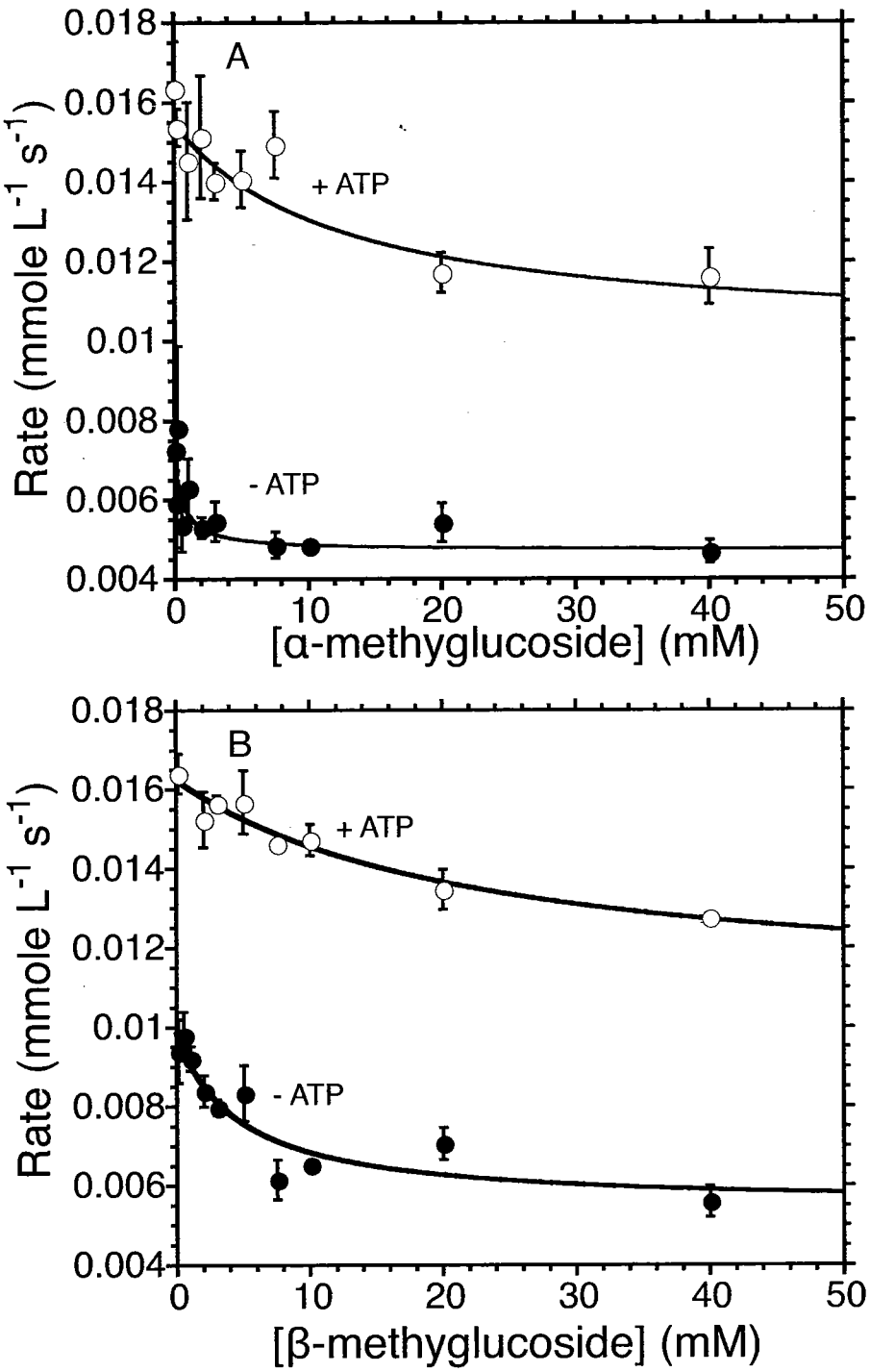
A
+ ATP
- ATP
Rate (mmole L-1 s-1)
[α-methyglucoside] (mM)
B
+ ATP
- ATP
Rate (mmole L-1 s-1)
[β-methyglucoside] (mM)
0.018
0.016
0.014
0.012
0.01
0.008
0.006
0.004
0
10
20
30
40
50

Figure 3.1. Inhibition of Initial Rates of Transport by Methyl-D-glucosides.

Ordinate: initial rate of transport in mmole L cell water^{-1} s^{-1}; Abscissa: intracellular inhibitor concentration. **A.** Inhibition of 2.5 mM 3MG exchange uptake in the presence of increasing concentration of α-methyl-D-glucoside with (○) and without (●) intracellular ATP. Curves drawn through points are computed by non-linear regression to the form $V_{i=0}$ - (V_{imax}* [I] / (K_i+ [I]) where $V_{i=0}$ is the rate in the absence of inhibitor, V_{imax} is the rate maximally inhibited, [I] is the concentration of inhibitor, and K_i is the apparent inhibition constant. $V_{i=0}$ = 0.007 mmole L^{-1} s^{-1}, V_{imax} = 0.002 mmole L^{-1} s^{-1}, and K_i = 0.6 mM in the absence of ATP and $V_{i=0}$ = 0.015 mmole L^{-1} s^{-1}, V_{imax} = 0.005 mmole L^{-1} s^{-1}, and K_i = 12 mM in the presence of ATP. **B.** Inhibition of 2.5 mM 3MG exchange uptake in the presence of increasing concentration of β-methyl-D-glucoside with (○) and without (●) intracellular ATP. Curves drawn through points are computed by non-linear regression to the form $V_{i=0}$ - (V_{imax}* [I] / (K_i+ [I]). $V_{i=0}$ = 0.009 mmole L^{-1} s^{-1}, V_{imax} = 0.004 mmole L^{-1} s^{-1}, and K_i = 4.6 mM in the absence of ATP and $V_{i=0}$ = 0.016 mmole L^{-1} s^{-1}, V_{imax} = 0.005 mmole L^{-1} s^{-1}, and K_i = 23 mM in the presence of ATP.

in the absence and presence of ATP respectively. While $K_{i(app)}$'s for β-methyl-D-glucoside are greater at 4.6 mM and 24 mM in the absence and presence of ATP respectively.

Exchange transport remains biphasic in the presence of GLUT1 inhibitors: Human red cell exchange sugar transport is biphasic in the presence of cytosolic ATP, displaying rapid equilibration of 66% of cell water and 20-fold slower equilibration of the remaining space. There is a simple test to distinguish between two explanations for biphasic sugar transport (*vide supra*). If biphasic sugar exchange reflects fast and slow transport of β- and α-D-glucose, specific GLUT1 inhibition should inhibit both fast and slow phases of transport. If biphasic transport reflects fast transport followed by a slower intracellular event, GLUT1 inhibitors should slow only the fast phase. Figure 3.2 shows and Table 3.1 summarizes the results of 3-O-methyl-D-glucose (3MG) exchange in the absence and presence of GLUT1 inhibitors and osmotic controls. Transport remains biphasic, but the effect of GLUT1 inhibition on both phases is less clear. Cytochalasin B (CCB) at a concentration of 10 μM effectively inhibits both fast and slow phases (three to five fold), however it appears that 100 μM phloretin inhibits only the fast phase (five fold) and not the slow phase. 3MG exchange exit is also biphasic with both phases inhibited by 10 μM CCB (not shown).

The effect of extracellular maltose is not as clear. At concentrations required for effective inhibition of exchange transport (100 mM) significant cell lysis occurs. This is corrected by resealing ghosts in the presence of a small amount of ^{14}C-sucrose and measuring the ratio of ^{3}H-sugar to ^{14}C-sucrose thereby subtracting the loss of signal due to ly-

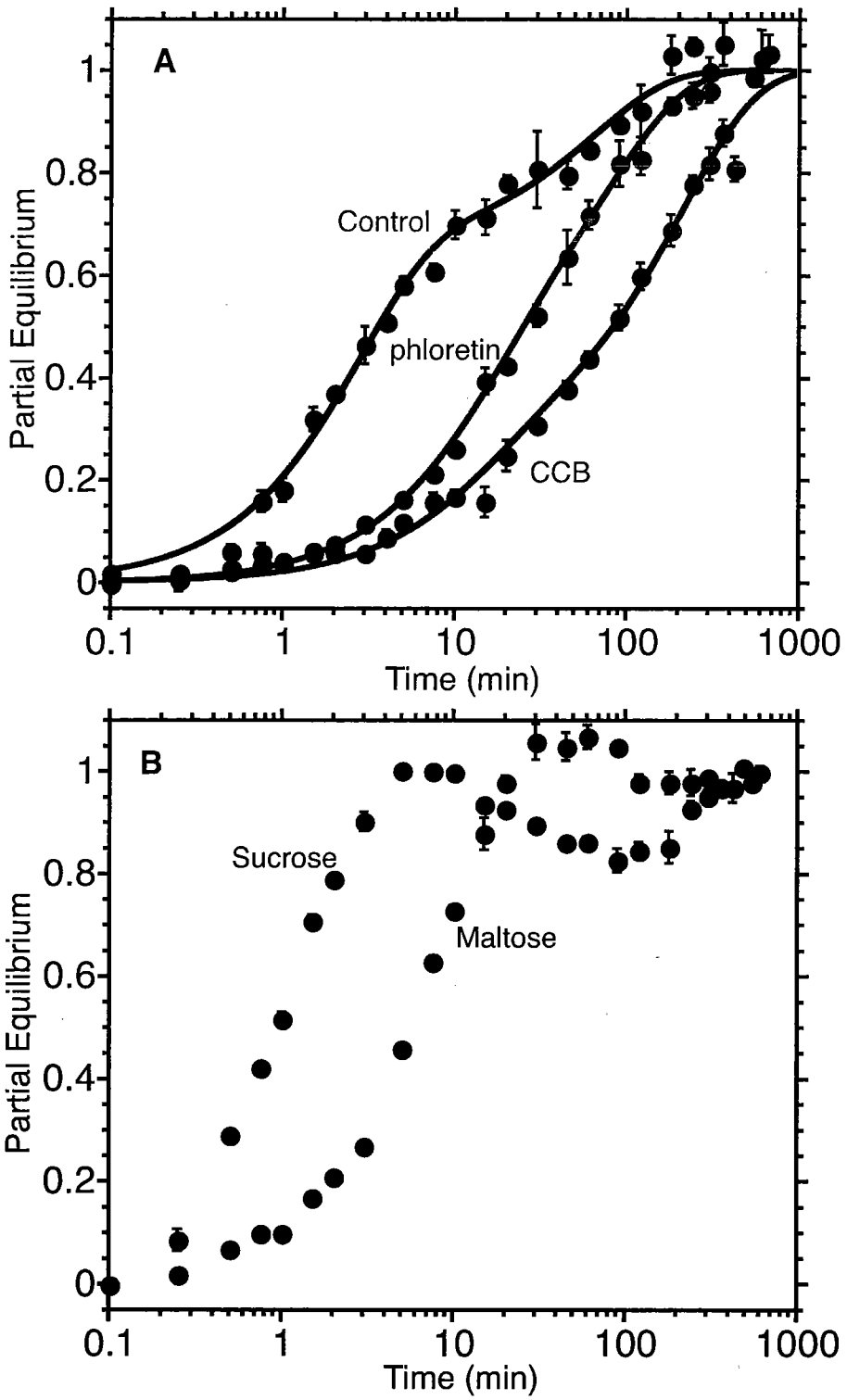
A
Control
phloretin
CCB
Partial Equilibrium
Time (min)
B
Sucrose
Maltose
Partial Equilibrium
Time (min)

Figure 3.2. Inhibition of 3MG Equilibrium Exchange Transport.

Ordinate: fractional equilibration; Abscissa: time in minutes (note log scale). **A.** Inhibition of 2.5 mM 3MG exchange in ghosts resealed with 4 mM ATP by intra- and extracellular inhibitors. Uninhibited (•) exchange is biphasic consistent with the filling of two compartments (physical or chemical). In the presence of 10 μM cytochalasin B (•), an intracellular binding inhibitor, transport remains biphasic and both phases of transport are inhibited nearly equally. Transport in the presence of 100 μM phloretin (•), an extracellular binding inhibitor, is biphasic however only the fast phase is inhibited. Curves drawn through the points were computed by nonlinear regression to assume the biexponential form: $A(1-e^{-k_1 t})+(1-A)(1-e^{-k_2 t})$ where k_1 and k_2 are the observed rate constants for phase 1 and 2 respectively and A is the fractional component of total uptake described by phase 1. Fit constants are shown in Table 3.1. **B.** Inhibition of 2.5 mM 3MG exchange in ghosts resealed with 4 mM ATP by extracellular maltose. 100 mM extracellular maltose (•) or sucrose (•) cause cell shrinkage and increase the initial intracellular 3MG concentration in validating the exchange condition. However, it appears extracellular maltose only inhibits the fast phase of transport as the two conditions reach equilibrium at nearly the same time.

Table 3.1. Effect of Inhibition on the Observed Rate Constants and Components for ATP Regulated 2.5 mM Equilibrium Exchange

Inhibitor	Fast k_{obs}[a]	Slow k_{obs}[a]	Fast Component Size[b]
--	0.36 ± 0.03	0.015 ± 0.003	66 ± 4
10 μM cytochalisn B	0.071 ± 0.018 (5.1)[c]	0.0047 ± 0.0004 (3.2)	26 ± 4
100 μM phloretin	0.075 ± 0.014 (4.8)	0.012 ± 0.001 (1.25)	40 ± 7

[a]All rate constants are first order and have units of min^{-1} and are shown as mean ± SEM.

[b]Fast component size represents the size (fraction of total 3MG accessible space) of the exchange transport component described by the fast rate constant and is shown as mean ± SEM. The size of the component described by the slow rate constant is 1 - fast fractional size.

[c]Numbers in () are the fold inhibition for each phase seen over control.

sis. While lysis can be corrected, the high extracellular osmolarity causes the ghosts to shrink. Shrinkage decreases intracellular volume thereby increasing the intracellular sugar concentration invalidating the equilibrium exchange transport condition and transport follows a counterflow time course (*vide infra*). The time course was repeated in the presence of 100 mM sucrose as an osmotic control. When maltose is compared to the sucrose control, it appears that only the first phase of transport is inhibited which is consistent with the other e2 inhibitor, phloretin .

Compartment sizes do not correlate with equilibrium anomer distributions: Exchange transport was examined in the presence and absence of ATP for several sugars, 3MG, D-glucose, 2-deoxy-D-glucose (2DG), and D-mannose. D-glucose and 3MG both have anomeric distributions of ~66% β- and 33% α. The two position seems important in determining the anomeric distribution as 2DG (missing the two position hydroxyl) is nearly equally populated as β- and α- (55% and 45% respectively) and D-mannose (the two position epimer of D-glucose) is 33% β- and 66% α. Equilibrium anomer distributions were measured by both proton NMR and by HPLC and give similar results. ATP induced biphasic transport for all tested sugar substrates, but the size of the fast compartment did not correlate with the %β- for each sugar (Table 3.2). The fast component size remained at ~67% of total transport for all substrates which is higher than expected for both 2DG and D-mannose but consistent with D-glucose and 3MG. Variation in component sizes between experiments necessitates simultaneous measurement of exchange of different sugars within the same ghosts. Figure 3.3 shows simultaneous exchange uptake

Table 3.2. Hexose Anomeric Proportions and Transport Compartmentalization

	Method for Determining Anomeric Proportions				
	Proton NMR		HPLC		
Sugar	% β[b] at equilibrium	% β[c] initially	% β[b] at equilibrium	% β[c] initially	Fast Transport Component[a]
D-glucose	66.8	13.0	64	--	74 ± 7
^{3}H-glucose[d]	--	--	69	--	
3MG	67.4	22.5	58[e], 63[f]	17	67 ± 11
^{3}H-3MG[d]	--	--	55	--	
2DG	54.6	75.0	57[g]	--	71 ± 10
D-mannose	36.7	12.3	32[g]	--	54 ± 5
Average	--	--	--	--	67

[a]Fast transport component represents the percentage (fraction of total 3MG accessible space) of the exchange transport component described by the fast rate constant and is shown as mean ± SEM. The size of the component described by the slow rate constant is 100 - fast fractional size. [b]% β seen after allowing dissolved sample to rest at room temperature for at least 48 hours. [c]% β seen after initially dissolved sample and allowing no more than 5 minutes to elapse on ice. [d]Radiolabeled substrates are only amenable to the HPLC analysis due to low concentration and are only available at anomeric equilibrium. [e]At 100 mM. [f]At 200 μM. [g]2DG and D-mannose are not baseline resolved with the HPLC method and numbers are calculated based on overlapping gaussian peak areas.

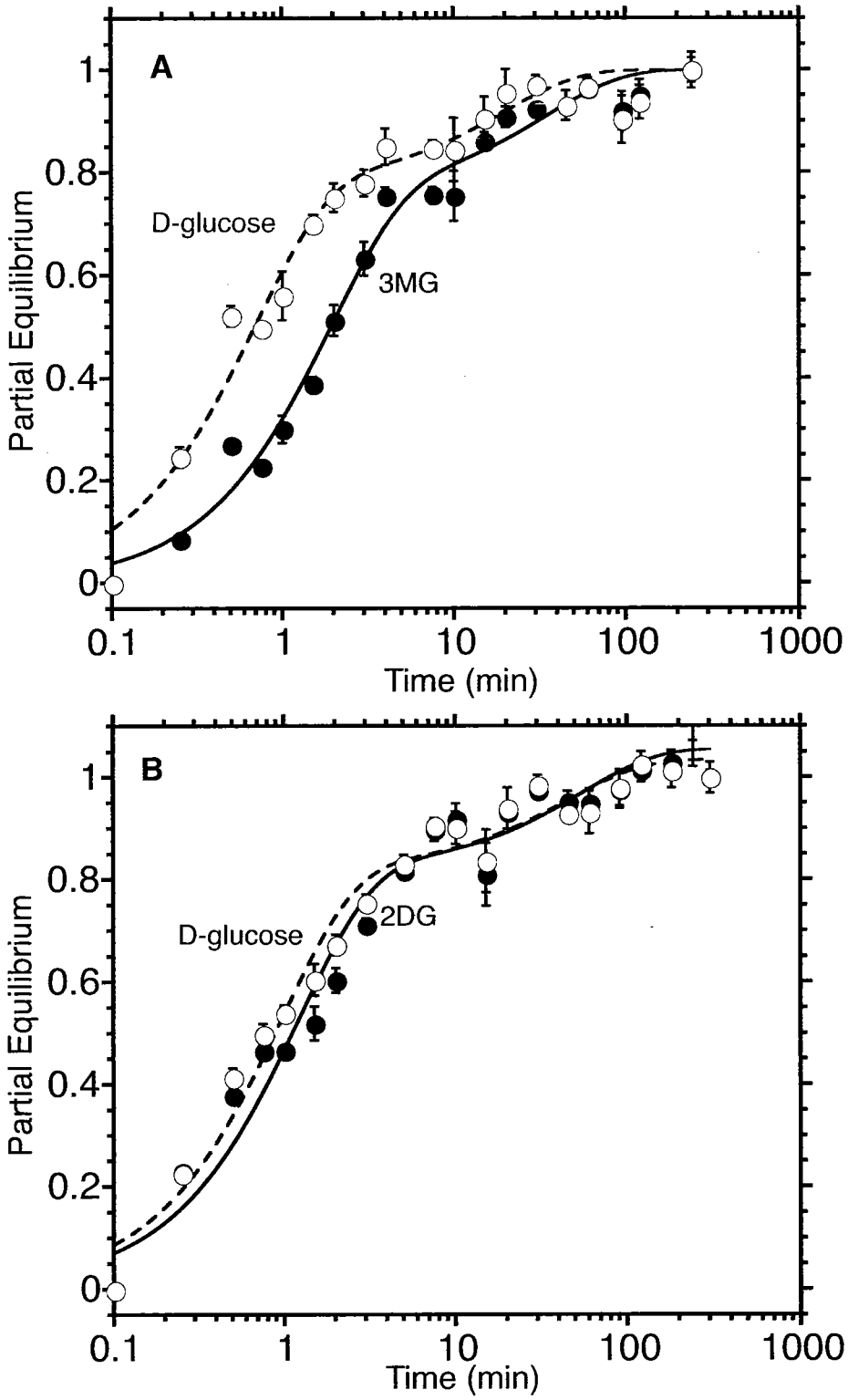
A
D-glucose
3MG
Partial Equilibrium
Time (min)
B
D-glucose
2DG
Partial Equilibrium
Time (min)

Figure 3.3. Simultaneous Exchange Transport of Multiple Sugar Substrates.

Ordinate: fractional equilibration; Abscissa: time in minutes (note log scale). **A.** Simultaneous exchange of 2.5 mM 3MG (•) and 2.5 mM D-glucose (○) in red cell ghosts containing 4 mM intracellular ATP. Curves drawn through the points were computed by nonlinear regression to assume the biexponential form: $A(1-e^{-k_1 t})+(1-A)(1-e^{-k_2 t})$ where k_1 and k_2 are the observed rate constants for phase 1 and 2 respectively and A is the fractional component of total uptake described by phase 1. For 3MG, $k_1 = 0.53 \pm 0.06$ min^{-1}, $k_2 = 0.03 \pm 0.01$ min^{-1}, and $A = 0.76 \pm 0.05$ and for D-glucose, $k_1 = 1.45 \pm 0.2$ min^{-1}, $k_2 = 0.05 \pm 0.02$ min^{-1}, and $A = 0.78 \pm 0.05$. **B.** Simultaneous exchange of 2.5 mM 2DG (•) and 2.5 mM D-glucose (○) in red cell ghosts containing 4 mM intracellular ATP. Curves drawn through the points were computed by nonlinear regression to assume the biexponential form: $A(1-e^{-k_1 t})+(1-A)(1-e^{-k_2 t})$ where k_1 and k_2 are the observed rate constants for phase 1 and 2 respectively and A is the fractional component of total uptake described by phase 1. For 2DG, $k_1 = 0.75 \pm 0.1$ min^{-1}, $k_2 = 0.04 \pm 0.03$ min^{-1}, and $A = 0.73 \pm 0.07$ and for D-glucose, $k_1 = 0.93 \pm 0.1$ min^{-1}, $k_2 = 0.04 \pm 0.02$ min^{-1}, and $A = 0.74 \pm 0.05$.

of D-glucose and 3MG and D-glucose and 2DG in ghosts resealed with ATP. There is no significant difference between the compartment sizes for the two sugars in either case.

Increasing the rate of anomerization has no effect on the second phase of transport: The 3MG anomerization rate has been previously measured by circular dichroism and found to be slower than the slow rate of transport (*vide supra*). But it remains to be determined whether this is true for other GLUT1 substrates that display biphasic transport. D-glucose, 2DG, and D-mannose do not have measurable CD signals so anomerization is measured by polarimetry. Table 3.3 and Figure 3.4 show anomerization rates for D-glucose, 3MG, 2DG, and D-mannose at 4, 20, and at 37 °C along with the activation energy. Based on the known mechanism, the uncatalyzed anomerization reaction is not expected to be concentration dependent; however, higher concentration of sugars give rise to more accurate rate determinations as there is an increase in the signal to noise ratio. For both D-glucose and 3MG the rate of anomerization at ice temperature is much slower than the slow rate of transport as required by the anomer barrier transport hypothesis. However, the same is not true for 2DG and D-mannose. Both 2-position glucose analogs display an increased anomerization rate compared with D-glucose, but unchanged activation energy. Anomerization rates approach the slow rate of transport, and for 2DG may actually be faster than the slow rate of transport although with the difficulty of accurately determining the slow rate of transport this remains uncertain.

If the rate of anomerization were faster than the slow rate of transport then transport of α-sugar would no longer be rate limiting. The rate of anomerization for D-glucose

Table 3.3. Sugar Anomerization Rates, Activation Energies, and Slow Phase Transport Rates

Sugar	Mutarotase (U/mL)[a]	[Sugar]	Anomerization Rate (min^{-1})			Activation Energy[b]	Slow Transport Rate (min^{-1})
			4 °C	20 °C	37 °C		
Glucose	0	10 mM	0.00509 ± 2e-05	0.0184 ± 5.82e-05	0.061563 ± 2.49e-04	52 ± 1	0.046 ± 0.024
		100 mM	0.00462 ± 2e-05	0.016793 ± 1.05e-05	0.067201 ± 3.33e-05	60 ± 2	
	1	10 mM	0.0568 ± 2e-04	0.10976 ± 5.44e-04	0.33771 ± 1.8e-03	45 ± 6	
		100 mM	0.01263 ± 2e-05	--	--	--	
	10	10 mM	0.318 ± 4e-03 0.397 ± 2e-03[a]	0.96217 ± 9.34e-03	1.7201 ± 2.16e-02	31 ± 6	0.069 ± 0.053[c]
		100 mM	0.09063 ± 7e-05	--	--	--	
	50	10	0.852 ± 8e-03	--	--	--	
	100	100	0.760 ± 3e-03	--	--	--	
3MG	0	10 mM	0.0045897 ± 1.53e-05	0.016223 ± 9.76e-05	0.050143 ± 2.34e-04	50 ± 1	0.019 ± 0.010
		100 mM	0.0049888 ± 7.26e-06	0.015622 ± 9.15e-06	0.061666 ± 6.58e-05	59 ± 3	
	10	10 mM	0.0041128 ± 2.76e-05	0.015972 ± 9.23e-05	0.053998 ± 2.14e-04	54 ± 1	
2DG	--	100 mM	0.038001 ± 5.04e-05	0.1322 ± 9.1e-05	0.59279 ± 8.64e-04	65 ± 3	0.016 ± 0.006
Mannose	--	100 mM	0.022925 ± 1.08e-04	0.07332 ± 8.99e-04	0.33936 ± 1.09e-03	66 ± 4	0.033 ± 0.017

[a]Lyophilized porcine kidney mutarotase was dissolved in kaline at 1000 U/mL and aliquots were diluted as necessary.

[b]Activation Energy in kJ/mole are calculated from Arrhenius plots.

[c]D-glucose exchange in the presence of extracellular and intracellular 500 U/mL exogenous mutarotase.

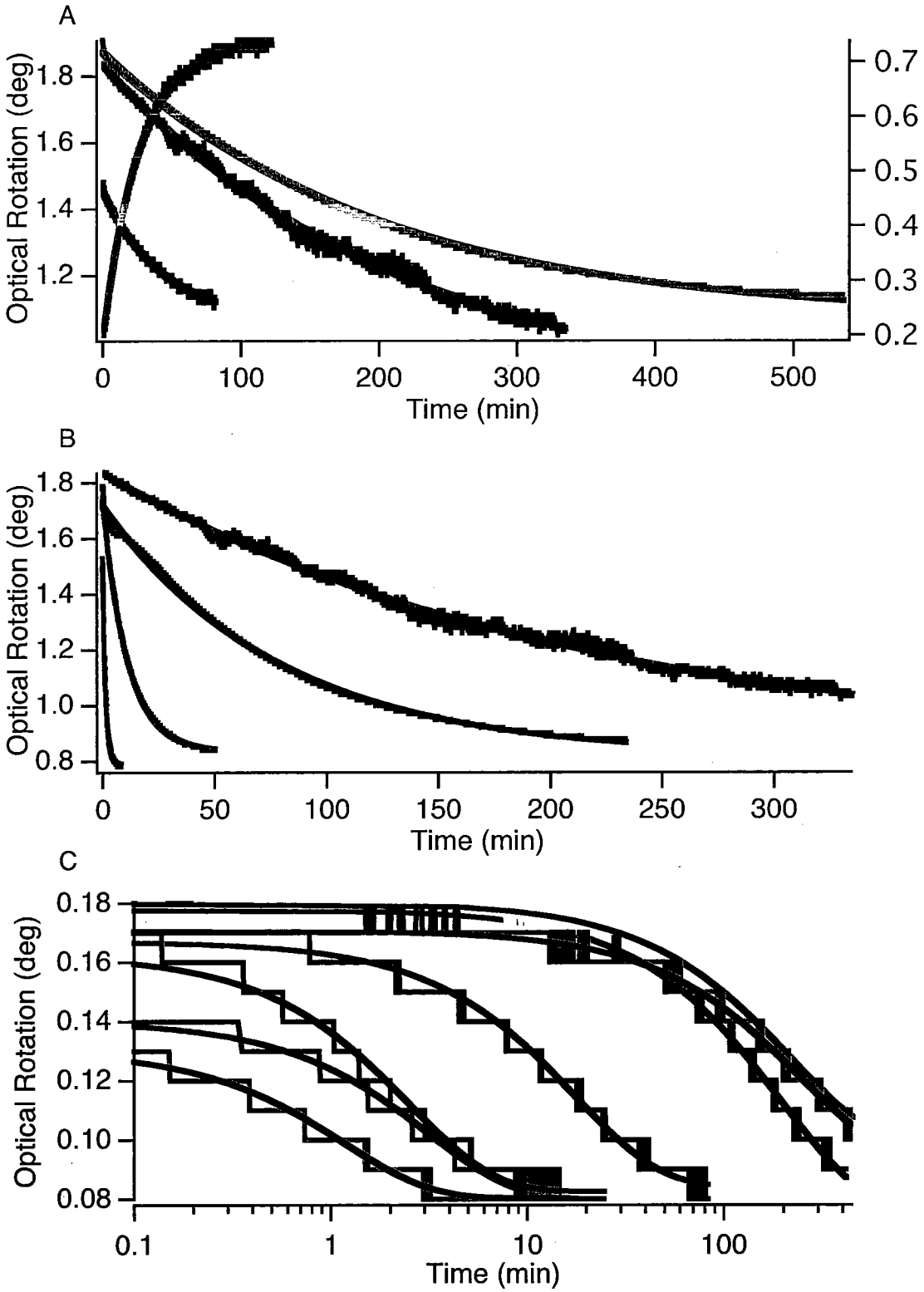
A
Optical Rotation (deg)
1.8
1.6
1.4
1.2
0.7
0.6
0.5
0.4
0.3
0.2
0
100
200
300
400
500
Time (min)
B
Optical Rotation (deg)
1.8
1.6
1.4
1.2
1.0
0.8
0
50
100
150
200
250
300
Time (min)
C
Optical Rotation (deg)
0.18
0.16
0.14
0.12
0.10
0.08
0.1
1
10
100
Time (min)

Figure 3.4. Anomerization of GLUT1 Hexose Substrates With and Without Exogenous Mutarotase.

Left ordinate: optical rotation (deg) for D-glucose, 3MG, and D-mannose; Right ordinate: optical rotation (deg) for 2DG; Abscissa: time in minutes (note scale) **A.** Anomerization of 100 mM α-D-glucose (—), 100 mM α-3MG (—), 100 mM α-D-mannose (—), and 100 mM β-2DG (—) at 4 °C. **B.** Anomerization of 100 mM α-D-glucose at 4 °C in the presence of exogenous porcine kidney mutarotase; 0 U/mL (—), 1 U/mL (—), 10 U/mL (—), and 100 U/mL (—). **C.** Anomerization of 10 mM α-D-glucose and 10 mM α- 3MG at 4 °C in the presence of exogenous porcine kidney mutarotase. Mutarotase has no effect on 3MG anomerization as 3MG with 0 U/mL mutarotase ( ) and 3MG with 10 U/mL mutarotse (—) follow the same time course. Increasing mutarotase concentrations, 0 U/mL (—), 1 U/mL (—), 10 U/mL (—), 10 U/mL in the presence of 4 mM ATP (—), and 50 U/mL with 4 mM ATP (—) correlate with decrease half-times for 10 mM D-glucose anomerization. For all plots, curves are drawn by nonlinear regression assuming single exponential decays of the form $Aexp^{-kt}$ for D-glucose, 3MG, and D-mannose, and a single exponential rise of the form $A(1-exp^{-kt})$ for 2DG, where A is the initial optical rotation and k is the observed anomerization rate constant. Constants for curve fits can be found in Table 3.3.

can be accelerated by addition of porcine kidney mutarotase, an enzyme that catalyzes the conversion of α- into β-D-glucose and β- into α-D-glucose without altering the equilibrium proportions. Table 3.3 also shows anomerization rates and activation energies for D-glucose and 3MG in the presence of mutarotase. Sufficient quantities of mutarotase increase the rate of anomerization to more than ten times faster than the slow rate of transport. In fact, the rate of anomerization of 10 mM D-glucose became too fast to measure at mutarotase concentrations above 50 U/mL. Simulations of transport show that if a significant quantity of mutarotase is resealed within red cell ghosts, then transport would become monophasic even in the presence of ATP (Figure 3.5). However, if mutarotase is only present externally, then transport would remain biphasic with only slight changes in the rates and compartment sizes (i.e. the fast phase would be a little faster and larger). Figure 3.5A shows transport in ghosts resealed in the absence and presence of 500 U/mL mutarotase and 4 mM ATP and predicted transport in the presence of varying activities of mutarotase. Transport in the presence of mutarotase appears to be unchanged. However, it would be difficult to see a difference if mutarotase is only active in the external medium (compare data with blue and green curves). Figure 3.5B shows an SDS-PAGE gel of ghosts that were resealed in the presence or absence of 500 U/mL mutarotase. Lanes 2 and 4 show media (i.e. both extracellular and intracellular proteins) while Lanes 3 and 5 show proteins associated with extensively washed resealed ghosts(only intracellular). Lane 5 indicates the presence of exogenous intracellular mutarotase. The staining intensity of mutarotase is reduced in washed ghosts because the extracellular volume is much

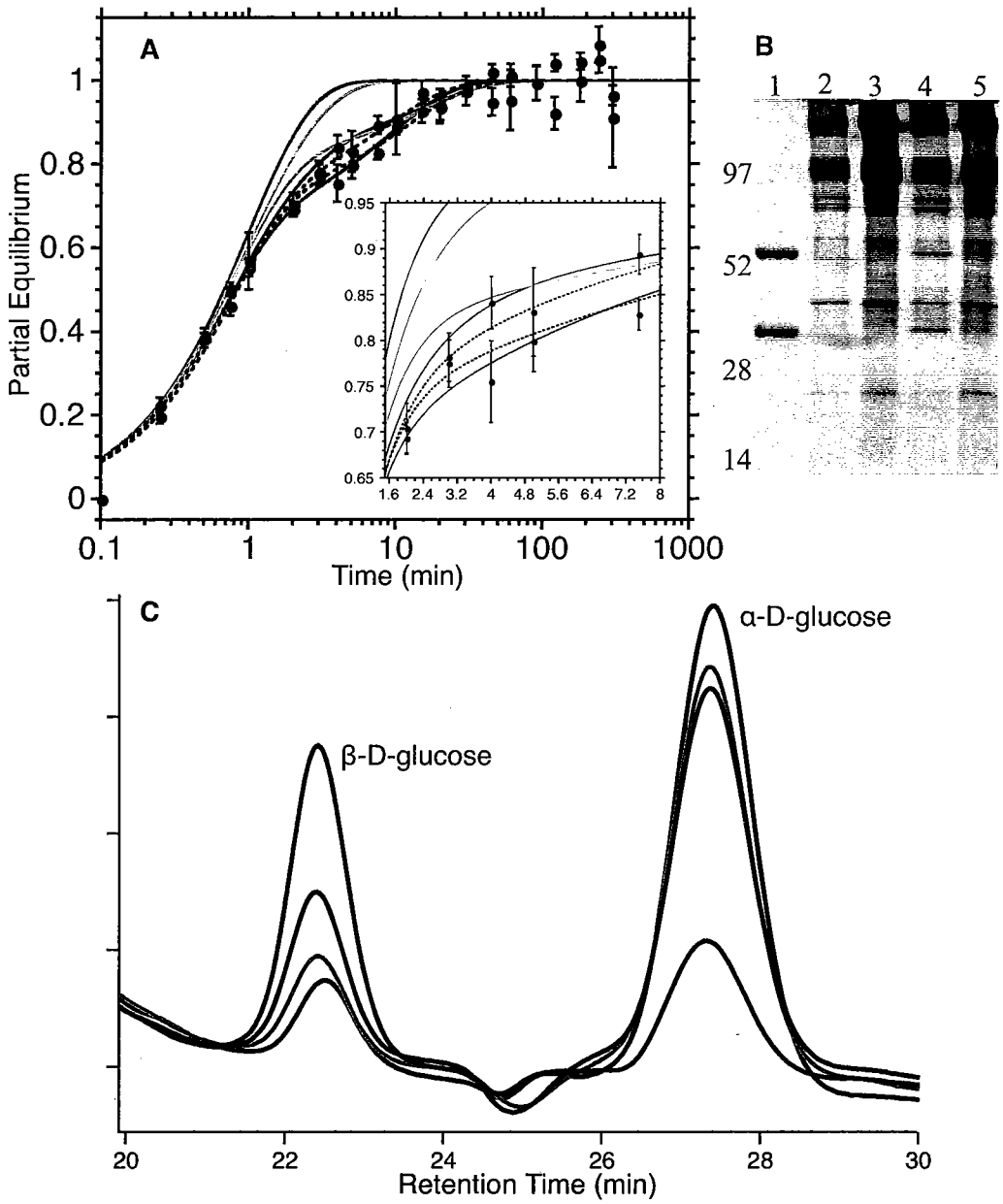

Figure 3.5. Effect of Mutarotase on D-glucose Exchange Kinetics.

A. Ordinate: fractional equilibrium; Abscissa: time in minutes (note scale). Transport of 2.5 mM D-glucose without (•) or with (•) 500 U/mL mutarotase resealed inside ghosts with 4 mM ATP. Dashed curves are drawn by nonlinear regression to

to assume the biexponential form: $A(1-e^{-k_1 t})+(1-A)(1-e^{-k_2 t})$ where k_1 and k_2 are the observed rate constants for phase 1 and 2 respectively and A is the fractional component of total uptake described by phase 1. For transport in the absence of mutarotase A = 0.71±0.05, k_1 =,1.4±0.2 min^{-1} and k_2 = 0.08±0.03 min^{-1}, and A =.71±0.06, k_1 = 1.3±0.2 min^{-1}, and k_2 = 0.11±0.03 min^{-1} in the presence of mutarotase. Transport is simulated according to equation 2.2 where K_α = 50 mM, K_β = 6.3 mM, V_α = 3 mM min^{-1}, and V_β = 5 min^{-1}, and the rate of anomerization is uncatalyzed where $k_\alpha + k_\beta = k_{obs}$ = 0.005 min^{-1} both inside and outside (—). If mutarotase is only present outside at 10% activity (—) or at 500 U/mL (—) (k_{obs} = 0.852 and 8.52 min^{-1} respectively) are shown. Simulated curves are shown if mutarotase is active both outside and inside at 10% activity ( ), 500 U/mL outside and 10% activity inside (—), and 500 U/mL activity both inside and outside (—). **B.** SDS-PAGE gel of erythrocyte ghosts resealed with and without mutarotase. Lane 1, mutarotase; Lane 2, resealing media without mutarotase; Lane 3, washed ghosts after resealing without mutarotase; Lane 4, resealing media containing 500 U/mL mutarotase; Lane 5, washed ghosts after resealing with mutarotase. **C.** Ordinate: change in refractive index; Abscissa: retention time in minutes. HPLC chromatograms of 2 mM D-glucose 1 hour after solubalizing in ice-cold kaline. Control D-glucose not exposed to ghosts (—), 13% β; extracellular D-glucose after incubation with ghosts resealed without exogenous mutarotase (—), 18% β; extracellular D-glucose after incubation with extensively washed ghosts resealed with 500 U/mL mutarotase (—), 64% β; and extracellular D-glucose as above but with 10 μM CCB and 100 μM pholoretin (—), 26% β.

larger than the intracellular volume. While showing that mutarotase is present in the intracellular medium of ghosts, this does not mean that incorporated mutarotase remains active. While ATP does not inhibit mutarotase (see Figure 3.4) a direct measurement of intracellular mutarotase activity is difficult. Extensively washed ghosts resealed with mutarotase and subsequently exposed to α-D-glucose for a short time, then assayed for total sugar anomeric composition show a larger amount of β-D-glucose than predicted by uncatalyzed annomerization. This effect is inhibited by the GLUT1 transport inhibitors CCB and phloretin (Figure 3.5C).

Direct measurements of anomer transport: A more direct approach is to ask the question, does GLUT1 preferentially transport one anomer over the other? If one were to sample red cell cytosol at an early time point in the time course of sugar transport, the anomer model predicts that there should be more β-anomer incorporated into the cell in the case of sugar uptake and less β-anomer in the cell in following sugar exit. An HPLC approach was employed to measure the anomeric composition of small amounts of sugar in answering this question. The resolution of the HPLC method for determining anomer proportions was examined by analysis of 3MG anomerization. Figure 3.6 shows chromatograms of freshly dissolved 100 μM 3MG taken at approximately 1 hour intervals. The initial proportion of β:α-3MG was 20:80. This ratio increases with a time course consistent with the previously measured anomerization rate (Figure 3.6B).

Because detection is through a change in refractive index, application of this type of analysis to transport determination requires a net movement of sugar either into or out

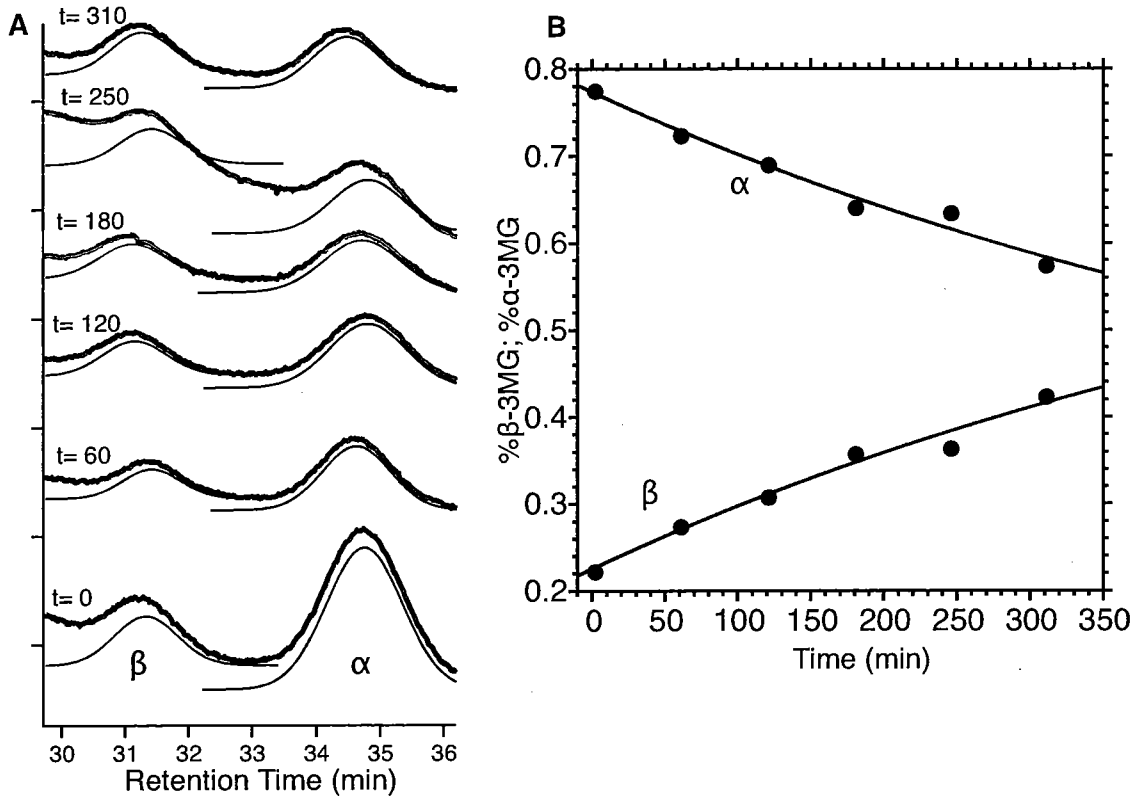

Figure 3.6. Determination of HPLC Method Precision.

A. Ordinate: change in refractive index; Abscissa: retention time in minutes. Chromatograms (—) of 100 μM 3MG after freshly dissolving in ice-cold kaline. Peaks are fit to gaussian distributions β-3MG (—) and α-3MG (—) and baseline adjusted for the resulting fit (—). **B.** Ordinate: %β-3MG, %α-3MG; Abscissa: retention time in minutes. Areas of the gaussian peaks are plotted as a percentage of total area vs incubation time at 4 °C, β-3MG (•), α-3MG (•) and compared to predicted values (—) based on the previously measured anomerization rate.

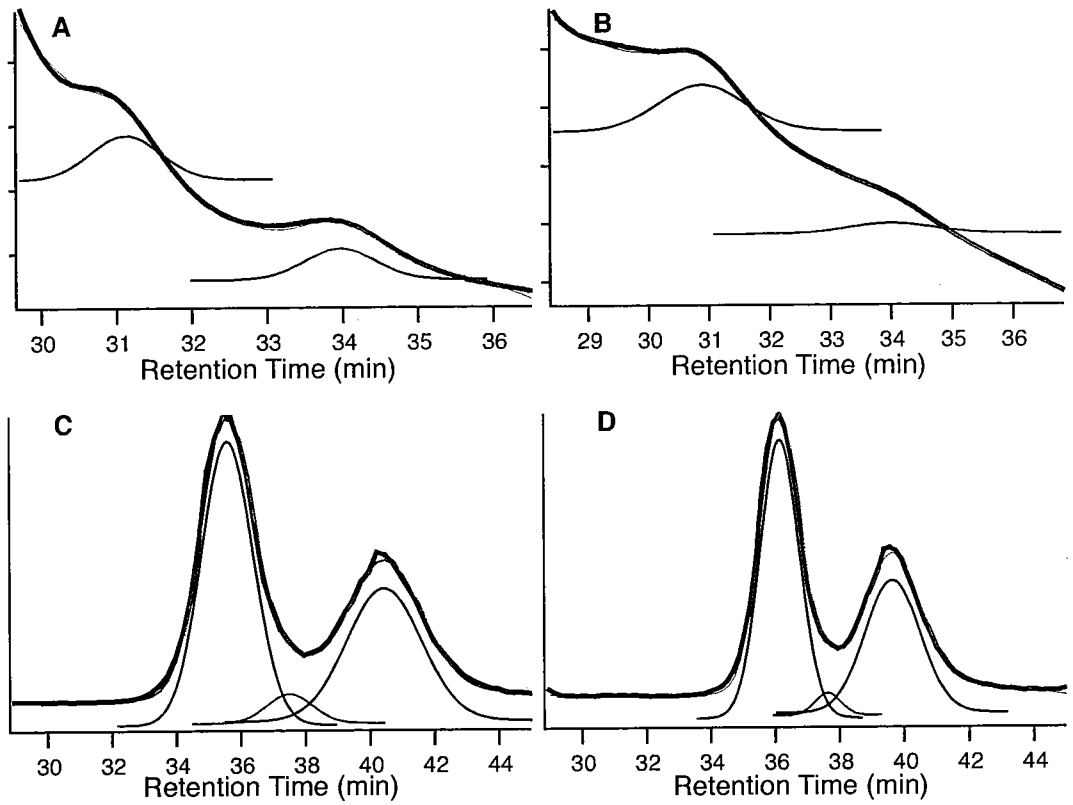

Figure 3.7. HPLC Anomeric Analysis of Extracellular 3MG Following 5 minutes of Net Uptake into Ghosts Without and With ATP.

A. Ordinate: change in refractive index; Abscissa: retention time in minutes. Analysis of unlabeled total (200 μM initially) extracellular 3MG in the absence of ATP. **B.** As in A but with 4 mM intracellular ATP. **C.** Ordinate: CPM's; Abscissa: retention time in minutes. Analysis of remaining extracellular ^{3}H-3MG in the absence of ATP. **D.** As in C but with 4 mM ATP. Chromatograms (—) are fit to a two (A and B) or three (C and D) gaussian peak function (—) and peaks for β- (—) and α-3MG (—) are shown as well as a smaller, third peak representing sugar that has mutarotated while on the column (—).

Table 3.4. Anomeric Analysis of Extracellular 3MG Post Transport

Uptake Time	% β remaining[a]	% β model prediction[b]
0.5 min 0 mM ATP	63 ± 10[c]	67[d]
5.0 min 0 mM ATP	64 ± 5[c]; 59 ± 1[e]	67[d]; 55[f]
0.5 min 4 mM ATP	71 ± 6[c]	64[d]
5.0 min 4 mM ATP	64 ± 4[c]; 57 ± 1[e]	56[d]; 42[f]
equilibrium ± ATP	64 ± 2[c]; 55 ± 1[e]	

[a]%β-3MG remaining extracellular as analyzed by HPLC a short time after mixing with ghosts lacking or containing intracellular ATP

[b]%β-3MG predicted to be remaining extracellular a short time after mixing with ghosts lacking or containing intracellular ATP as described by Eq. 2.2 where $K_{m(app)}$ = 26.9 mM and V_{max} = 1.02 mmol min-1 L cell water-1 for α-3MG, $K_{m(app)}$ = 4.8 mM and V_{max} = 1.41 mmol min-1 L cell water-1 for β-3MG in the presence of ATP.

[c]Analysis of unlabeled 3MG.

[d]Prediction based on an α:β equilibrium of 33:67 as seen for unlabeled 3MG.

[e]Analysis of radiolabeled ^{3}H-3MG.

[f]Prediction based on an α:β equilibrium of 45:55 as seen for ^{3}H-3MG.

of the cell. Hence these experiments reflect net transport not exchange transport measurements. At early time points where the greatest difference of anomer ratios is expected, the amount of total sugar within ghosts is too small to measure by refractive index and measurements were characterized by extremely poor signal to noise ratios. Therefore, the extracellular sugar remaining in solution was analyzed. Figure 3.7 shows chromatograms of extracellular medium containing 200 μM 3MG before and after incubation with an equal volume of ghosts resealed with and without ATP. If β-3MG is the preferred transport substrate, a higher percentage of α-sugar would remain in the media. Time course simulations suggest that the maximal difference occurs following 5 minutes of uptake. Table 3.4 shows the measured anomeric compositions and model predictions. There is no change in the anomeric compositions of extracellular sugar after transport. This signal to noise after 5 minutes of transport, while still adequate to determine anomer proportions, was less than ideal, so to improve the specific signal, the experiments were repeated with radiolabeled 3MG and detected by an in-line radiometric scintillation counter (Figure 3.7 and Table 3.4). It is interesting to note that ^{3}H-3MG does not have the same equilibrium anomeric percentages as unlabeled 3MG.

The advent of detecting radiolabeled 3MG, allowed examination of the 3MG anomeric proportions that are transported into ghosts by sampling the cytosol directly. The use of radiolabels drastically increases signal to noise and also allows the equilibrium exchange transport condition to be examined. The extraction procedure to isolate cytosolic sugar (lysis in ice-cold 3% perchloric acid and neutralization with sodium bi-

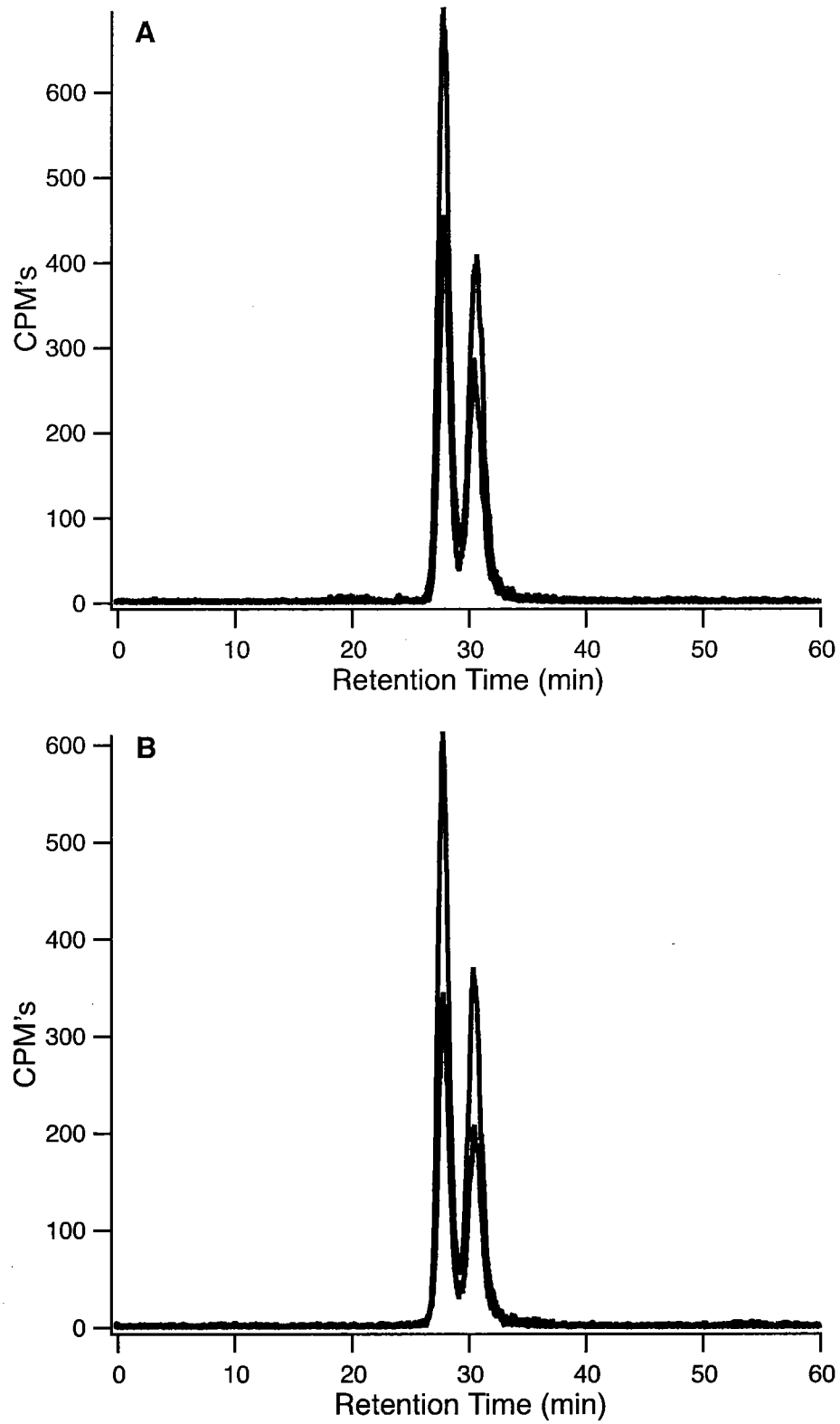
A
600
500
400
300
200
100
0
CPM's
0
10
20
30
40
50
60
Retention Time (min)
B
600
500
400
300
200
100
0
CPM's
0
10
20
30
40
50
60
Retention Time (min)

Figure 3.8. Anomeric Analysis of Intracellular ^{3}H-3MG Following Transport.

Ordinate: CPM's; Abscissa: retention time in minutes. **A.** Chromatograms of intracellular 3MG following net uptake intervals of 30 seconds (—) and 5 minutes (—). **B.** Chromatograms of intracellular 3MG following equilibrium exchange intervals of 30 seconds (—) and 5 minutes (—).

Table 3.5. Anomeric Analysis of Intracellular 3MG Following Uptake

Condition		% β[a]	% β Model[b]	n[c]
Zero-Trans Uptake 0 mM ATP	30 seconds	53% ± 2%	67%[d]; 55[e]	9
Zero-Trans Uptake 4 mM ATP	30 seconds	56% ± 1%	93%[d]; 89%[e]	12
	5 minutes	56% ± 1%	85%[d]; 78%[e]	3
Exchange Uptake 0 mM ATP	15 seconds	53 ± 1%	67%[d]; 55[e]	3
	30 seconds	51% ± 2%	67%[d]; 55[e]	3
Exchange Uptake 4 mM ATP	30 seconds	57% ± 1%	96%[d]; 97%[e]	3
	5 minutes	57% ± 1%	83%[d]; 93%[e]	3
Stock Solutions		55% ± 1%	-	12

[a]%β-^{3}H-3MG intracellular as analyzed by HPLC a short time after mixing with ghosts lacking or containing intracellular ATP.

[b]%β-3MG predicted to be remaining extracellular a short time after mixing with ghosts lacking or containing intracellular ATP as described by Eq. 2.2 where $K_{m(app)}$ = 26.9 mM and V_{max} = 1.02 mmol min-1 L cell water-1 for α-3MG, $K_{m(app)}$ = 4.8 mM and V_{max} = 1.41 mmol min-1 L cell water-1 for β-3MG in the presence of ATP for zero-trans uptake and $K_{m(app)}$ = 37 mM and V_{max} = 0.53 mmol min-1 L cell water-1 for α-3MG, $K_{m(app)}$ = 4.7 mM and V_{max} = 1.48 mmol min-1 L cell water-1 for β-3MG in the presence of ATP for equilibrium exchange uptake.

[c]Number of experiments.

[d]Prediction based on an α:β equilibrium of 33:67 as seen for unlabeled 3MG.

[e]Prediction based on an α:β equilibrium of 45:55 as seen for ^{3}H-3MG.

carbonate) was used on a freshly dissolved sample of unlabeled 3MG and had no measurable impact on anomer ratios (20:80 β:α). Figure 3.8 shows radio chromatograms for 3MG extracted from ghosts resealed with ATP after a short interval of transport. Even at the earliest times when the β- to α-3MG ratio is predicted to be greatest, there is no difference in the anomeric proportions (Table 3.5).

Incubation of human red blood cells with 2,4-dinitrophenol: Picric acid and 2,4-dinitrphenol (DNP) are known to cause echinocytosis of red blood cells when added to the extracellular medium (237, 246-247). 3MG exchange transport in freshly obtained red blood cells that were either incubated with either 0 or 10 mM DNP for 10 minutes prior to start of transport measurements. Figure 3.9 shows that in the absence of DNP treatment, fresh red cells display biphasic transport as expected. DNP treatment, however, abolishes the biphasic nature resulting in monophasic exchange with kinetic properties consistent with ATP depleted ghosts. HPLC analysis of cytosolic nucleotides ensures that DNP treatment does not alter the metabolic potential of the red cell. Metabolically depleted red blood cells display high AMP:ATP ratios while DNP treated cells look like control.

Discussion

Human GLUT1 mediated 3-O-methylglucose exchange kinetics in red blood cells and blood cell ghosts are biphasic, where 66 % of the total 3MG accessible space fills quickly and the remaining 33 % fills slowly, in the presence of ATP at all sugar concen-

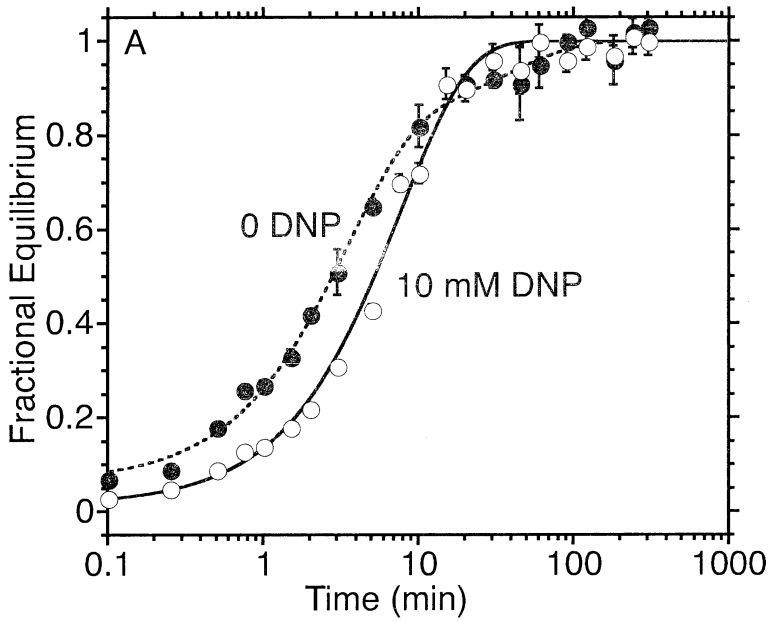
A
Fractional Equilibrium
1
0.8
0.6
0.4
0.2
0
0 DNP
10 mM DNP
0.1
1
10
100
1000
Time (min)

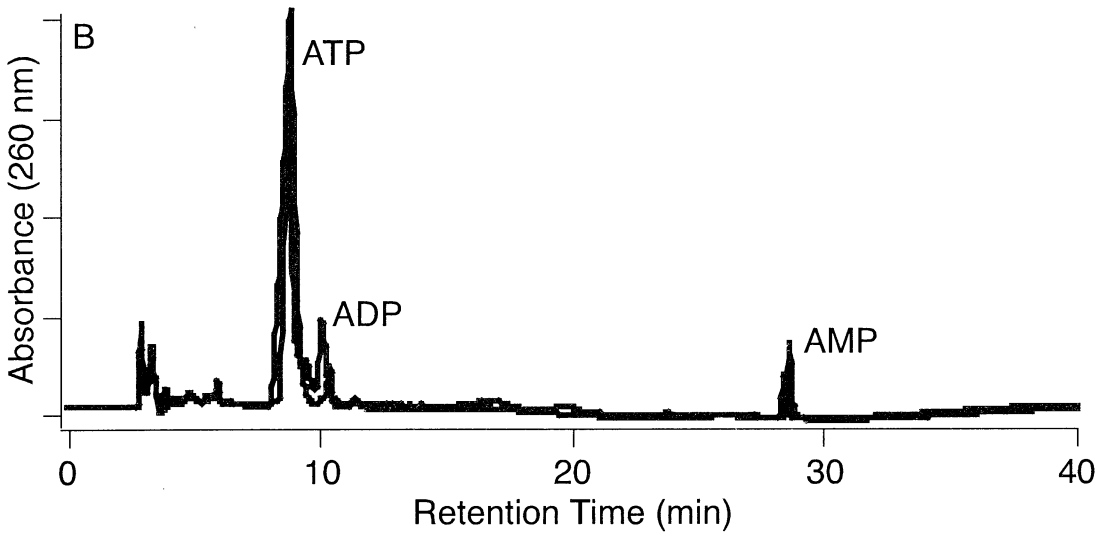
B
Absorbance (260 nm)
ATP
ADP
AMP
0
10
20
30
40
Retention Time (min)

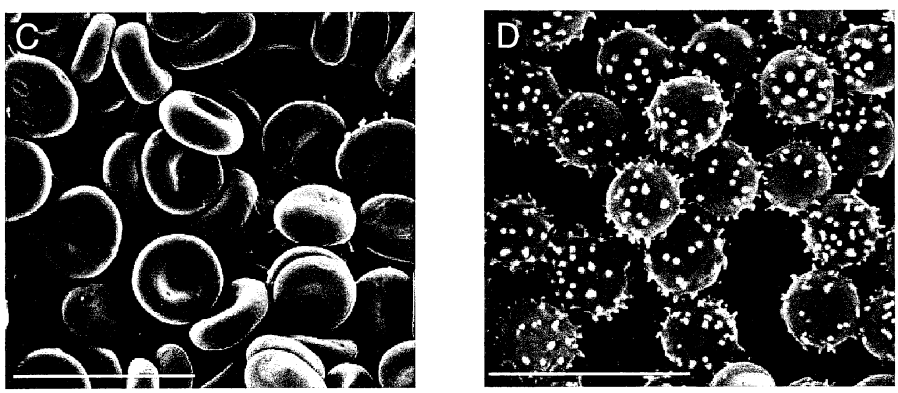
C
D

Figure 3.9. 3MG Exchange in Fresh Red Cells Treated with and without DNP.

A. Ordinate: Fractional equilibrium; Abscissa: time in minutes. Exchange Transport of 2.5 mM 3MG in fresh red cells following 10 minute treatment with DNP (○) or no treatment. (●). Curves drawn through points are computed by non-linear regression to the forms $1-e^{-kt}$ for DNP treated cells and $A(1-e^{-k1t})+(1-A)(1-e^{-k2t})$ where $k = 0.13 \pm 0.01$ min^{-1} for DNP treated and $A = 0.75 \pm 0.05$, $k1 = 0.29 \pm 0.03$ min^{-1}, and $k2 = 0.025 \pm 0.01$ min^{-1} for untreated cells. **B.** Ordinate: CPM's; Abscissa: retention time in minutes Chromatograms of intracellular nucleotides 3 hours post treatment with ± 10 mM DNP (—) and with no treatment (—). **C.** Scanning electron micrograph of fresh, untreated red blood cells used in A and B. **D.** Scanning electron micrograph of fresh, DNP treated red cells used in A and B. The white bar represents 10 μM in both C and D.

trations tested. This observation is incompatible with previous models of ATP regulation of GLUT1, specifically that ATP induces a conformational change allowing direct binding and occlusion of sugar by GLUT1. Two alternative hypotheses have been recently proposed. In one hypothesis, ATP binding confers onto GLUT1 a specificity for β-3MG versus α-3MG so that β-3MG is rapidly transported accounting for the 66 % quickly filling space and α-3MG is transported slowing accounting for the remaining space. While anomer specificity of human GLUT1 has been studied before, there is little consensus as to whether GLUT1 displays anomer specificity, and if so, which anomer is preferred. The other hypothesis requires that there is an undefined diffusion barrier beneath the cell membrane arranged in a manner such that only 66 % of total cytosol is accessible to the intracellular binding site of GLUT1 while 100 % of cytosol is accessible to the intracellular binding site of ENT1. While there is evidence for a non-uniform distribution of sugar in erythrocyte cytosol (6) (112) (100) (110) and for plausible diffusion barriers (170), a mechanism for forming a diffusion barrier is not understood. This work tests the former, biochemically simpler, hypothesis and shows the hypothesis to be untenable by several methods.

Previous data and transport simulation predict that β-3MG is the preferred GLUT1 substrate in the presence of intracellular ATP. In fact, the predicted $K_{m(app)}$ for α-3MG is 7.3 fold greater than for β-3MG. This suggests that methyl-glucosides should also display a similar anomeric preference for binding in the presence of ATP. Measured inhibition of 2.5 mM 3MG equilibrium exchange with α- and β-methylglucoside shows a

difference for the $K_{i(app)}$ for the two epimers, however the difference is not as expected. In the absence of ATP, α-methylglucoside has a $K_{i(app)}$ 7.6 times lower than β-methylglucoside suggesting that α-anomers are the preferred binding substrate in the ATP free state. In the presence of ATP, α-methylglucoside is still the more potent inhibitor, but the ratio is reduced to nearly 1.8. Substitutions on the anomeric hydroxyl (α-methyl and β-methyl) are not substrates for GLUT1 and in fact are only inhibitors at the e1 site (inside) (175). Based on this and other information it has been proposed that the e2 (outside) site interacts with sugar at carbon 1, the anomeric side, while the e1 site binds carbon 4 and 5 (217). This suggests that discrimination of anomer binding would occur at the e2 site rather than at the e1. The difference in methyglucoside binding could be accounted for by the methyl moiety being positioned to interact with a small hydrophobic pocket in the axial position while being positioned away in the equatorial position; or steric hindrance of β-methylglucoside binding but not for α-methylglucoside.

It is also interesting to note that inhibition for both glucosides is only 50% maximally. This suggests that the GLUT1 tetramer is capable of binding a single methylglucoside effectively inhibiting one "dimer" but allowing the other to freely transport. This type of incomplete inhibition has been observed in GLUT1 before and thought to be due to cooperative interactions between the GLUT1 subunits. The binding of one cytochalasin B to the GLUT1 tetramer actually increases the rate of sugar transport (90). Other e1 inhibitor studies also have suggested that some cytochalasin or forskolin derivatives bind with negative coopertivity, where the binding of one molecule decreases the affinity for a

second molecule (Trista Robichaud, unpublished results). Not withstanding these complications, the incompatibility of methylglucoside inhibition of transport with the anomer barrier hypothesis is not sufficient to disprove it.

3MG exchange transport remains biphasic in the presence of both e1 and e2 inhibitors. This is entirely consistent with the anomer hypothesis. As both α- and β-3MG are transported through GLUT1, inhibition of GLUT1 transport should inhibit both phases of transport. However, it appears that cytochalasin B inhibits both phases of transport while phloretin and extracellular maltose do not.

The maltose inhibition data are consistent with only the first phase of transport being inhibited. The concentration necessary for sufficient inhibition also perturbs the ghost size and therefore 3MG substrates resulting in transport reminiscent of counterflow. In counterflow transport, where the unidirectional uptake is measured when $[S_i] > [S_o]$ and net transport is out of the cell, and the unidirectional uptake is characterized by a limited concentrating effect where the radiolabel inside is at a higher concentration than observed at equilibrium; the carrier behaves as a poor antiporter. Under conditions of low initial intracellular substrate concentrations and intracellular ATP, counterflow transport in human red cells displays an additional feature not described previously after the expected counterflow transient (*vide infra*). Intracellular radiolabel concentrations, instead of falling to equilibrium, undershoot to a value below equilibrium and then slowly refill. The time course of sucrose (a sugar that does not interact with GLUT1) modulation of 3MG exchange is consistent with counterflow in the presence of ATP presumably due to

a change in cell volume by the increased extracellular osmolarity. Maltose inhibition under the same conditions is constant with the first phase of transport (the counterflow transient) being inhibited. If, however, the second phase were to be inhibited, the undershoot should also be visible. It is not and the maltose inhibited time course reaches equilibrium and roughly the same time as the sucrose modified time course.

CCB binds at the e1 site while phloretin and maltose bind at the e2 site, and all are competitive inhibitors of GLUT1 mediated exchange transport (218). However, at sub-saturating substrate concentrations the inhibition type may be more complicated. Could it be that CCB is a competitive inhibitor of both α- and β- sugar efflux and a non-competitive inhibitor of α- and β- sugar influx and therefore inhibits both sugar influxes equally as the competitive inhibition occurs at the predicted anomer nondiscriminatory site? The e2 inhibitor on the other hand is noncompetitive for sugar efflux and competitive for influx and may compete unequally with α- and β- sugar on the outside. This seems unlikely because both $K_{m(app)}$ for α- and β- 3MG would be factored by the value $(1+ [I] /K_I)$ and would therefore show the same fold inhibition. These results are inconsistent with the anomer barrier hypothesis.

While all hexoses exist in a dynamic equilibrium between α- and β-anomers, not all hexoses display the 1:2 ratio of α:β as seen for D-glucose and 3-O-methylglucose. The anomeric barrier hypothesis predicts that the sizes of the fast and slow phase are dependent on the anomeric proportions. This, while true for D-glucose and 3MG, is not observed for other GLUT1 substrates. Transport of 2-deoxy-glucose (55% β) and D-

mannose (33% β) remains biphasic with a 70% fast filling component and a 30% slow filling component. While the D-mannose data suggest that the anomer hypothesis is incorrect, the alternative hypothesis that β-anomers are preferred for D-glucose, 3MG, and 2DG, and α- is the preferred substrate for D-mannose is tenable, but difficult to fathom structurally.

A second tenet of the anomeric hypothesis is that the rate of anomerization (interconversion between the α- and β-anomers) must be equal to or less than the slow rate of transport. Anomerization rates and transport rates for several GLUT1 substrates were measured. This requirement was observed to be true for D-glucose, 3MG and D-mannose. 2DG may however be transported more slowly than its anomerization rate, but the degree of certainty is low owing to the difficulty in accurately measuring the rate for the slow phase of transport. The anomerization rate of D-glucose can be accelerated by more than 1000-fold by the addition of exogenous mutarotase. Transport of D-glucose in the presence of mutarotase remains biphasic which is incompatible with the anomer hypothesis.

The most compelling evidence against the anomer hypothesis is obtained upon measurement of the anomeric composition of freshly transported sugar. Under all conditions, the anomeric composition of transported 3MG does not deviate from 66% β, 33% α even though transport simulations predict deviations of up to 97%.

HPLC analysis of transported 3MG also refutes the broader chemical barrier hypothesis. Here, 3MG and other sugars are proposed to be converted into another form

within the red cell ghost cytoplasm accounting for the second observed phase of transport. The second form must also be a substrate for GLUT1 or other passive carrier in the red cell membrane as there is no greater available cytosolic space for 3MG than observed for uridine which would be required if the modified sugar is not transported. 3MG is reported to be a poor substrate for hexokinase (173) nor is it a substrate for glucose oxidase (data not shown). HPLC chromatograms of equilibrated intracellular 3MG show no additional peaks from stock. Control experiments where ^{3}H-3MG is incubated with exogenous S. cerevisiae hexokinase and ATP or recombinant D-glucose oxidase show earlier eluting peaks after prolonged incubation times. While the stock ^{3}H-3MG does contain small amounts of tritium impurities that slowly and nonspecifically diffuse across the ghost cell membrane, the concentration of these impurities does not account for 33% of the total tritium signal.

These data refute the hypothesis that GLUT1 displays an anomeric preference for β-pyranoses in the presence of ATP. If high specific transport of β-anomers and low transport of α-anomers does not explain biphasic exchange transport seen with intracellular ATP, then what does? An alternative hypothesis, described earlier, suggests that there is a diffusion barrier associated with the red cell membrane under ATP replete conditions. The proposed diffusion barrier isolates areas of red cell membrane that have no GLUT1 from patches that contain GLUT1, but is indiscriminate with respect to other transporters. A tenet of this hypothesis (*vide supra*) is that agents that promote spheroechinocytosis will also induce monophasic transport even in the presence of cytosolic ATP. Exchange

transport in 2,4-dinitrophenol treated of red cells is monophasic even while the treated red cells are ATP replete. This observations supports the hypothesis that there are factors beyond the GLUT1-ATP complex necessary for sugar transport complexity. The only caveat being that DNP does not directly block ATP binding to or action on GLUT1.

Data presented here is also incompatible with the diffusion barrier hypothesis. If biphasic transport results from fast movement through GLUT1 into an isolated cytosolic compartment followed by slow diffusion into the remaining cytosolic space, then GLUT1 inhibitors should only inhibit the fast phase of transport. This is indeed the case for the exofacial inhibitors phloretin and maltose. However, cytochalasin B appears to inhibit both the slow and fast phases of transport nearly equally.

If a diffusion barrier cannot explain the ability of cytochalasin B to inhibit both phases of transport while phloretin and maltose do not, then some other explanation must exist. Maltose is cell membrane impermeant and cannot interact with intracellular species (90). Phloretin and CCB however are quite hydrophobic and readily diffuse across the cell membrane. CCB, while being a potent D-glucose transport inhibitor, also interacts with other proteins, inhibiting other carrier proteins and actin polymerization (219, 220). If movement between cytosolic compartments is an enzyme mediated process rather than stokesian diffusion, then it is possible that cytochalasin B may inhibit the movement of sugar between intracellular compartments. The dose response for biphasic 3MG transport suggests that the second phase of transport is not saturable, but the concentrations tested may be below the operational $K_{m(app)}$.

The knowledge that cytochalasin B interacts with the actin cytoskeleton allows for the possibility that the diffusion barrier is comprised of actin filaments. The red cell membrane cytoskeleton is thought to be relatively simple (221, 222). The major component is spectrin, which forms an $\alpha_2\beta_2$-tetramer and is arranged in a hub and spoke network with each spectrin tetramer comprising a spoke. The hub is comprised of a short 14-subunit actin filament plus adducin, tropomyosin, and tropomodulin. Tropomyosin and tropomodulin act as filament capping proteins which stabilized the actin filaments from de-polymerization (223). The spectrin tetramer is anchored to the erythrocyte membrane through a peripheral membrane protein, ankyrin, which is bound to a dimeric form of the anion exchanger and actin filaments are anchored by the peripheral membrane protein band 4.1 which binds to glycophorin. The 14-subunit actin filament is 36 nm long parallel to the membrane (224, 225). While specrin is anchored to the membrane, it is thought to extend 30 to 50 nm into the cytosol (224, 226) (Figure 3.10).

If the volume of a red cell ghost were calculated as a sphere of an average diameter of 5 μm, then the intracellular volume would be 65 μm^3 (65 fL). Biphasic transport consists of two filling compartments with the fast phase composing approximately 66% and the slow phase 33%. If the slow phase of sugar transport represents equilibration of a compartment contained within the center of the sphere, then the radius of that compartment is 1.73 μm meaning that the edge of the small compartment is 770 nm away from the cell membrane, or roughly twenty times the thickness of the membrane skeleton. A reversal of the two compartment spaces allows the thickness to be shortened to 335 nm,

but would require the center of the cell to fill with sugar more rapidly than the membrane proximal region. As the ATP containing red cell ghost is not a sphere and has a shape which maximizes surface area to volume ratios (a sphere has the minimum surface area to volume ratio), then the distance of the small compartment from the cell membrane would be as much as ten times less than the calculated 335 nm and may, in-fact, abut the cell membrane at some locations (Figure 3.7). Could the cytoskeleton form the diffusion barrier?

Magnesium ATP is required for actin filament formation (G-Actin → F-Actin) and is required for biphasic sugar exchange. Electronmicrographs suggest that the spectrin network is more dense than previously thought. In stretched erythrocyte membrane skeleton, there are normally five to six spectrin molecules per actin filament and near 200 actin filaments per square micron, however in living red cell ghosts it appears that there are four to five spectrin molecules per actin filament, but nearly double the density of the actin filaments (227). Cytochalasin B inhibits actin polymerization and when actin is polymerized in the presence of CCB, a denser network of shorter filaments are formed which may account for the decreased slow rate constant (228). If the cytoskeleton is involved in forming a diffusion barrier, then reagents that disrupt the erythrocyte cell shape and/or membrane cytoskeleton should also have effects on GLUT1 mediated transport. Other cytochalasins (CCE and CCD) have little affinity for GLUT1 and do not inhibit sugar transport (90, 229, 230), while still altering actin filament formation (231, 232). The effect of these compounds on sugar exchange time courses have not been studied.

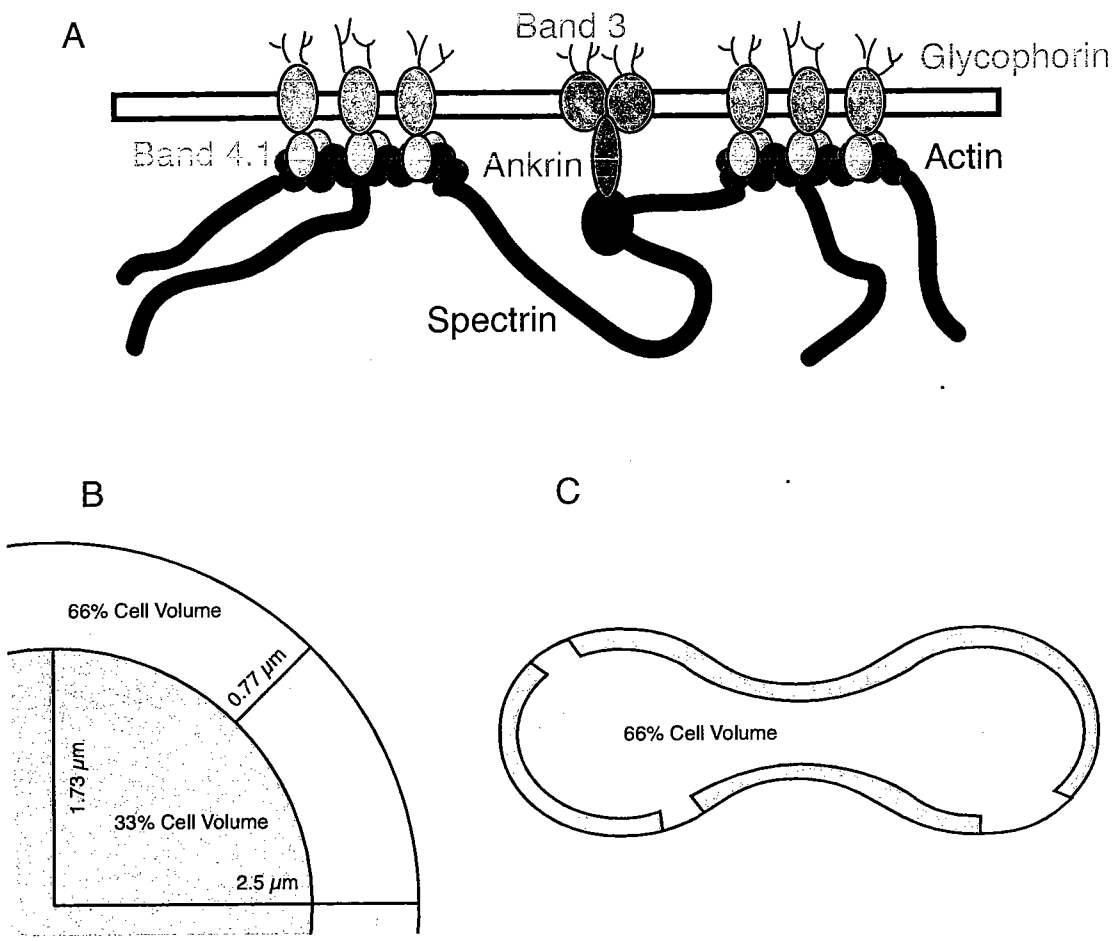

Figure 3.10. Erythrocyte Cytoskeleton and Formation of an Unstirred Layer.

A. The erythrocyte cytoskeleton is mostly comprised of spectrin, which is anchored to the plasma membrane through ankrin and the anion transporter (Band 3) and short actin filaments also anchored to the membrane through Band 4.1 and glycophorin (221). **B.** Sizes of two cytosolic compartments assuming that the larger compartment is proximal to the cell membrane and cell shape is a sphere with a radius of 2.5 μm. **C.** Approximate sizes of two cytosolic compartments in a discocyte where the larger compartment is abutting the membrane in isolated patches.

Conclusion

Sugar transport into and out of red cells is biphasic in the presence of ATP. Biphasic transport does not result from the differential transport of β- and α-sugar anomers as shown by several independent methods. In fact, GLUT1 shows little to no anomer discrimination in either the ATP free or ATP bound state. Transported sugars are not modified by cytoplasm which leads to the rejection of the chemical barrier hypothesis and the adoption of the physical barrier hypothesis. Cytochalasin B inhibition of both phases of transport gives insight into the nature of the diffusion barrier and suggests the possibility of cytoskeleton involvement in its formation.

CHAPTER IV

COUNTERFLOW SUGAR TRANSPORT IN THE HUMAN ERYTHROCYTE SHOWS COMPLEXITY NOT EXPLAINED BY A DIFFUSION BARRIER ALONE

Abstract

Human erythrocyte glucose sugar transport was examined in resealed ghosts under counterflow conditions, where intracellular [sugar] >> extracelular [sugar] and unidirectional uptake is measured. Counterflow transport in ghosts resealed in the absence of cytosolic ATP behaves as observed with other carrier systems, but does not fit well to a symmetric, simple carrier. When ATP is resealed within erythrocyte ghosts, counterflow transport shows a previously unobserved feature. Following the normal counterflow transient where the specific activity (radiolabel) is temporarily concentrated within the cytoplasm, the specific activity of imported sugar undershoots the equilibrium specific activity and then slowly rises back to equilibrium. This occurs when the initial intracellular sugar concentration is less than or equal to 10 mM. The presence of this undershoot is consistent with the presence of an intracellular diffusion barrier and inconsistent with sugar binding or chemical modification. Simultaneous measurement of unidirectional sugar exit is inconsistent with a diffusion barrier as exit is monophasic under all conditions. Transport simulations predict that exit is biphasic in the presence of an intracellular diffusion barrier or if movement across the diffusion barrier were enzyme mediated. To

account for these discrepancies, a model is proposed in which a diffusion barrier separates two cytosolic compartments that are adjacent to the cell membrane. The larger compartment is accessible to sugar transported by GLUT1 while the smaller compartment contains an allosterically regulated sugar exporter that is active only under conditions of limiting extracellular sugar and high intracellular sugar. This allows for efficient exit of total cytosolic sugar but fast reequilibration with only 66% cell water thereby increasing the available sugar for delivery to metabolizing tissues.

Introduction

Glucose transport in human erythrocytes is complex and incompatible with available carrier models for facilitated bilayer diffusion (7, 76, 80, 106). Naftalin and Holman have shown that a cytosolic diffusion barrier can account for the differences in observed kinetic behavior and predicted behavior based on the models of Lieb and Stein (6, 97). Biphasic net-uptake in human red blood cells is seen as direct kinetic evidence for the presence of a cytosolic diffusion barrier (113) however the exact nature of the diffusion barrier remains in question. Intracellular ATP concentrations are involved in regulating the observed transport complexity. Transport complexity is lost in ghosted erythrocytes where cytosolic factors are removed; but retained when ghosts are resealed with exogenous ATP (80, 121, 122).

Equilibrium exchange of 3-O-methyl-D-glucose in red cell ghosts is consistent with the hypothesis that the red cell cytosol contains an ATP dependent diffusion barrier.

Human erythrocyte ghosts display monophasic exchange kinetics when resealed with zero intracellular ATP and biphasic exchange when resealed with 4 mM intracellular ATP. Monophasic exchange is described as the equilibration of a single cytosolic compartment (total cytosol) while biphasic exchange is consistent with the filling of two serial compartments, the first 66% of total cytosol and the second being the remaining 33%. An alternative hypothesis that the two components of biphasic exchange are due to the differential transport of β- and α-anomers is unsubstantiated and has been rejected in favor of a physical barrier. Direct evidence of other transport systems (mainly uridine) in human erythrocytes shows the physical barrier is either restricted to isolated membrane patches containing GLUT1 or is specific to the diffusion of sugar. In the current chapter, the counterflow transport condition is used to further examine the effect of a diffusional barrier on erythrocyte net sugar transport and to gain further insights into the observed, ATP dependent, complexities of human red cell hexose transfer.

Carrier-mediated counterflow transport occurs under conditions where the extracellular substrate concentration is much less than intracellular concentration. Net flux is in the direction of inside to outside, but the unidirectional flux from outside to inside is measured by the use of radiolabels. Counterflow transport is often used as a criterion to reject a channel or pore model for facilitated diffusion (2, 233). A carrier system can couple the diffusion of two substrates (even a carrier that only transports one substrate molecule at a time). If one substrate is present at the same concentration on both sides of the membrane, and a second substrate for the same carrier has a substantial concentration

gradient across the membrane, then the flow of the second substrate down its concentration gradient may drive the first substrate against its own gradient. This type of substrate coupling is obligate for many antiporters. These two substrates do not need to be chemically different, but can be the radiolabeled equivalent of each other. As the second substrate flows down its concentration gradient, it will eventually reach equilibrium and the condition responsible for counterflow will disappear. The counterflow concentrating effect on substrate one is therefore a transitory effect and after the disappearance of second substrate's concentration gradient, the first substrate will return to equilibrium concentrations. Please see Stein for an in-depth analysis of counterflow transport (2).

The use of counterflow transport in human erythrocyte ghosts lacking or containing ATP will investigate the physical barrier hypothesis and determine what steps occur subsequent to sugar uptake by GLUT1.

Materials and Methods

Materials: ^{3}H-3-O-methylglucose and ^{14}C-3-O-methylglucose were purchased from Sigma Chemicals. Human blood was purchased from Biological Specialties Cooperation. Potassium Chloride was purchased from Fisher Scientific. Other reagents were purchased from Sigma Chemicals.

Solutions: Kaline consisted of 150 mM KCl, 5 mM $MgCl_2$, 5 mM EGTA, 5mM HEPES, pH 7.4. Lysis buffer contained 10 mM Tris-HCl, 2mM EDTA, pH 7.4. Stripping solution

is 2 mM EDTA, 15.4 mM NaOH, pH 12. Stop solution consisted of 20 μM CCB and 200 μM phloretin in ice-cold Kaline.

Red Cells: Red cells were isolated by washing whole human blood in 4 or more volumes ice-cold Kaline and centrifuging at 10,000 x g for 15 minutes at 4 °C. Serum and buffy coat were removed by aspiration. Cells were resupended in 4 volumes of sugar free or sugar containing Kaline and incubated for 1 hour at 37 °C to deplete or load intracellular sugar.

Red Cell Ghosts: Ghosts were hypotonically lysed by re-suspending washed red cells in 10 volumes of lysis buffer for 10 minutes. Membranes were harvested by centrifugation at 27,000 x g for 20 minutes. Ghosts were continually washed with lysis buffer centrifugation cycles until light pink (about 3 cycles). Ghosts were then washed with 10 volumes ice-cold kaline and collected by centrifugation at 27,000 x g. Membranes were then resealed by incubating in 4 volumes of kaline ± 4 mM ATP at 37 °C for 1 hour and then harvested by centrifugation at 27,000 x g for 15 minutes at 4 °C and then kept on ice until use.

3-O-methylglucose counterflow uptake and exit: Ghosts were resealed with 2.5, 5, 10, 20, 40, or 80 mM 3MG, centrifuged, and the supernatant removed. Red cells were incubated with the above concentrations of 3MG at 37 °C for 2 hours, then treated in the same manner as ghosts. Radiolabel ^{14}C-3MG (50 nCi of per mL of cells) was added and allowed to equilibrate overnight. Transport was initiated by mixing the ghosts with 20 volumes of ice-cold kaline containing 100 μM 3MG and 0.5 μCi/mL ^{3}H-3MG. In this man-

ner, the ^{3}H label will monitor external 3MG taken up into the ghost/cells and the ^{14}C label will show the exit of internal sugar. Transport was allowed to proceed for a period as short at 6 seconds and as long as 10 hours when 10 volumes of ice-cold stop buffer was added and ghosts were centrifuged at 14,000 x g for 1 minute. The supernatant was removed by aspiration and ghosts were washed with 20 volumes of sugar stop buffer, recentrifuged and supernatant aspirated. The ghosts pellet was then extracted with 500 µL of 3% percholoric acid, centrifuged, and samples of the clear supernatant were counted in duplicate. Zero time points were collected by the addition of sugar stop solution followed by transport medium and immediately processed. The radioactivity associated with cells at zero time was subtracted from the total following an uptake interval and used to normalize the exit data. Equilibrium time points were collected using an overnight uptake interval. Uptake time points were normalized to the equilibrium time point. All solutions and tubes used in the assay were pre-incubated on ice for 30 minutes prior to the start of the experiment. Triplicate samples were processed at each time point.

Curve fitting procedures and transport simulation: Counterflow sugar exit was analyzed by nonlinear regression using the software package KaleidaGraph™ 4.0 (Synergy Software, Reading, PA). Counterflow sugar uptake and exit were simulated by using BerkleyMadona 8.3.12 using fourth-order Runge-Kutta numerical integration.

Results

Counterflow transport in ghosts lacking and containing intracellular ATP and in red blood cells: In order to determine the feasibility of using the counterflow condition in analyzing the hypothesized diffusion barrier, the time course of unidirectional 3MG uptake was monitored in ghosts with and without intracellular ATP and fresh red blood cells equilibrated with 10 mM nonradiolabeled intracellular 3MG and resuspended in 100 μM extracellular 3MG spiked with tracer radiolabeled 3MG at 4 °C. Figure 4.1 shows that in the absence of intracellular ATP, the normal counterflow situation results where initial external sugar temporarily concentrates within the ghosts until the internal and external specific activities (ratio of radiolabeled to unlabeled 3MG) are equal, at which point net radiolabel flux is from inside to outside until equilibrium is reached. This is expected for all passive, carrier-mediated, transport systems (2). Resealing ghosts with 4 mM ATP has a profound effect on the time course of counterflow transport. The normal counterflow concentrating effect is still observed with an increase in the rate constant for reaching the counterflow transient peak, but the degree of concentrating is reduced by one-third. However, the most interesting feature occurs during the late time-point values (40 to 200 min) following the counterflow transient. Here, the intracellular specific activity falls below the equilibrium value. This undershoot is also observed in fresh red blood cells and there is a hint that the fresh red cells may return to equilibrium near 200 minutes. Is this undershoot indicative of intracellular compartmentalization?

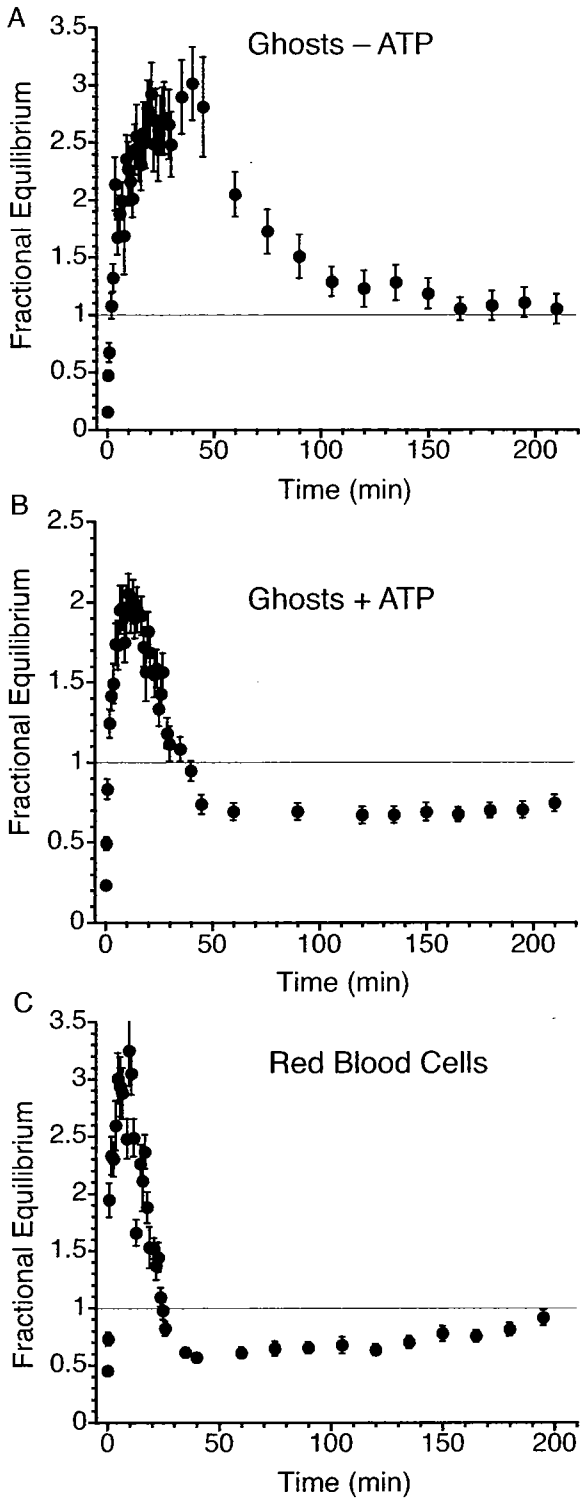
A
Ghosts – ATP
Fractional Equilibrium
Time (min)
B
Ghosts + ATP
Fractional Equilibrium
Time (min)
C
Red Blood Cells
Fractional Equilibrium
Time (min)

Figure 4.1. Time course of counteflow transport uptake in ghosts and red blood cells.

Ordinate: fractional equilibration; Abscissa: time in minutes. **A.** The time course of counterflow uptake in ghosts lacking intracellular ATP. **B.** The time course of counterflow uptake in ghosts containing 4 mM ATP. **C.** The time course of counterflow uptake in fresh red blood cells. For all cases, the initial extracellular 3MG concentration is 100 μM and the intracellular 3MG concentration is 10 mM. The horizontal line at the fractional equilibrium value of 1 represent equilibrium.

To further expand on the ATP effect on counterflow transport, the initial intracellular sugar was varied. Figure 4.2 shows counterflow uptake in cells containing 2.5, 5, 10, 20, 40, and 80 mM intracellular 3MG and exposed to 100 μM extracellular 3MG. In the absence of intracellular ATP, the normal counterflow situation results where initial external sugar temporarily concentrates within the ghosts until the internal and external specific activities equilibrate. In all cases, we see that ATP decreases the time of the counterflow concentrating affect, presumably by a stimulation of exchange transport. Furthermore, at initial intracellular 3MG concentrations at or below 10 mM the undershoot is present. After the initial concentrating of imported sugar, the sugar is rapidly exported to attain levels below equilibrium so that the internal sugar concentration is less than external concentration. Imported sugar then slowly increases returning to the equilibrium level. Counterflow transport has been studied by this and other laboratories but only at initial intracellular sugar concentrations of 76 mM or higher which explains why the undershoot was not previously observed (100, 110, 111, 234).

Simultaneous unidirectional exit from ghosts resealed with and without intracellular ATP: The time course of exit in the above counterflow experiments was measured simultaneously with the use of ^{14}C-3MG. Figure 4.3 shows that ATP accelerates the time course of exit under all substrate concentrations. This is somewhat surprising as the diffusion barrier hypothesis predicts a slowing of the exit time (97). Experimental exit is best described as a monoexpential decay even in the presence of ATP (except where the initial intracellular 3MG concentration of 2.5 mM condition where exit is

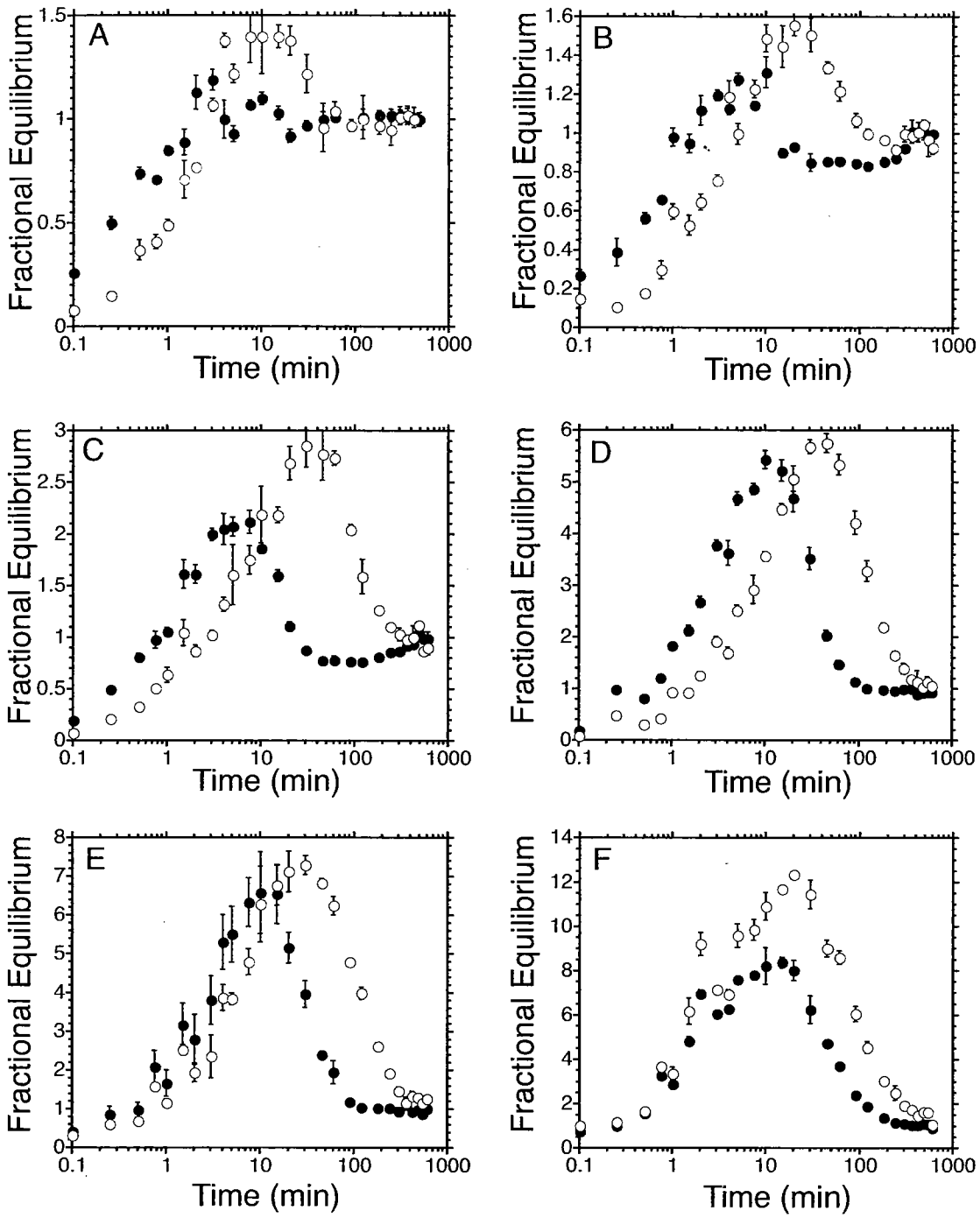
A
B
C
D
E
F
Fractional Equilibrium
Time (min)
0.1
1
10
100
1000

Figure 4.2. Effect of ATP and intracellular 3MG concentration on counterflow uptake.

Ordinate: fractional equilibration; Abscissa: time in minutes (note log scale). Uptake of 100 μM 3MG is shown in cell lacking (○) or containing (●) 4 mM ATP and intracellular ^{14}C-3MG. The concentration of intracellular 3MG is varied for each panel. **A.** 2.5 mM intracellular 3MG. **B.** 5.0 mM intracellular 3MG. **C.** 10 mM intracellular 3MG. **D.** 20 mM intracellular 3MG. **E.** 40 mM intracellular 3MG. F. 80 mM intracellular 3MG. The presence of intracellular ATP decreases the observed concentrating effect by approximately one-third for initial intracellular 3MG concentrations of 10 mM or less and for an initial intracellular 3MG concentration of 80 mM. ATP also induces an observable undershoot following the counterflow transient when the initial intracellular 3MG concentrations is 10 mM or less.

biphasic). Table 4.1 summarizes fit parameters for exit in ghosts lacking and containing ATP. The observation of single exponential kinetics is perplexing as equilibrium exchange transport experiments show biphasic sugar exit (*vide supra*).

Simulation of the counterflow time course kinetics:

Simple carrier simulations: Counterflow transport in erythrocyte ghosts resealed without ATP can be simulated by the simple carrier model. The simple carrier can be solved for the interaction with two substrates, S and P, where S and P are chemically identical except for isotopic label, and takes the form where total transport of S is described by:

$$v^S = v^S_{21} - v^S_{12} \qquad \text{Eq. 4.1}$$

and v^S_{12} is the unidirectional flux of S from side 1 to side 2 taking the form:

$$v^S_{12} = \frac{\frac{S_1}{K} + \frac{S_1 S_2}{K^2} + \frac{S_1 P_2}{K^2}}{R_{00} + R_{12}\left(\frac{S_1 + P_1}{K}\right) + R_{21}\left(\frac{S_2 + P_2}{K}\right) + R_{ee}\left(\frac{S_1 P_2 + S_2 P_1 + S_1 S_2 + P_1 P_2}{K^2}\right)} \qquad \text{Eq. 4.2}$$

and

$$v^S_{21} = \frac{\frac{S_2}{K} + \frac{S_1 S_2}{K^2} + \frac{S_2 P_1}{K^2}}{R_{00} + R_{12}\left(\frac{S_1 + P_1}{K}\right) + R_{21}\left(\frac{S_2 + P_2}{K}\right) + R_{ee}\left(\frac{S_1 P_2 + S_2 P_1 + S_1 S_2 + P_1 P_2}{K^2}\right)}$$

where S_2 is the concentration of substrate S at side 2 (outside), S_1 is the substrate concentration at side 1, K is the intrinsic affinity constant for substrates S and P, R_{12} is the reciprocal of V_{max} for zero-trans exit, R_{21} is the reciprocal of V_{max} for zero-trans uptake, and R_{ee} is the reciprocal of V_{max} for equilibrium exchange. R_{00} is the reciprocal of the maxi-

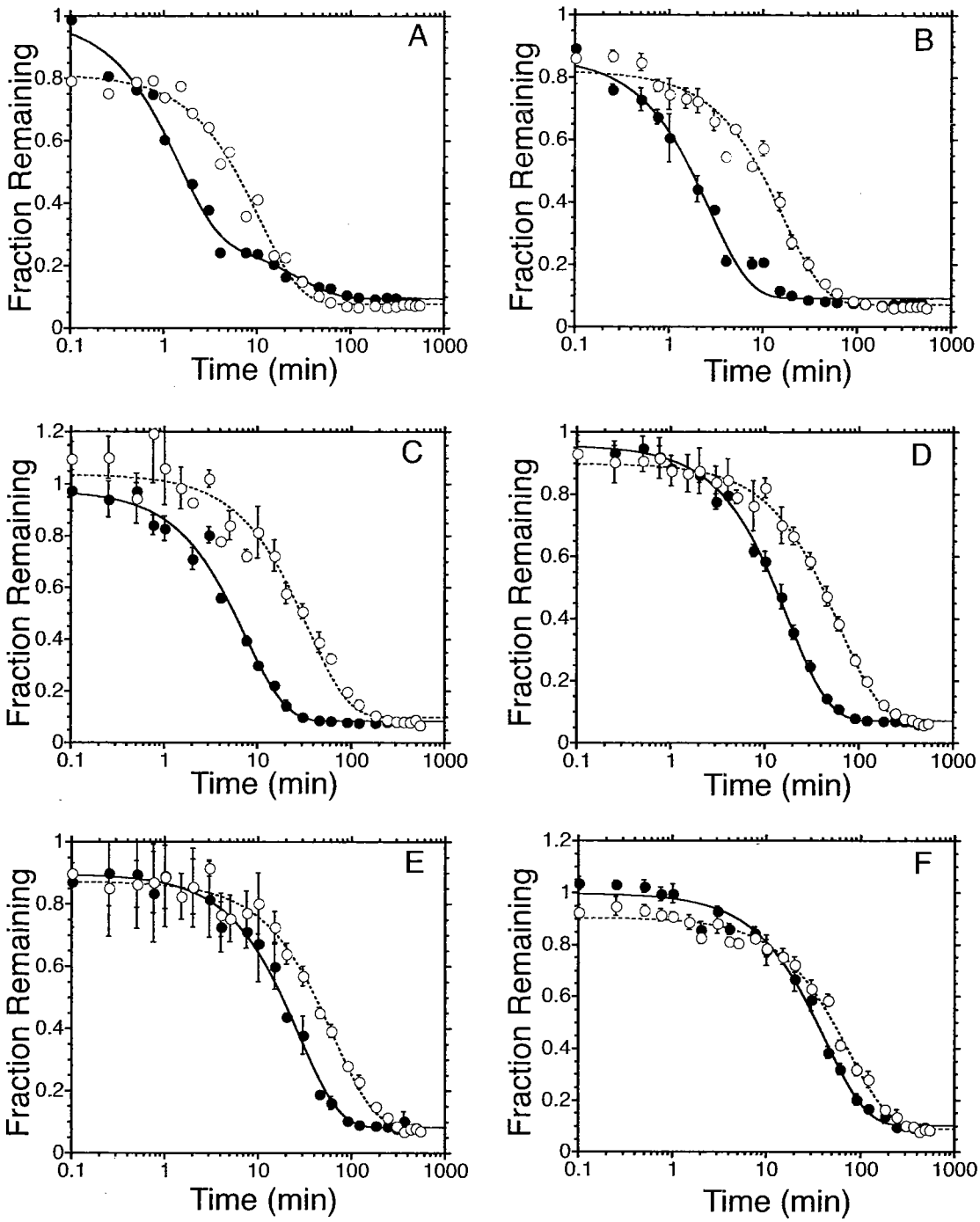
A
B
C
D
E
F
Fraction Remaining
Time (min)
0.1
1
10
100
1000
0
0.2
0.4
0.6
0.8
1
1.2

Figure 4.3. Effect of ATP and Intracellular 3MG Concentration on the Simultaneous Measurement of Exit During Counterflow Uptake.

Ordinate: fraction of intracellular sugar remaining; Abscissa: time in minutes (note log scale). Exit of ^{14}C-3MG is shown in cell lacking (○) or containing (●) 4 mM ATP and extracellular 100 μM 3MG. The concentration of intracellular 3MG is varied for each panel. **A.** 2.5 mM intracellular 3MG. **B.** 5.0 mM intracellular 3MG. **C.** 10 mM intracellular 3MG. **D.** 20 mM intracellular 3MG. **E.** 40 mM intracellular 3MG. **F.** 80 mM intracellular 3MG. The presence of intracellular ATP decreases the observed exit time in all cases. At the lowest intracellular 3MG concentration tested (2.5 mM) exit is biphasic in the presence of ATP. Curves drawn through the points are computed by nonlinear regression and take the forms: e^{-kt} for exit where k is the observed rate constant and for 2.5 mM +ATP $A(e^{-k1t})+(1-A)(e^{-k2t})$ where k1 is the observed rate constant for the fast phase of exit, k2 is the observed rate constant for the slow phase, and A is the fractional component of total exit described by the fast phase. Values for k, k1, k2, and A are shown in Table 4.1.

Table 4.1. Effect of Intracellular 3MG Concentration and ATP on the Rate Constants of 3MG Exit

[3MG]	- ATP	+ ATP		
	k_{obs}[a]	fast k_{obs}[ab]	slow k_{obs}[a]	fast component size[c]
2.5	0.09 ± 0.006	0.798 ± 0.12	0.026 ± 0.022	0.70 ± 0.048
5	0.10 ± 0.01	0.46 ± 0.04	--	--
10	0.026 ± 0.003	0.15 ± 0.01	--	--
20	0.021 ± 0,002	0.06 ± 0.002	--	--
40	0.023 ± 0.003	0.04 ± 0.004	--	--
80	0.018 ± 0.002	0.02 ± 0.001	--	--

[a]Rate constants are first-order and have unit of min^{-1}

[b]Fast k_{obs} is for the biphasic fit for 2.5 mM in the presence of ATP and represents the only k_{obs} for the other conditions

[c]The fraction of the total exit described by the fast rate constant. The fraction described by the slow rate is calculated as 1-fast component size

mal rate of movement of binding sites between the two membrane sides for the empty carrier. Total transport of P is described similarly where S and P are swapped in the above equations. A representative fit is shown in Figure 4.4. The parameters of the simple carrier for each time course is shown in Table 4.2. However the parameters required to accurately predict the time course are not consistent with other kinetic information. Ghosts resealed without intracellular ATP display transacceleration, where R_{ee} is less than R_{12} and R_{21}, which is not observed in the simulations.

Fixed-Site Carrier Simulations: The fixed-site carrier can likewise be solved for the counterflow condition for transport (100) of S and P where the unidirectional uptake of S from side 2 to 1 is:

$$v_{21}^{S}=\frac{V\frac{S_2}{K}+V_{ee}\frac{S_2(S_1+P_1)}{\alpha\lambda K^2}}{1+\frac{S_1+P_1}{\lambda K}+\frac{S_2+P_2}{K}+\frac{(S_2+P_2)(S_1+P_1)}{\alpha\lambda K^2}} \qquad \text{Eq. 4.3}$$

where V is the maximal rate of transport of zero-trans exit, and V_{ee} is the maximal rate of equilibrium exchange. K is $K_{m(app)}$ for zero-trans uptake and λK is the $K_{m(app)}$ for zero-trans exit. The degree of coopertivaty between the two sites is described by α. The unidirectional exit of S is obtained by interchanging subscripts 1 and 2 and λV and λK for V and K in the numerator. The fixed-site carrier is much better at simulating the counterflow time courses in the absence of ATP as shown in Figure 4.4 and Table 4.2. The simulated parameters for each time course is fairly internally consistent and show that the carrier displays transacceleration as V_{ee} is greater than V.

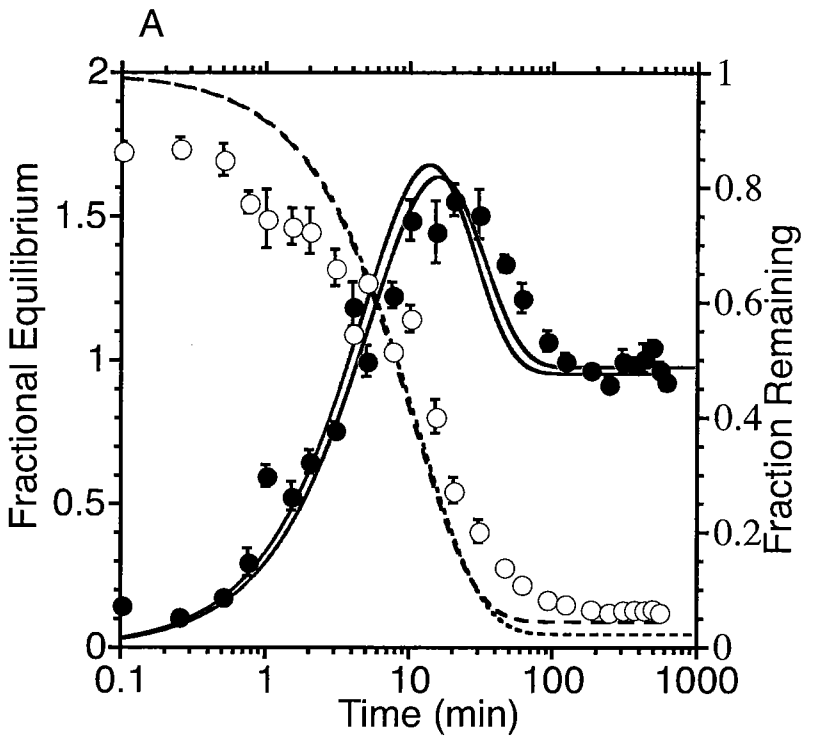
A
Fractional Equilibrium
Fraction Remaining
Time (min)
0
0.5
1
1.5
2
0.2
0.4
0.6
0.8
0.1
1
10
100
1000

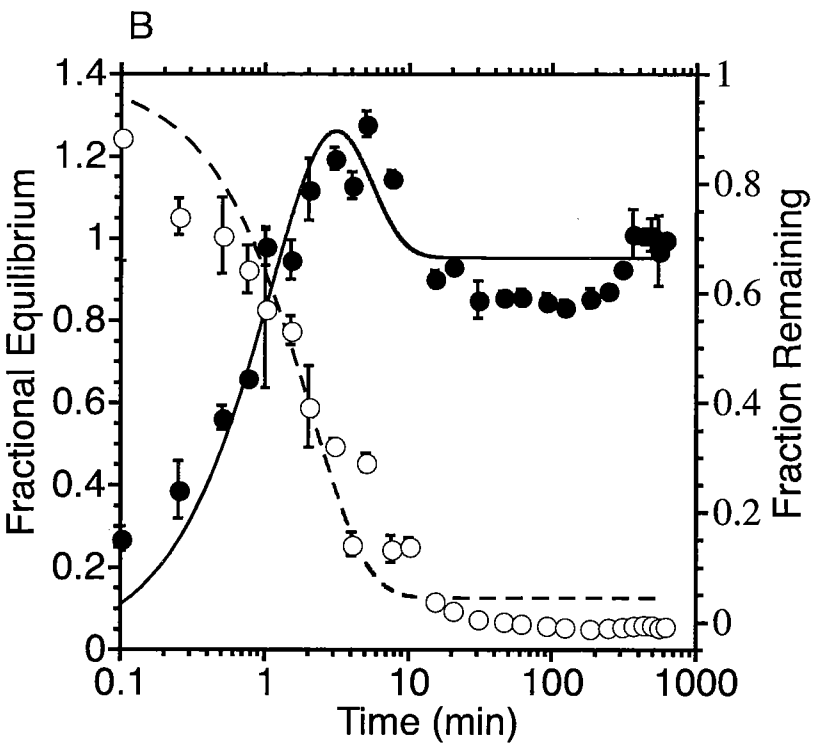
B
Fractional Equilibrium
Fraction Remaining
Time (min)
0
0.2
0.4
0.6
0.8
1
1.2
1.4
0.2
0.4
0.6
0.8
0.1
1
10
100
1000

Figure 4.4. Simple and Fixed-Site Carrier Transport Simulations.

Left Ordinate: fractional equilibration; Right Ordinate: fraction of intracellular sugar remaining; Abscissa: time in minutes (note log scale). **A.** Counterflow uptake of 100 μM ^{3}H-3MG (•) and exit of 5 mM ^{14}C-3MG (○) is shown in ghosts lacking intracellular ATP. The simple carrier is able to adequately describe uptake (—) and exit (·····). The fixed-site carrier is also shown for uptake (—) and exit (·····). Parameters for both models are shown in Table 4.2. **B.** Counterflow uptake of 100 μM ^{3}H-3MG (•) and exit of 5 mM ^{14}C-3MG (○) is shown in ghosts containing 4 mM intracellular ATP. The fixed-site carrier is unable to predict the observed undershoot present in uptake (—) but fits well with exit (·····). Parameters for the fixed-site carrier are K = 0.42 mM, V = 0.43 mM min^{-1}, V_{ee} = 6.1 mM min^{-1}, α = 9.5 and λ = 10.

Table 4.2. Simulation Parameters for Counterflow in the Absence of ATP

Simple Carrier Parameters[a]

[3MG] [b]	K[c]	R_{12}[d]	R_{21}[d]	R_{ee}[d]
2.5	1.0	1.4e-07	6.4	6.3e-06
5	1.7	2.6e-07	6.7	8.5e-06
10	1.3	2.3e-07	21.5	3.6e-06
20	1.0	4.9e-07	35.7	3.3e-06
40	1.4	2.5e-07	21.5	6.8e-06
80	1.3	1.8e-07	15.6	6.0e-06

Fixed-Site Carrier Parameters[e]

[3MG] [b]	K[c]	V[f]	V_{ee}[f]	α[g]	λ[h]
2.5	1.2	0.2	10	0.4	9
5	10	0.89	4.8	0.1	8
10	6.2	0.2	6.5	0.6	10
20	2.3	0.7	5.2	0.2	10
40	10	0.25	9.6	0.35	10
80	10	2.4	2.7	0.1	9

[a]The simple carrier is described in equation 4.2

[b]Concentration (in mM) of initial intracellular 3MG

[c]The intrinsic affinity constant, in mM

[d]Resistance terms described in equation 4.2 in terms of min mM^{-1}

[e]The fixed-site carrier is described by equation 4.3

[f]V_{max} as described by equation 4.3 in mM min^{-1}

[g]Coopertivity factor

[h]Asymmetry factor

Simulations with the inclusion of a intracellular diffusion barrier: The fixed-site or simple carrier models however are unable to predict the undershoot seen for 3MG counterflow transport in the presence of intracellular ATP and low initial intracellular 3MG (Figure 4.4). This undershoot may result from an intracellular diffusion barrier and transport simulations that consider this probability may give insights into the nature of the diffusion barrier. If a fixed-site carrier is coupled to the diffusion through a physical barrier, then the resulting total transport scheme is as follows:

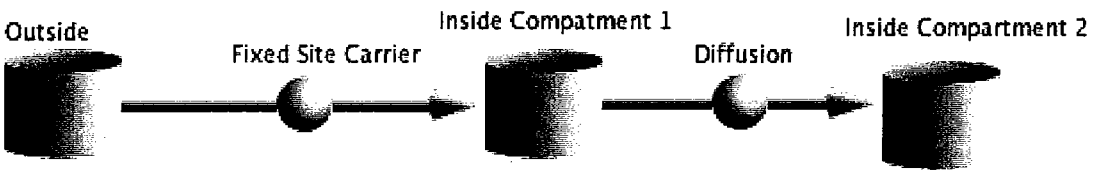

where movement of substrate between the outside and the first intracellular compartment is governed by equation 4.3 and movement between compartment 1 and compartment 2 is modeled by a simple first order reaction of the form:

$$d^S=(S_{C1}-S_{C2})k_d \qquad \text{Eq. 4.4}$$

where d^S is the net flux from compartment 1 to compartment 2, S_{C1} is the concentration of S in compartment 1, S_{C2} is the concentration of S in compartment 2, and k_d is the rate of movement between the two compartments. For the counterflow simulations, the fractional volume of cytosol occupied by compartment 1 is set between 0.6 to 0.8 as seen for compartmentalization under equilibrium exchange conditions (*vide supra*). The cytosolic diffusion barrier model is quite capable of describing the counterflow record in the pres-

ence of ATP and an initial intracellular concentration of 2.5 mM 3MG. Figure 4.5 shows that simulations reproduce both the counterflow transient and the observed undershoot. This model requires that exit be biphasic which is indeed the case when the initial intracellular 3MG concentration is 2.5 mM. However, the model breaks down when simulating the counterflow time course when the intracellular concentration is above 2.5 mM. Here, the model can accurately predict the counterflow transient and observed undershoot, but requires that simulated exit be biphasic (which is not observed) and slower than observed experimentally (Figure 4.5). How is it that uptake is consistent with the movement of sugar into two cytosolic compartments, but exit only shows one?

Simulations with the inclusion of a catalyzed barrier: The above diffusion model allows substrate in one compartment to diffuse independently of substrate in the second compartment. If d^S were not governed by simple diffusion, but instead were an enzyme mediated process, then perhaps substrate in intracellular compartment 2 could inhibit movement of substrate from compartment 1 into compartment 2. This could in principle allow for slow diffusion of substrate between both compartments when substrate is present in both, but as the counterflow time course proceeds and substrate in compartment one is depleted due to transport through GLUT1 to the extracellular space, then the inhibition of movement in the direction of compartment 2 to compartment 1 is lost while inhibition of movement from compartment 1 to compartment 2 is retained. Here the net movement of substrate S is described by:

$$d^S = d^S_{C1\rightarrow C2} - d^S_{C2\rightarrow C1} \qquad \text{Eq. 4.5}$$

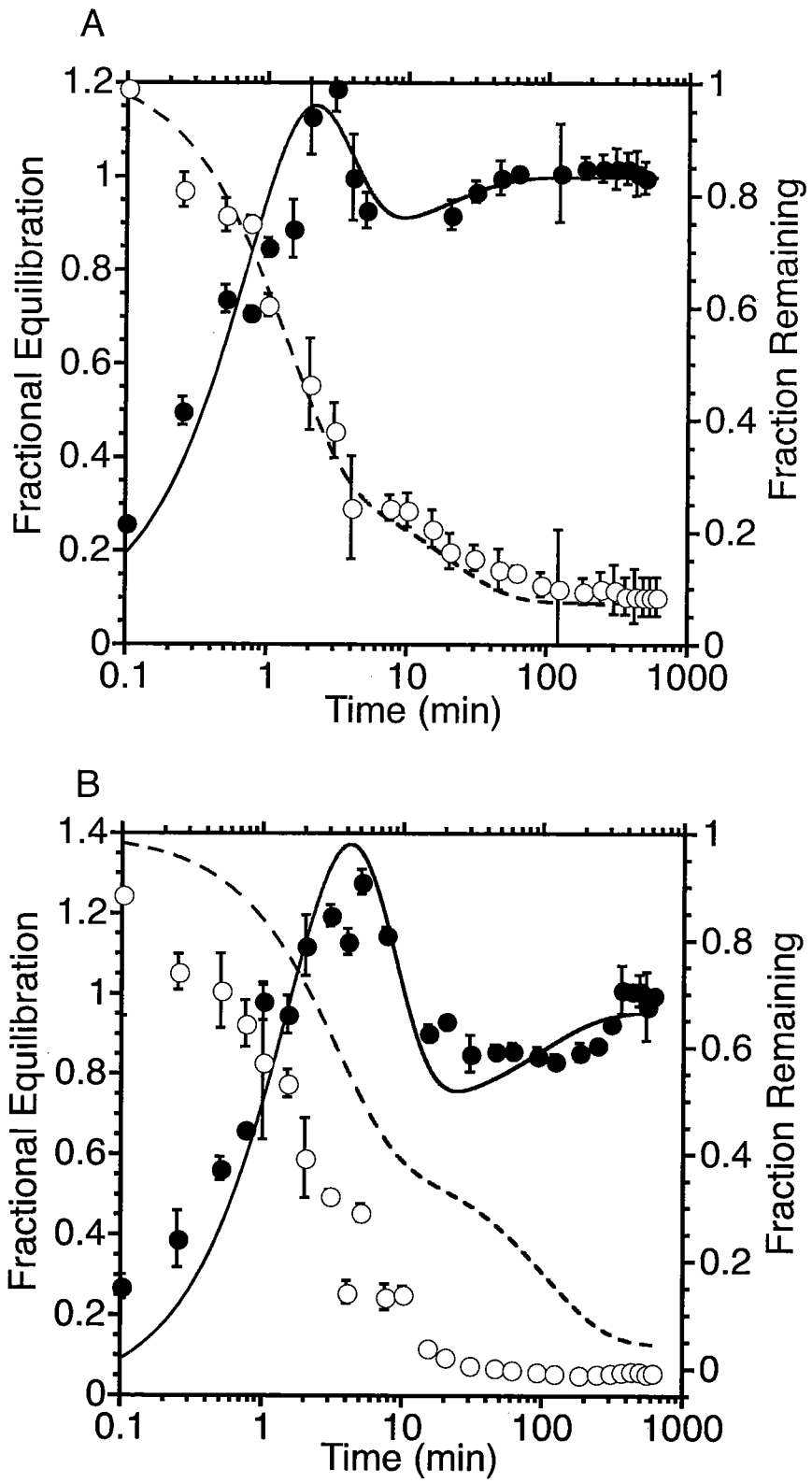
A
1.2
1
0.8
0.6
0.4
0.2
0
Fractional Equilibration
1
0.8
0.6
0.4
0.2
0
Fraction Remaining
0.1
1
10
100
1000
Time (min)
B
1.4
1.2
1
0.8
0.6
0.4
0.2
0
Fractional Equilibration
1
0.8
0.6
0.4
0.2
0
Fraction Remaining
0.1
1
10
100
1000
Time (min)

Figure 4.5. Simulations of Counterflow Transport in the Presence of ATP by a Fixed-Site Carrier and Diffusion Barrier Model.

Left Ordinate: fractional equilibration; Right Ordinate: fraction of intracellular sugar remaining; Abscissa: time in minutes (note log scale). **A.** Counterflow uptake of 100 μM ^{3}H-3MG (•) and exit of 2.5 mM ^{14}C-3MG (○) is shown in ghosts containing intracellular ATP. Transport simulation base on the fixed-site carrier and an additional diffusion barrier described by Eq. 4.4 is shown for uptake (—) and exit (·····). K = 1.5 mM, V = 1.4 mM min^{-1}, V_{ee} = 10 mM min^{-1}, α = 0.3, and λ = 10 for the fixed-site carrier and k_D = 0.01 min^{-1} and the fractional size of C_1 is 0.8. **B.** Counterflow uptake of 100 μM ^{3}H-3MG (•) and exit of 5 mM ^{14}C-3MG (○) is shown in ghosts containing intracellular ATP. Transport simulation base on the fixed-site carrier and an additional diffusion barrier described by Eq. 4.4 is shown for uptake (—) and exit (·····). K = 5.2 mM, V = 1.0 mM min^{-1}, V_{ee} = 4.7 mM min^{-1}, α = 0.1, and λ = 10 for the fixed-site carrier and k_D = 0.003 min^{-1} and the fractional size of C_1 is 0.67.

where the unidirectional flow of S from C1 to C2 in the presence of a second sugar P is

$$d^{S}_{C1\rightarrow C2}=\frac{V_1 S_{C1}}{K_1\left(1+\frac{P_{C1}}{K_1}+\frac{S_{C2}+P_{C2}}{K_2}\right)+S_{C1}} \qquad \text{Eq. 4.6}$$

where V_1 is V_{max} for the movement of substrate from C1 to C2, K_1 is the affinity constant for substrate in C1, and K_2 is the affinity constant for substrate in C2. The unidirectional flow from C2 to C1, $d^{S}_{C2\rightarrow C1}$, is obtained by interchanging C1 and C2 and subscripts 1 and 2 and $V_2K_1 = V_1K_2$. Movement of substrate P is obtained by interchanging S and P. In this model, both S and P in each compartments compete for movement between compartments.

Alternatively S and P to be competitive when present in the same compartment, while substrate in the other compartment behaves as non-competitive inhibitors. Here, the unidirectional flow from C1 to C2 is described by:

$$d^{S}_{C1\rightarrow C2}=\frac{\frac{V_d}{\left(1+\frac{S_{C2}+P_{C2}}{K_{I2}}\right)}S_{C1}}{K_m\left(1+\frac{P_{C1}}{K_m}\right)+S_{C1}} \qquad \text{Eq. 4.7}$$

where V_d is the maximal rate of movement between the two compartments, K_m is the affinity constant, K_2 is the inhibitory constant by substrate in compartment 2. Unidirectional flow from C2 to C1 is obtained by interchanging C2 and C1 and subscripts 1 and 2 where K_1 is the inhibitory constant by substrate in compartment 1. The flow for substrate P is obtained by interchanging S and P.

Both models can describe movement of substrate through two physical or chemical compartments. Figure 4.6 shows counterflow simulations where $d^{S}_{C2\rightarrow C1}$ is described by equation 4.7. Simulations with $d^{S}_{C2\rightarrow C1}$ described by equation 4.6 give similar results. The simulations show that an enzyme mediated diffusion process is capable of fitting both the counterflow transient and the undershoot of uptake very well. In fact, the simulations here fit the undershoot better than the simple diffusion model. The data show a lag in the refilling of the undershoot which can not be explained by simple diffusion, but appears to be fit well by an inhibited enzyme model. The inhibited enzyme model also allows sugar exit to be nearly monophasic. Exit is simulated as being biphasic, but the difference between the two rate constants is small enough that experimental data may appear monophasic. However, the simulated exit time course still does not fit well with experimental data. Simulated exit proceeds several times slower than observed exit. The predicted completion of exit coincides with the reversal of the undershoot while the data shows exit finishing upon completion of the counterflow transient.

Simulations with a single route of uptake and parallel exit pathways: In order that exit from both intracellular compartments may finish before the second compartments refills, the second intracellular compartment must exit directly to the extracellular space. Substrate in both intracellular compartments exits in parallel, but uptake occurs in series first through compartment 1 and then through compartment 2. The resulting flow path is as follows:

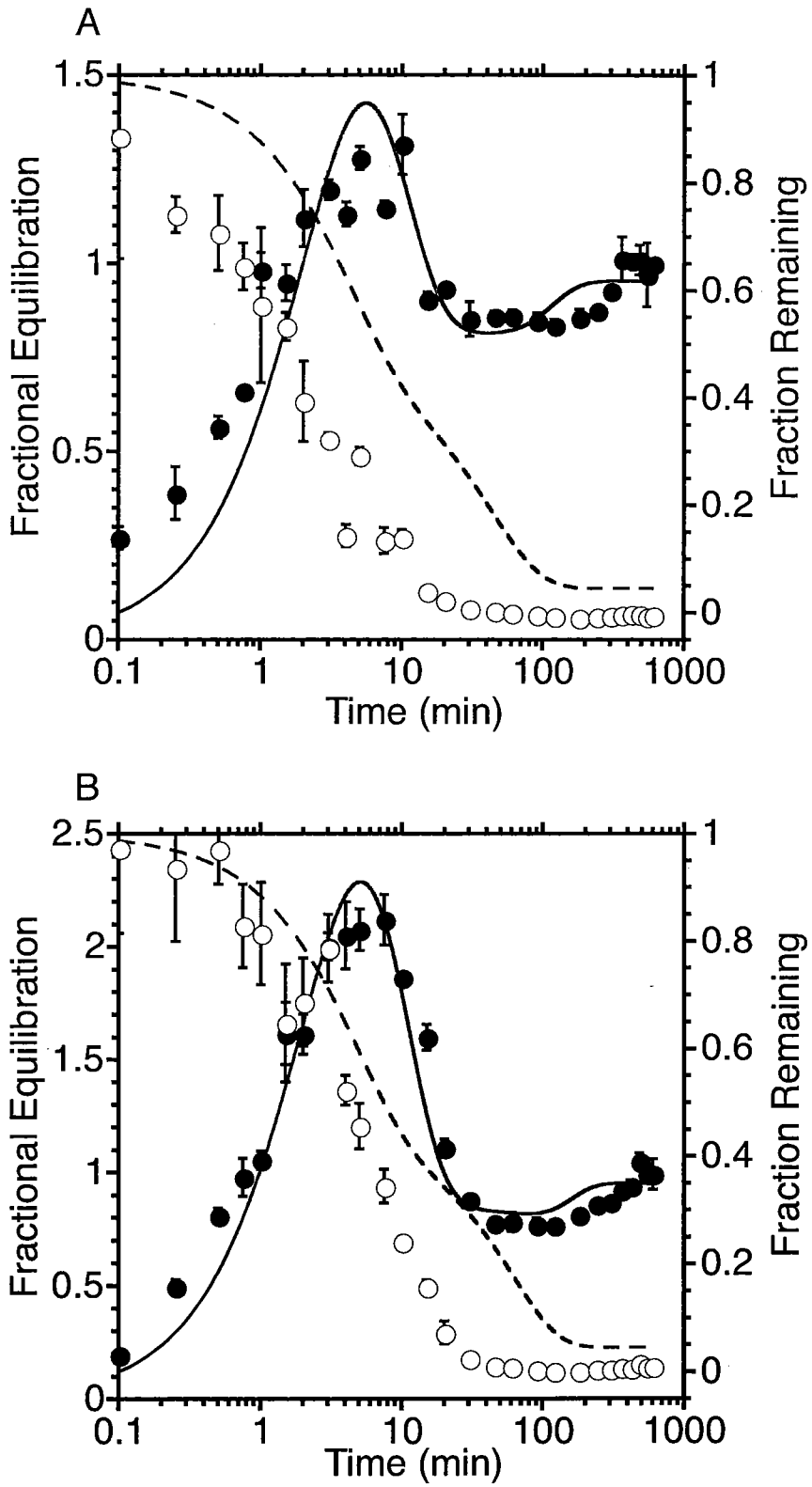
A
1.5
1
0.5
0
Fractional Equilibration
1
0.8
0.6
0.4
0.2
0
Fraction Remaining
0.1
1
10
100
1000
Time (min)
B
2.5
2
1.5
1
0.5
0
Fractional Equilibration
1
0.8
0.6
0.4
0.2
0
Fraction Remaining
0.1
1
10
100
1000
Time (min)

Figure 4.6. Simulations of Counterflow Transport in the Presence of ATP by a Fixed-Site Carrier and Enzyme Inhibition Diffusion Barrier Model.

Left Ordinate: fractional equilibration; Right Ordinate: fraction of intracellular sugar remaining;; Abscissa: time in minutes (note log scale). **A.** Counterflow uptake of 100 μM ^{3}H-3MG (•) and exit of 5 mM ^{14}C-3MG (○) is shown in ghosts containing intracellular ATP. **B.** Counterflow uptake of 100 μM ^{3}H-3MG (•) and exit of 10 mM ^{14}C-3MG (○) is shown in ghosts containing intracellular ATP. Transport simulation is based on the fixed-site carrier and an additional diffusion barrier described by Eq. 4.6 is shown for uptake (—) and exit (·····). K = 5.2 mM, V = 0.75 mM min^{-1}, V_{ee} = 4.2 mM min^{-1}, α = 0.1, and λ = 10 for the fixed-site carrier and K_m = 15 mM, V = 0.24 mM min^{-1}, K_{I1} = K_{I2} = 1 mM for diffusion and the fractional size of C1 is 0.67 for both A and B.

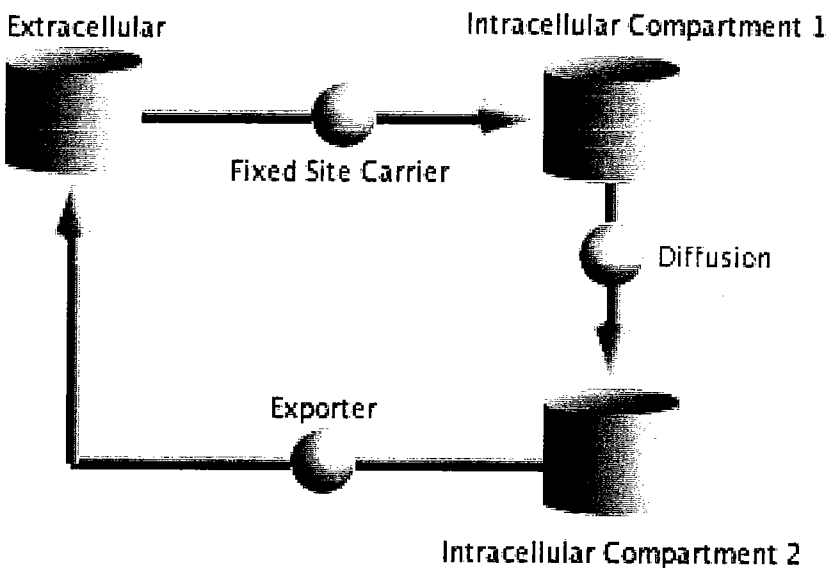

where substrate movement between the extracellular and intracellular compartment 1 (both uptake and exit) is through GLUT1 as a fixed-site carrier, movement between intracellular compartment 1 and compartment 2 (in both directions) is either simple diffusion (Eq. 4.4) or enzyme mediated (Eq. 4.6 or 4.7) and exit from compartment 2 is mediated through a specific sugar exporter.

Other transport kinetic experiments may give us insight into the mechanism of this proposed exporter. Biphasic sugar exit is observed under equilibrium exchange conditions suggesting that exit from compartment 2 proceeds through compartment 1 when sugar is present extracellularly. Also, unidirectional exit is biphasic under counterflow conditions when the initial intracellular 3MG concentration is 2.5 mM suggesting that there is a threshold sugar concentration in compartment 2 for activation of the exporter. Uptake appears to proceed into two compartments in series suggesting that the movement between the intracellular compartment 2 and extracellular space is nonreversible. By

permitting the proposed exporter to be active only when an intracellular activating site is filled and an extracellular inhibitory site is empty ensures that the there is a minimum intracellular concentration and little extracellular concentration as shown below.

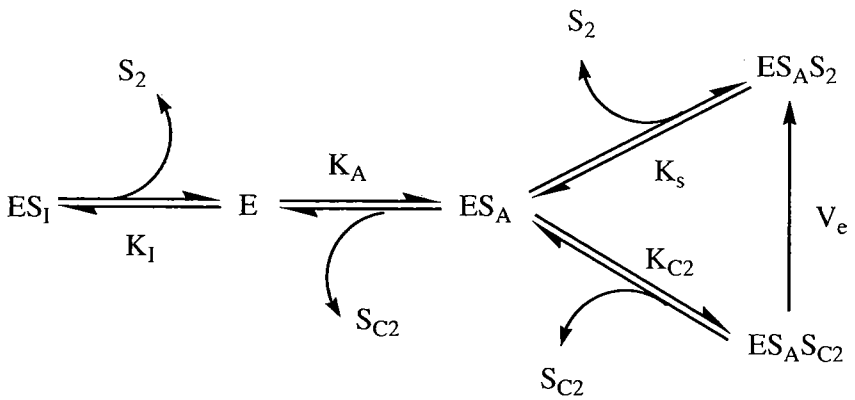

In this case, exit of substrate S is described by:

$$v^{S}_{C2\to 2} = \frac{\left(\frac{S_{C2}{}^{2}}{K_A K_{C2}} + \frac{P_{C2}S_{C2}}{K_A K_{C2}}\right)V_e}{1+\frac{S_{C2}+P_{C2}}{K_A} + \frac{S_{C2}{}^{2}+2P_{C2}S_{C2}+P_{C2}{}^{2}}{K_A K_{C2}} + \frac{S_{C2}S_2+S_{C2}P_2+P_{C2}S_2+P_{C2}P_2}{K_A K_2} + \frac{S_2+P_2}{K_I}} \quad \text{Eq. 4.8}$$

where S_{C2} is the concentration of S in the second intracellular compartment, P_{C2} is the concentration of P in the second intracellular compartment, S_2 and P_2 are the concentrations of S and P extracellularly (on side 2 of the membrane) and V_e is the V_{max} for export. K_{C2} and K_2 are the affinity constants for the active site in the intracellular compartment 2 and extracellularly, K_A is the affinity constant for an allosterically activating site in compartment 2, and K_I is the affinity constant for the extracellular inhibitory site. Exit of P can be obtained by interchanging S and P in the numerator. Figure 4.7 shows the simulated time course of counterflow transport with the scheme outlined above, where the movement between extracellular and intracellular compartment 1 is a fixed-site or simple

carrier, movement between intracellular compartment 1 and 2 is defined by simple diffusion (Eq. 4.4) and exit from compartment 2 into extracellular space is defined as above. Simulated uptake shows that the counterflow transient as well as the observed undershoot are fit well and exit is consistent with a single fast observed phase. While the second transporter model is able predict the observed counterflow time course for each individual initial intracellular 3MG concentration, the parameters required to do so are not internally consistent. This indicates that while the hypothesis has merit, the exact kinetics require additional refinement.

Hydrolyzable ATP is required for the counterflow undershoot: Transport simulations of 3MG counterflow data suggest that red cells compartmentalize intracellular sugar and that a large compartment is allowed to import and export sugar and the smaller compartment only allows sugar exit. For exit to be apparently nonreversible, the exit of sugar needs to be coupled to a second process. ATP hydrolysis is one possible candidate as ATP is required for the observed counterflow undershoot and the hydrolysis of ATP is coupled to a great number of other transporters. The use of the nonhydrolyzable ATP analogue 5'-adenylyl imidodiphosphate (AMP-PNP) has been previously shown to mimic ATP regulation of glucose transport in red cell ghosts (127). The fractional equilibration, measured at 30 minutes where the maximum undershoot occurs, is shown in Figure 4.8 for ghosts containing 0 ATP, 4 mM ATP, and 4 mM AMP-PNP. While ghosts resealed with ATP clearly show the undershoot by a fractional equilibrium of less than 1, the 0 ATP and AMP-PNP containing ghosts show a fractional equilibrium greater than 1.

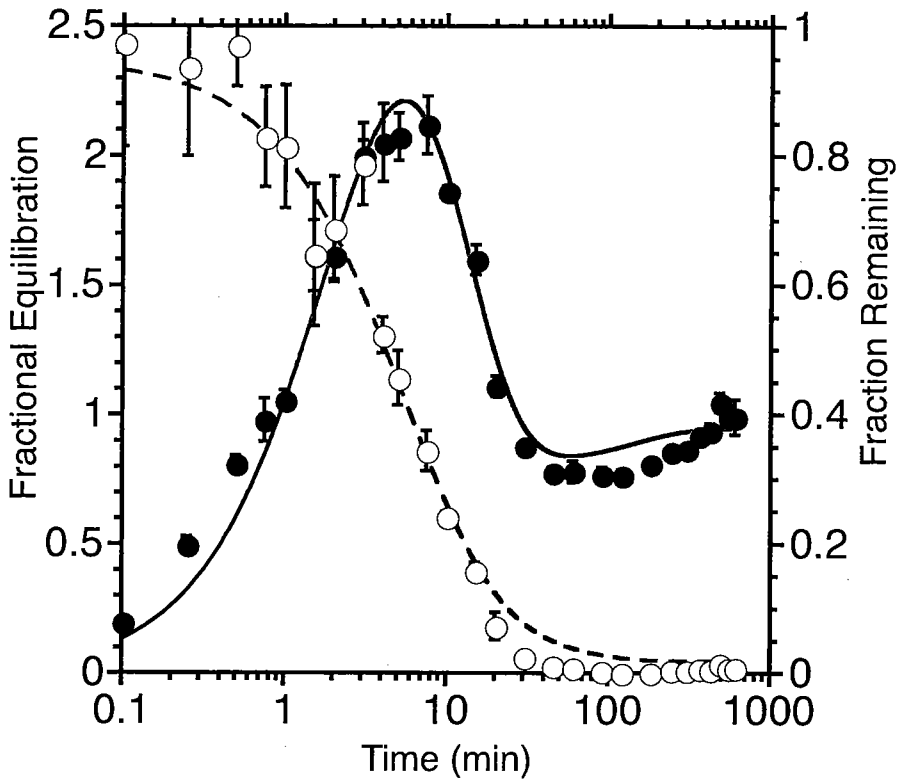

Figure 4.7. Simulation of Counterflow Transport with Intracellular Compartmentalization and a Sugar Exporter.

Ordinate: fractional equilibration and fraction remaining intracellular; Abscissa: time in minutes (note log scale). Counterflow uptake of 100 μM ^{3}H-3MG (•) and exit of 10 mM ^{14}C-3MG (○) is shown in ghosts containing intracellular ATP. Transport simulation is based on the fixed-site carrier, a diffusion barrier described by Eq. 4.4, and an exporter described by Eq. 4.8 is shown for uptake (—) and exit (·····). K = 5.2 mM, V = 0.75 mM min^{-1}, V_{ee} = 4.2 mM min^{-1}, α = 0.1, and λ = 10 for the fixed-site carrier, K_{C2} = 2 mM, K_2 = 10 mM K_A = 1 mM, V_e = 6 mM min^{-1}, K_I = 0.001 mM for diffusion and the fractional size of C1 is 0.67.

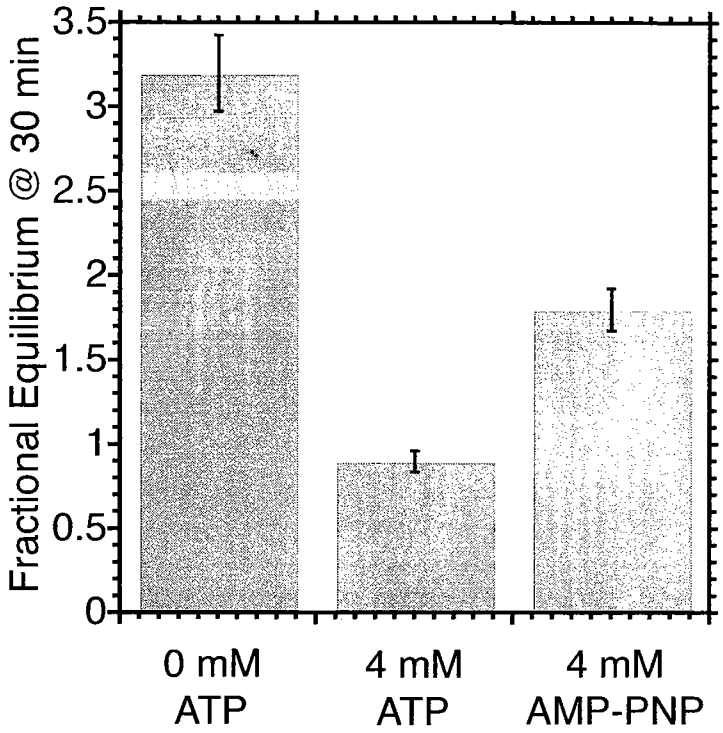

Figure 4.8. Affect of a Nonhydrolyzable ATP Analogue on the Counterflow Undershoot.

Ordinate: fractional equilibration at 30 minutes; Abscissa: Condition. 0 ATP, 4 mM ATP, and 4 mM AMP-PNP are resealed in erythrocyte ghosts containing 10 mM 3MG and assayed for fractional equilibrium of 100 μM ^{3}H-3MG uptake at 30 minutes. ATP induces the observed undershoot while AMP-PNP does not.

Discussion

Equilibrium exchange and net uptake of 3MG in human red cell ghosts containing intracellular ATP is consistent with transport occurring into two diffusionally isolated cytosolic compartments (*vide supra*) (113). In the present study, counterflow conditions are used to obtain a more detailed analysis of the proposed ATP dependent diffusion barrier. Counterflow transport, in which initial $[S_i] > [S_o]$ and unidirectional uptake is measured, is consistent with a fixed-site carrier mechanism and no cytosolic compartmentalization in the absence of cytoplasmic ATP. When ghosts are resealed with cytosolic ATP, counterflow transport displays kinetics that are inconsistent with a simple or fixed-site carrier. At low initial intracellular 3MG concentrations ($\leq$ 10 mM) the time course for counterflow displays an additional, previously undescribed feature. After the expected counterflow transient, where imported sugar is temporarily concentrated within the ghosts, fractional accumulation of extracellular sugar does not return to unity but instead falls to a value less than unity and then slowly rises. This observation has been attributed to the slow filling of a second cytosolic compartment. The undershoot is not an obligate consequence of a diffusional barrier however, and it is not observed at initial intracellular 3MG concentrations above 10 mM. This explains why the undershoot has not been previously described as previous counterflow experiments used conditions where the intracellular sugar concentration was 75 mM or greater (100, 110, 111, 234).

The addition of a simple diffusion barrier to transport simulations is unable to simulate the observed counterflow time course for both uptake and exit in the presence of

ATP. Transport simulations with an unstirred layer do show the newly observed undershoot, but require that exit be biphasic. Counterflow unidirectional exit displays monophasic kinetics at initial intracellular 3MG concentrations above 2.5 mM.

Cytochalasin B, an intracellular binding GLUT1 inhibitor is capable of inhibiting both phases of transport under equilibrium exchange conditions (*vide supra*). If sugar flux between the two intracellular compartments were enzyme mediated, then the CCB inhibition data and the counterflow time courses may be explained. While modeling flow between the intracellular compartments as an inhibitable, enzyme catalyzed reaction faithfully reproduces the experimental time course of uptake, it does not accurately describe the time course of exit. Exit simulations remain biphasic, but difference in rates of exit from intracellular compartment 1 into the extracellular space and exit from compartment 2 into compartment 1 become small so that exit almost appears as one phase. However, the simulated time course for exit is much longer than is actually observed.

Completion of the exit time course finishes with the counterflow transient and not with the refilling of the undershoot. This is indicative of a process where both intracellular compartments are capable of exporting sugar directly to interstitium in parallel, but only allowing uptake into compartments in series (compartment 1 fills directly, compartment 2 fills from compartment 1). Previous results suggest that if the cytosol is compartmentalized, both compartments must be adjacent to cell membrane as uridine transport remains monophasic in the presence of intracellular ATP (*vide supra*). If sugar in compartment 1 is accessible to the extracellular space through GLUT1, then for sugar in

compartment to be directly accessible to the extracelluar space as well, there must also be an additional sugar transporter in compartment 2.

Here, a hypothesis is presented wherein human red blood cells contain an intracellular diffusion barrier separating the cytosol into two compartments under ATP-replete conditions (Figure 4.9). The larger compartment is directly accessible to membrane containing GLUT1. The second cytosolic compartment is accessible to membrane containing a sugar transporter that appears to catalyze the irreversible export of sugar (based on transport simulations as models containing a reversible transport system between interstitium and compartment 2 do not simulate the observed time courses). Diffusion of sugar between the two compartments may or may not be mediated by an enzymatic process.

The transport simulations based on this hypothesis are capable of qualitatively fitting the observed counterflow time courses, however the exact parameters are inconsistent when comparisons are made between conditions of different initial intracellular 3MG loading concentrations. This shows that while the hypothesis may have merit, the mechanistic details for the flux of 3MG between the cytosolic compartments, and between the cytolic compartment and extracellular space remain unknown.

Proposed properties of the sugar exporter: There are several conditions placed on the activity of the hypothesized sugar export. 1) The exporter is inactive when intracellular [sugar] = extracellular [sugar]. Equilibrium exchange displays biphasic exchange for both uptake and exit suggesting that exit from the second intracellular compartment occurs via the first intracellular compartment (*vide supra*). If the proposed exporter were

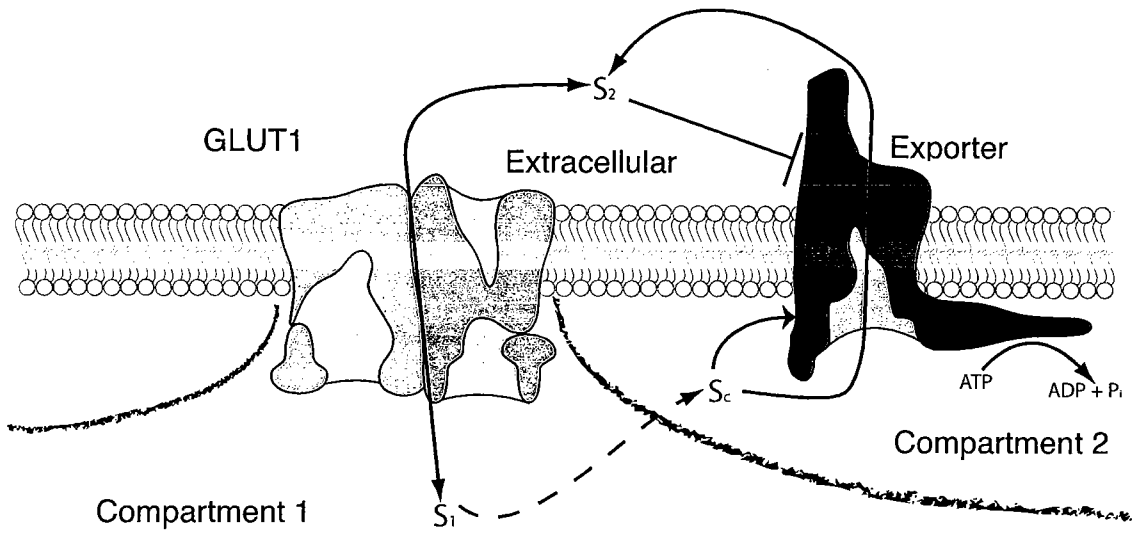

Figure 4.9. Exporter Hypothesis.

The intracellular space is divided into two compartments between which sugar can slowly diffuse. The sugar in compartment 1 is directly exchanged with extracellular sugar by GLUT1. The sugar in compartment 2 is directly effluxed into the extracellular space when the sugar concentration in compartment 2 is sufficiently high and when extracellular sugar concentration is sufficiently low.

active under exchange conditions, then exit would be monophasic. This would be accomplished if the exporter contained an extracellular sugar inhibition site. 2) The GLUT1 inhibitors cytochalasin B and/or phloretin also inhibit the exporter. If the exporter is not inhibitable by the stop solution, then sugar present in the second cytosolic compartment would be lost during the washing steps which removes extracellular sugar. This would cause the second phase of transport to be unobservable and the intracellular 3MG accessible volume would be less than intracellular uridine accessible volume (*vide supra*). 3) There is a minimal threshold for intracellular [sugar]. If the exporter were always active, then counterflow transport when the intracelluar 3MG concentration is 2.5 mM would display monophasic exit. Also, sub-saturating zero-trans exit would be monophasic which is not observed (data not shown). However, saturating zero-trans exit would appear monophasic (113).

Identification of plausible candidates for the sugar exporter: Recently the human red blood cell membrane proteome was analyzed by mass spectroscopy (235). Pasini *et. al.* found many, low-abundance integral membrane proteins of unknown or hypothetical function. Several of these may be good candidates for the hypothetical sugar exporter, including several ATP-binding cassette efflux pumps with currently unknown substrates.

GLUT1 is also a potential target as GLUT1 has been shown to have multiple functional states and oligomeric forms (85-87) and is an ATP binding protein (90, 124, 126). Could GLUT1 be acting as a fixed-site carrier in one membrane domain, and as a

sugar exporter in another? Purified GLUT1 has been shown to not hydrolyze ATP *in vitro*, however the proposed properties of the exporter (sensitivity to transmembrane glucose gradients) may make *in vitro* ATP assays difficult.

Physiological significance: What advantage is obtained from a glucose exporter in erythrocytes? Perhaps the benefit is not realized by the red cell, but rather, by cells to which glucose is subsequently transferred. When serum glucose levels fall acutely due to net transfer of glucose to tissue interstitium and cells, red cell cytoplasmic glucose (45-50% of total blood glucose) becomes a significant additional source of glucose. If 30-40% of the red cell glucose were compartmentalized such that it is available for rapid exit, but that space does not quickly reequilibrate, then the total blood sugar available for metabolizing tissues is increased by approximately 15% to 20%. Regulation of erythrocyte glucose transport therefore permits controlled expansion/contraction of the blood glucose space available for exchange with the interstitium of glycolytically active tissues. The effect may be most pronounced in skeletal muscle and in brain-endothelial capillaries. The plasma water space is relatively small in skeletal muscle (149) necessitating efficient extraction of blood glucose while the capillary bed is fenestrated thus facilitating rapid depletion of serum nutrients (151). Brain endothelial cells constitute only 0.1% of brain mass yet almost all of the glucose utilized by cerebral neurons and astrocytes must enter the brain by GLUT1-mediated, trans-endothelial cell transport (236). Hence efficient glucose transfer from blood to tissue is essential to both peripheral and central glucose homeostasis.

Conclusion

Counterflow 3MG transport in red ghosts containing intracellular ATP is not consistent with a simple diffusion barrier hypothesis. While the counterflow uptake can be simulated by a diffusion barrier, the simultaneous exit can not. Uptake is consistent with transport into two cytosolic, diffusionally isolated compartments, while unidirectional exit is consistent with export directly from both compartments. In order to qualitatively explain the observed behavior, a second glucose export process must be hypothesized.

Chapter V

CONCLUSIONS AND FUTURE DIRECTIONS

Glucose transport in human red blood cells displays a functional complexity that defies common mechanistic description, while glucose transport in non-primate red blood cells display simpler kinetics that fit with current models for carrier mediated transport. How is it that human red cells display kinetic anomalies whereas rat and rabbit red cells function as expected when the sequence identity of human GLUT1 and rat and rabbit GLUT1 is 98.4% (55, 103, 104)? Several lines of evidence now suggest that red cell factors other than GLUT1 primary structure contribute to human red cell glucose transport complexity. This thesis addresses several hypotheses for the mechanism of ATP regulation of erythrocyte glucose transport and how these can give rise to anomalous sugar transport behavior.

Previous reports have suggested the ATP-induced biphasic sugar exchange kinetics result from the fast exchange of sugar between interstitium and high-affinity cytosolic sugar binding sites, and the slow exchange of bound sugar with bulk cytosol (112). Data presented in this thesis are inconsistent with this hypothesis.

Equilibrium exchange transport of 3MG in human erythrocyte ghosts lacking ATP displays simple, single exponential kinetics which is consistent with the exchange of a single substrate between two compartments, extracellular interstitium and intracellular cytoplasm. Exchange transport in erythrocyte ghosts containing 4 mM ATP, however, de-

viates from single exponential kinetics. ATP-loaded ghosts display biphasic 3MG exchange for both unidirectional uptake and unidirectional exit where 67% of total sugar transported is faster than the exchange rate observed without ATP and the remaining 33% exchanged more slowly than the rate observed without ATP. This is consistent with either the exchange of two substrates between two compartments as above, or with the exchange of a single substrate between three compartments, interstitium and two diffusionally isolated cytosolic compartments.

The component sizes of biphasic exchange support the hypothesis that ATP induces GLUT1 anomeric discrimination as the anomeric proportions of both 3MG and D-glucose consist of 66.6% β-anomer and 33.3% α-anomer. Time course simulations confirm that the hypothesis is tenable, however several lines of direct experimental evidence refute this hypothesis. Biochemical analysis shows that GLUT1 displays little to no preference for either sugar anomer in the absence or presence of cytosolic ATP. Equilibrium exchange transport experiments with other GLUT1 sugar substrates with differing anomeric ratios display the same 66:33 ratio of biphasic component sizes as seen for 3MG. Massive acceleration of anomerization by exogenous mutarotase has little effect on the time course of D-glucose exchange in the presence of ATP when transport simulation predicts monophasic kinetics. Chromatographic analysis of intracellular equilibrium 3MG indicates only two species (α-3MG and β-3MG) comprising greater than 99% of total sugar.

The indefensibility of the two substrate, one intracellular compartment hypothesis suggests that red blood cell ghosts contain two intracellular compartments in the presence of ATP, and only contain one in the absence of ATP. The compartmentalization of red cell cytosol, however, is specific to 3MG as uridine exchange mediated by ENT1 is monophasic under all conditions. The two cytosolic sugar compartments are not due to high capacity sugar binding as the total intracellular 3MG and uridine spaces are equal and unaltered by intracellular ATP.

The ATP state is also associated with changes in red cell ghost morpholoy. Upon ATP depletion, normal red cell discosytes become highly crenated spheroechinocytes in which GLUT1 anisotropic membrane distribution appears to be lost. Chemically induced spheroechinocytosis causes a loss of biphasic transport even in the presence of replete ATP. Cytochalasin B, a potent GLUT1 and F-actin polymerization inhibitor is capable of inhibiting both phases of GLUT1 mediated exchange transport while other GLUT1 inhibitors inhibit only the fast phase of 3MG exchange.

Counterflow transport, in which unidirectional uptake is measured under conditions where the intracellular sugar concentration is greater than the extracellular sugar concentration, is consistent with the presence of two intracellular compartments in ATP replete ghosts. However, simultaneously measured unidirectional exit suggests that both compartments export intracellular sugar to interstitum at equal rates.

Together, these results suggest the following hypothesis. ATP replete human red blood cells are biconcave discocytes which contain two diffusionally isolated compart-

ments. Both compartments are adjacent to the red cell plasma membrane, but GLUT1 is found only in membrane patches abutting the larger cytosolic compartment. Membrane adjacent to the second, smaller compartment contains a specific glucose exporter. This exporter is allosterically regulated in a manner such that it is active only when intracompartmental [sugar] is high and extracellular [sugar] is low. The human equilibrative nucleoside transporter (ENT1) is imbedded in membrane adjacent to both compartments allowing efficient facilitated diffusion of uridine into total cytosol. Intracellular ATP depletion causes a morphological change whereby red blood cells become spheroechinocytes and the anisotropic distribution of GLUT1 and/or the diffusion barrier separating the two cytosolic compartments is lost. The sugar exporter is hypothesized to be ATP-dependent thereby accounting for its lack of activity under ATP-depleted conditions.

The physiological implications of this hypothesis are significant. Human red blood cells are thought not just to distribute oxygen to metabolizing tissues, but also to help in the delivery of energy in the form of glucose. There is ample evidence to suggest that both blood plasma glucose and red cell cytosolic glucose are capable of being depleted during capillary bed transit (153, 154). If 30% of red cell cytosol is able to quickly export glucose, but only slowly reequilibrate, during capillary transit, then the apparent glucose concentration available for uptake by metabolizing tissues is increased. If, for example, 4 mmoles of total blood (plasma and red cell cytosol) glucose were quickly removed from 1 L of whole blood containing 5 mM glucose, then the plasma glucose concentration available to metabolizing tissues would be 1.2 mM instead of the expected 1

mM. This is an apparent increase of ~20%. If red cells become ATP depleted, the cell morphology changes (becoming a spheroechinocyte), disrupting the cytosolic and GLUT1 compartmentalization allowing total red cell intracellular space to quickly fill and intracellular ATP levels to rise.

While the kinetic data presented in this thesis are consistent with the development of the above hypothesis, it is not sufficient to confirm the existence of compartmentalization of red cell cytosol and of a sugar exporter. Specific biochemical evidence is needed. The formulation and subsequent rejection of the differential anomer transport hypothesis presented in this thesis is a prime example of how kinetic analysis alone is insufficient.

The connection between red cell morphology and ATP modification of 3MG equilibrium exchange may or may not be causative. Reagents that artificially promote echinocytosis without changing intracellular ATP levels are useful in determining the exact relationship between cell shape and mono- or biphasic sugar exchange kinetics. Small chemical compounds such as 2,4-dinitrophenol and picric acid have been shown to induce echinocytosis at 4 °C (237). Investigating 3MG exchange kinetics in DNP or picric acid treated red cells will expand upon the role of red cell structure and function.DNP treatment causes the loss of biphasic 3MG exchange transport while not altering ATP levels. However, it is not known if DNP interferes with ATP binding to or action on GLUT1.

Red cell cytosolic factors involved in the formation of a diffusion barrier remain unknown although there is evidence to suggest that the membrane/cytoskeleton may be involved. 3MG exchange in the presence of chemical factors that alter the cytoskeleton

and do not inhibit GLUT1 or change intracellular ATP concentrations (157) would permit evaluation of the role of the cytoskeleton in the ATP regulation of erythrocyte glucose transport. Other members of the cytochalasin family (CCE and CCD) may be reagents of choice.

Direct visualization of diffusion in red cell cytosol may also confirm or reject the compartmentalization hypothesis. It was hoped that the use of 2-NBDG (a fluorescent glucose analog) would allow for temporal and spacial measurements of sugar uptake and exit into and out of red cell ghosts. However, 2-NBDG, while an inhibitor of GLUT1, is only a very poor substrate for GLUT1 mediated facilitated diffusion (data not shown). Yet, the use of 2-NBDG and/or other fluorescent water soluble probes may still allow for the visualization of a cytosolic diffusion barrier. Fluorescence loss in photobleaching (FLIP) experiments use 2-photon excitation to selectively and continuously photobleach a small volume of cytosol and the fluorescence loss in the surrounding area is observed (238). Fluorescent molecules that are directly accessible to the photobleaching volume quickly lose their fluorescence, while molecules that are diffusionally isolated remain fluorescent. FLIP has been used to study nuclear and cytoslic localization of Map kinases (239), the diffusional mobility of vesicle bound and free Ras GTPases (240), and compartmentalization of cytosol and periplasmic space during the prokaryote caulobacter cell division (241). The same analysis could, in principle, be applied to red cell ghosts to visualize 2-NBDG compartmentalization. An alternative approach is to use a fluorescent glucose binding protein recently developed (Anthony Cura, unpublished results) (242) to

spatially visualize glucose or 3MG uptake. However, the dimensions of the red cell compartments may be too small for the resolution limit of light microscopy (~200 nm).

The hypothetical sugar exporter also requires biochemical identification and further characterization. Several sugar transport experiments in erythrocyte ghosts will help to characterize the exporter. If human red blood cells contain an ATP-dependent sugar exporter, then inside-out vesicles prepared from red blood cell membranes should show a burst of ATP hydrolysis when exposed to a sufficient concentration of 3MG. Similarly, raising the extracellular sugar concentration and monitoring the time course of 10 mM 3MG exit from ghosts resealed with ATP will identify the minimal external concentration that inhibits the exporter. The above hypothesis predicts that the time course of exit should become biphasic above some external 3MG concentration. Identification of the sugar exporter may prove difficult, but biochemical and proteomic approaches may serve in fishing out the proposed transporter. Labeling of red cell erythrocyte membrane proteins with reactive glucose derivatives in conjunction with mass spectrometry should allow the identification of potential targets. Several hexose-modified protein labeling reagents are available, and it has been reported that glucosyl- and maltosyl-isothiocyanates label Band 3 proteins (243)(244) while an aryl azide glucose derivative labels Band 1, Band 3, and Band 4.5 (245). Labeling of non-GLUT1 proteins should be glucose or maltose inhibitable and perhaps cytochalasin B or ATP sensitive.

The work presented in this thesis advances the knowledge of human red cell glucose transport and expands the role played of erythrocytes in human glucose homeostasis.

While it has been thought that glucose transport is regulated in human red cells by ATP, it was unclear how red cell intracellular ATP levels would fall in response to the metabolic demand of other tissues. The hypothesis detailed here offers a plausible explanation by which the ATP-replete red cell is primed for export of intracellular sugar when plasma glucose levels fall, and the ATP-depleted red cell can quickly reequilibrate total cytosolic glucose levels through GLUT1.

BIBLIOGRAPHY

(1) Widdas, W. F. (1952) Inability of diffusion to account for placental glucose transfer in the sheep and consideration of the kinetics of a possible carrier transfer. J. Physiol. (London) 118, 23–39.

(2) Stein, W. D. (1986) Transport and diffusion across cell membranes, Academic Press, New York.

(3) Lieb, W. R., and Stein, W. D. (1974) Testing and characterizing the simpler pore. Biochim. Biophys. Acta 373, 165-177.

(4) Trimmer, J. S., and Agnew, W. S. (1989) Molecular diversity of voltage-sensitive Na channels. Annu. Rev. Physiol. 51, 401-418.

(5) MacKinnon, R. (2003) Potassium channels. FEBS Lett 555, 62-5.

(6) Lieb, W. R., and Stein, W. D. (1974) Testing and characterizing the simple carrier. Biochim. Biophys. Acta 373, 178–196.

(7) Baker, G. F., Basketter, D. A., and Widdas, W. F. (1978) Asymmetry of the hexose transfer system in human erythrocytes. Experiments with non-transportable inhibitors. J Physiol (Lond) 278, 377-88.

(8) Amzel, L. M., and Pedersen, P. L. (1983) Proton atpases: structure and mechanism. Annu Rev Biochem 52, 801-824.

(9) Hediger, M. A., Budarf, M. L., Emanuel, B. S., Mohandas, T. K., and Wright, E. M. (1989) Assignment of the human intestinal Na+/glucose cotransporter gene (SGLT1) to the q11.2----qter region of chromosome 22. Genomics 4, 297-300.

(10) Ren, Q., Kang, K. H., and Paulsen, I. T. (2004) TransportDB: a relational database of cellular membrane transport systems. Nucleic Acids Res 32, D284-8.

(11) Czech, M. P. (1980) Insulin action and the regulation of hexose transport. Diabetes 29, 399-409.

(12) Alonso, M. J., Heine-Suner, D., Calvo, M., Rosell, J., Gimenez, J., Ramos, M. D., Telleria, J. J., Palacio, A., Estivill, X., and Casals, T. b. (2007) Spectrum of mutations in the CFTR gene in cystic fibrosis patients of Spanish ancestry. Ann Hum Genet 71, 194-201.

(13) Schmitt, N., Calloe, K., Nielsen, N. H., Buschmann, M., Speckmann, E. J., Schulze-Bahr, E., and Schwarz, M. (2007) The novel C-terminal KCNQ1 mutation M520R alters protein trafficking. Biochem Biophys Res Commun 358, 304-10.

(14) Ocorr, K., Reeves, N. L., Wessells, R. J., Fink, M., Chen, H. S., Akasaka, T., Yasuda, S., Metzger, J. M., Giles, W., Posakony, J. W., and Bodmer, R. (2007) KCNQ potassium channel mutations cause cardiac arrhythmias in Drosophila that mimic the effects of aging. Proc Natl Acad Sci U S A 104, 3943-8.

(15) Monty, J. F., Llanos, R. M., Mercer, J. F., and Kramer, D. R. (2005) Copper exposure induces trafficking of the menkes protein in intestinal epithelium of ATP7A transgenic mice. J Nutr 135, 2762-6.

(16) Richardson, D. R., and Suryo Rahmanto, Y. (2007) Differential regulation of the Menkes and Wilson disease copper transporters by hormones: an integrated model of metal transport in the placenta. Biochem J 402, e1-3.

(17) Pfeiffer, R. F. (2007) Wilson's Disease. Semin Neurol 27, 123-32.

(18) Leggio, L., Gasbarrini, G., and Addolorato, G. (2007) Wilson's disease. Lancet 369, 902.

(19) Dawson, R. J., and Locher, K. P. (2007) Structure of the multidrug ABC transporter Sav1866 from Staphylococcus aureus in complex with AMP-PNP. FEBS Lett 581, 935-8.

(20) Gottschalk, B., Broker, G., Kuhn, M., Aymanns, S., Gleich-Theurer, U., and Spellerberg, B. (2006) Transport of multidrug resistance substrates by the Streptococcus agalactiae hemolysin transporter. J Bacteriol 188, 5984-92.

(21) Seidner, G., Alvarez, M. G., Yeh, J. I., O'Driscoll, K. R., Klepper, J., Stump, T. S., Wang, D., Spinner, N. B., Birnbaum, M. J., and De Vivo, D. C. (1998) GLUT-1 deficiency syndrome caused by haploinsufficiency of the blood-brain barrier hexose carrier. Nat Genet 18, 188-91.

(22) Klepper, J., and Voit, T. (2002) Facilitated glucose transporter protein type 1 (GLUT1) deficiency syndrome: impaired glucose transport into brain-- a review. Eur J Pediatr 161, 295-304.

(23) Joost, H. G., Bell, G. I., Best, J. D., Birnbaum, M. J., Charron, M. J., Chen, Y. T., Doege, H., James, D. E., Lodish, H. F., Moley, K. H., Moley, J. F., Mueckler, M.,

Rogers, S., Schurmann, A., Seino, S., and Thorens, B. (2002) Nomenclature of the GLUT/SLC2A family of sugar/polyol transport facilitators. Am J Physiol Endocrinol Metab 282, E974-6.

(24) Wood, I. S., and Trayhurn, P. (2003) Glucose transporters (GLUT and SGLT): expanded families of sugar transport proteins. Br J Nutr 89, 3-9.

(25) Kayano, T., Burant, C. F., Fukumoto, H., Gould, G. W., Fan, Y. S., Eddy, R. L., Byers, M. G., Shows, T. B., Seino, S., and Bell, G. I. (1990) Human facilitative glucose transporters. Isolation, functional characterization, and gene localization of cDNAs encoding an isoform (GLUT5) expressed in small intestine, kidney, muscle, and adipose tissue and an unusual glucose transporter pseudogene-like sequence (GLUT6). J. Biol. Chem. 265, 13276-82.

(26) Li, S. R., Alcolado, J. C., Stocks, J., Baroni, M. G., Oelbaum, R. S., and Galton, D. J. (1991) Genetic polymorphisms at the human liver/islet glucose transporter (GLUT2) gene locus in Caucasian and West Indian subjects with type 2 (non-insulin-dependent) diabetes mellitus. Biochimica et Biophysica Acta 1097, 293-8.

(27) Patel, P., Bell, G. I., Cook, J. T., Turner, R. C., and Wainscoat, J. S. (1991) Multiple restriction fragment length polymorphisms at the GLUT2 locus: GLUT2 haplotypes for genetic analysis of type 2 (non-insulin-dependent) diabetes mellitus. Diabetologia 34, 817-21.

(28) Oelbaum, R. S. (1992) Analysis of three glucose transporter genes in a Caucasian population: no associations with non-insulin-dependent diabetes and obesity. Clinical Genetics 42, 260-6.

(29) Uldry, M., Ibberson, M., Hosokawa, M., and Thorens, B. (2002) GLUT2 is a high affinity glucosamine transporter. FEBS Lett 524, 199-203.

(30) Haber, R. S., Weinstein, S. P., O'Boyle, E., and Morgello, S. (1993) Tissue distribution of the human GLUT3 glucose transporter. Endocrinology 132, 2538-43.

(31) Maher, F., Vannucci, S. J., and Simpson, I. A. (1993) Glucose transporter isoforms in brain: absence of GLUT3 from the blood-brain barrier. Journal of Cerebral Blood Flow & Metabolism 13, 342-5.

(32) Yano, H., Seino, Y., Inagaki, N., Hinokio, Y., Yamamoto, T., Yasuda, K., Masuda, K., Someya, Y., and Imura, H. (1991) Tissue distribution and species difference of the brain type glucose transporter (GLUT3). Biochem Biophys Res Commun 174, 470-7.

(33) Kern, M., Wells, J. A., Stephens, J. M., Elton, C. W., Friedman, J. E., Tapscott, E. B., Pekala, P. H., and Dohm, G. L. (1990) Insulin responsiveness in skeletal muscle is determined by glucose transporter (Glut4) protein level. Biochemical Journal 270, 397-400.

(34) Davidson, N. O., Hausman, A. M., Ifkovits, C. A., Buse, J. B., Gould, G. W., Burant, C. F., and Bell, G. I. (1992) Human intestinal glucose transporter expression and localization of GLUT5. American Journal of Physiology.

(35) Concha, II, Velasquez, F. V., Martinez, J. M., Angulo, C., Droppelmann, A., Reyes, A. M., Slebe, J. C., Vera, J. C., and Golde, D. W. (1997) Human erythrocytes express GLUT5 and transport fructose. Blood 89, 4190-5.

(36) Mueckler, M. (1994) Facilitative glucose transporters. Eur J Biochem 219, 713-25.

(37) Joost, H. G., and Thorens, B. (2001) The extended GLUT-family of sugar/polyol transport facilitators: nomenclature, sequence characteristics, and potential function of its novel members (review). Mol Membr Biol 18, 247-56.

(38) Wu, X., Li, W., Sharma, V., Godzik, A., and Freeze, H. H. (2002) Cloning and characterization of glucose transporter 11, a novel sugar transporter that is alternatively spliced in various tissues. Mol Genet Metab 76, 37-45.

(39) Doege, H., Bocianski, A., Scheepers, A., Axer, H., Eckel, J., Joost, H. G., and Schurmann, A. (2001) Characterization of human glucose transporter (GLUT) 11 (encoded by SLC2A11), a novel sugar-transport facilitator specifically expressed in heart and skeletal muscle. Biochem J 359, 443-9.

(40) Carayannopoulos, M. O., Chi, M. M., Cui, Y., Pingsterhaus, J. M., McKnight, R. A., Mueckler, M., Devaskar, S. U., and Moley, K. H. (2000) GLUT8 is a glucose transporter responsible for insulin-stimulated glucose uptake in the blastocyst. Proc Natl Acad Sci U S A 97, 7313-8.

(41) Dawson, P. A., Mychaleckyj, J. C., Fossey, S. C., Mihic, S. J., Craddock, A. L., and Bowden, D. W. (2001) Sequence and functional analysis of glut10: a glucose

transporter in the type 2 diabetes-linked region of chromosome 20q12-13.1. Mol Genet Metab 74, 186-99.

(42) Andersen, G., Rose, C. S., Hamid, Y. H., Drivsholm, T., Borch-Johnsen, K., Hansen, T., and Pedersen, O. (2003) Genetic variation of the GLUT10 glucose transporter (SLC2A10) and relationships to type 2 diabetes and intermediary traits. Diabetes 52, 2445-8.

(43) Rogers, S., Chandler, J. D., Clarke, A. L., Petrou, S., and Best, J. D. (2003) Glucose transporter GLUT12-functional characterization in Xenopus laevis oocytes. Biochem Biophys Res Commun 308, 422-6.

(44) Marger, M. D., and Saier, M. J. (1993) A major superfamily of transmembrane facilitators that catalyse uniport, symport and antiport [see comments]. [Review]. Trends in Biochemical Sciences 18, 13-20.

(45) Pao, S. S., Paulsen, I. T., and Saier, M. H., Jr. (1998) Major facilitator superfamily. Microbiol Mol Biol Rev 62, 1-34.

(46) Saier, M. H., Jr., Beatty, J. T., Goffeau, A., Harley, K. T., Heijne, W. H., Huang, S. C., Jack, D. L., Jahn, P. S., Lew, K., Liu, J., Pao, S. S., Paulsen, I. T., Tseng, T. T., and Virk, P. S. (1999) The major facilitator superfamily. J Mol Microbiol Biotechnol 1, 257-79.

(47) Abramson, J., Kaback, H. R., and Iwata, S. (2004) Structural comparison of lactose permease and the glycerol-3-phosphate antiporter: members of the major facilitator superfamily. Curr Opin Struct Biol 14, 413-9.

(48) Abramson, J., Smirnova, I., Kasho, V., Verner, G., Kaback, H. R., and Iwata, S. (2003) Structure and mechanism of the lactose permease of Escherichia coli. Science 301, 610-5.

(49) Huang, Y., Lemieux, M. J., Song, J., Auer, M., and Wang, D. N. (2003) Structure and mechanism of the glycerol-3-phosphate transporter from Escherichia coli. Science 301, 616-20.

(50) Hirai, T., Heymann, J. A., Maloney, P. C., and Subramaniam, S. (2003) Structural model for 12-helix transporters belonging to the major facilitator superfamily. J Bacteriol 185, 1712-8.

(51) Hirai, T., Heymann, J. A., Shi, D., Sarker, R., Maloney, P. C., and Subramaniam, S. (2002) Three-dimensional structure of a bacterial oxalate transporter. Nat Struct Biol 9, 597-600.

(52) Purhonen, P., Lundback, A. K., Lemonnier, R., Leblanc, G., and Hebert, H. (2005) Three-dimensional structure of the sugar symporter melibiose permease from cryo-electron microscopy. J Struct Biol 152, 76-83.

(53) Kaback, H. R. (2005) Structure and mechanism of the lactose permease. C R Biol 328, 557-67.

(54) Guan, L., and Kaback, H. R. (2006) Lessons from lactose permease. Annu Rev Biophys Biomol Struct 35, 67-91.

(55) Mueckler, M., Caruso, C., Baldwin, S. A., Panico, M., Blench, I., Morris, H. R., Allard, W. J., Lienhard, G. E., and Lodish, H. F. (1985) Sequence and structure of a human glucose transporter. Science 229, 941-945.

(56) Hresko, R. C., Kruse, M., Strube, M., and Mueckler, M. (1994) Topology of the Glut 1 glucose transporter deduced from glycosylation scanning mutagenesis. J. Biol. Chem. 269, 20482-8.

(57) Olsowski, A., Monden, I., and Keller, K. (1998) Cysteine-scanning mutagenesis of flanking regions at the boundary between external loop I or IV and transmembrane segment II or VII in the GLUT1 glucose transporter. Biochemistry 37, 10738-45.

(58) Hruz, P. W., and Mueckler, M. M. (1999) Cysteine-scanning mutagenesis of transmembrane segment 7 of the GLUT1 glucose transporter. J Biol Chem 274, 36176-80.

(59) Mueckler, M., and Makepeace, C. (2006) Transmembrane segment 12 of the Glut1 glucose transporter is an outer helix and is not directly involved in the transport mechanism. J Biol Chem 281, 36993-8.

(60) Mueckler, M., and Makepeace, C. (2005) Cysteine-scanning mutagenesis and substituted cysteine accessibility analysis of transmembrane segment 4 of the Glut1 glucose transporter. J Biol Chem 280, 39562-8.

(61) Mueckler, M., Roach, W., and Makepeace, C. (2004) Transmembrane segment 3 of the Glut1 glucose transporter is an outer helix. J Biol Chem 279, 46876-81.

(62) Hruz, P. W., and Mueckler, M. M. (2000) Cysteine-scanning mutagenesis of transmembrane segment 11 of the GLUT1 facilitative glucose transporter. Biochemistry 39, 9367-72.

(63) Mueckler, M., and Makepeace, C. (1999) Transmembrane segment 5 of the Glut1 glucose transporter is an amphipathic helix that forms part of the sugar permeation pathway. J Biol Chem 274, 10923-6.

(64) Deziel, M. R., Jung, C. Y., and Rothstein, A. (1985) The topology of the major band 4.5 protein component of the human erythrocyte membrane: characterization of reactive cysteine residues. Biochim Biophys Acta 819, 83-92.

(65) Heinze, M., Monden, I., and Keller, K. (2004) Cysteine-scanning mutagenesis of transmembrane segment 1 of glucose transporter GLUT1: extracellular accessibility of helix positions. Biochemistry 43, 931-6.

(66) Olsowski, A., Monden, I., Krause, G., and Keller, K. (2000) Cysteine scanning mutagenesis of helices 2 and 7 in GLUT1 identifies an exofacial cleft in both transmembrane segments. Biochemistry 39, 2469-74.

(67) Mueckler, M., and Makepeace, C. (2004) Analysis of transmembrane segment 8 of the GLUT1 glucose transporter by cysteine-scanning mutagenesis and substituted cysteine accessibility. J Biol Chem 279, 10494-9.

(68) Mueckler, M., and Makepeace, C. (2002) Analysis of transmembrane segment 10 of the Glut1 glucose transporter by cysteine-scanning mutagenesis and substituted cysteine accessibility. J Biol Chem 277, 3498-503.

(69) Jarvis, S. M., Hammond, J. R., Paterson, A. R., and Clanachan, A. S. (1983) Nucleoside transport in human erythrocytes. A simple carrier with directional symmetry in fresh cells, but with directional asymmetry in cells from outdated blood. Biochem J 210, 457-61.

(70) Plagemann, P. G., Wohlhueter, R. M., and Erbe, J. (1982) Nucleoside transport in human erythrocytes. A simple carrier with directional symmetry and differential mobility of loaded and empty carrier. J Biol Chem 257, 12069-74.

(71) Ginsburg, H., and Cabantchik, Z. I. (1977) On uridine transport in human red blood cells. J Gen Physiol 70, 679-80.

(72) Cabantchik, Z. I., and Ginsburg, H. (1977) Transport of uridine in human red blood cells. Demonstration of a simple carrier-mediated process. J Gen Physiol 69, 75-96.

(73) Rosenberg, R. (1981) L-Leucine transport in human red blood cells: a detailed kinetic analysis. J Membr Biol 62, 79-93.

(74) Hoare, D. G. (1972) The transport of L-leucine in human erythrocytes: a new kinetic analysis. J Physiol 221, 311-29.

(75) Carruthers, A. (1990) Facilitated diffusion of glucose. Physiol. Rev. 70, 1135-1176.

(76) Miller, D. M. (1968) The kinetics of selective biological transport. IV. Assessment of three carrier systems using the erythrocyte-monosaccharide transport data. Biophys J 8, 1339-52.

(77) Lowe, A. G., and Walmsley, A. R. (1986) The kinetics of glucose transport in human red blood cells. Biochim. Biophys. Acta 857, 146-154.

(78) Karlish, S. J. D., Lieb, W. R., Ram, D., and Stein, W. D. (1972) Kinetic Parameters of glucose efflux from human red blood cells under zero-trans conditions. Biochim. Biophys. Acta 255, 126-132.

(79) Baker, G. F., and Naftalin, R. J. (1979) Evidence of multiple operational affinities for D-glucose inside the human erythrocyte membrane. Biochim. Biophys. Acta 550, 474-484.

(80) Carruthers, A., and Melchior, D. L. (1983) Asymmetric or symmetric? Cytosolic modulation of human erythrocyte hexose transfer. Biochim. Biophys. Acta 728, 254-266.

(81) Hankin, B. L., Lieb, W. R., and Stein, W. D. (1972) Rejection criteria for the asymmetric carrier and their application to glucose transport in the human red blood cell. Biochim. Biophys. Acta 288, 114-126.

(82) Lieb, W. R., and Stein, W. D. (1977) Is there a high affinity site for sugar transport at the inner face of the human red cell membrane? J. Theor. Biol. 69, 311-319.

(83) Harris, E. J. (1983) An analytical study of the kinetics of glucose movement in human erythrocytes. J. Physiol. 173, 344-353.

(84) Taylor, L. P., and Holman, G. D. (1981) Symmetrical kinetic parameters for 3-O-methyl-D-glucose transport in adipocytes in the presence and in the absence of insulin. Biochim. Biophys. Acta 642, 325-335.

(85) Hebert, D. N., and Carruthers, A. (1991) Cholate-solubilized erythrocyte glucose transporters exist as a mixture of homodimers and homotetramers. Biochemistry 30, 4654-4658.

(86) Graybill, C., van Hoek, A. N., Desai, D., Carruthers, A. M., and Carruthers, A. (2006) Ultrastructure of human erythrocyte GLUT1. Biochemistry 45, 8096-107.

(87) Zottola, R. J., Cloherty, E. K., Coderre, P. E., Hansen, A., Hebert, D. N., and Carruthers, A. (1995) Glucose transporter function is controlled by transporter oligomeric structure. A single, intramolecular disulfide promotes GLUT1 tetramerization. Biochemistry 34, 9734-47.

(88) Pessino, A., Hebert, D. N., Woon, C. W., Harrison, S. A., Clancy, B. M., Buxton, J. M., Carruthers, A., and Czech, M. P. (1991) Evidence that functional erythrocyte-type glucose transporters are oligomers. J. Biol. Chem. 266, 20213-20217.

(89) Levine, K. B., Hamill, S., Cloherty, E. K., and Carruthers, A. (2001) Alanine Scanning Mutagenesis of the Human Erythrocyte Glucose Transporter Putative ATP Binding Domain. Blood Cells, Molecules and Disease 27, 139-142.

(90) Cloherty, E. K., Levine, K. B., and Carruthers, A. (2001) The red blood cell glucose transporter presents multiple, nucleotide-sensitive sugar exit sites. Biochemistry 40, 15549-61.

(91) Hebert, D. N., and Carruthers, A. (1992) Glucose transporter oligomeric structure determines transporter function. Reversible redox-dependent interconversions of tetrameric and dimeric GLUT1. J. Biol. Chem. 267, 23829-38.

(92) Helgerson, A. L., and Carruthers, A. (1987) Equilibrium ligand binding to the human erythrocyte sugar transporter. Evidence for two sugar-binding sites per carrier. J. Biol. Chem. 262, 5464-5475.

(93) Carruthers, A., and Helgerson, A. L. (1991) Inhibitions of sugar transport produced by ligands binding at opposite sides of the membrane. Evidence for simultaneous occupation of the carrier by maltose and cytochalasin B. Biochemistry 30, 3907-15.

(94) Sultzman, L. A., and Carruthers, A. (1999) Stop-flow analysis of cooperative interactions between GLUT1 sugar import and export sites. Biochemistry 38, 6640-50.

(95) Hamill, S., Cloherty, E. K., and Carruthers, A. (1999) The human erythrocyte sugar transporter presents two sugar import sites. Biochemistry 38, 16974-83.

(96) Baker, G. F., and Widdas, W. F. (1973) The asymmetry of the facilitated transfer system for hexoses in human red cells and the simple kinetics of a two component model. J. Physiol. (London) 231, 143–165.

(97) Naftalin, R. J., and Holman, G. D. (1977) Transport of sugars in human red cells, in Membrane transport in red cells (Ellory, J. C., and Lew, V. L., Eds.) pp 257-300, Academic Press, New York.

(98) Holman, G. D. (1980) An allosteric pore model for sugar transport in human erythrocytes. Biochim. Biophys. Acta 599, 202–213.

(99) Carruthers, A. (1991) Mechanisms for the facilitated diffusion of substrates across cell membranes. Biochemistry 30, 3898-3906.

(100) Helgerson, A. L., and Carruthers, A. (1989) Analysis of protein-mediated 3-O-methylglucose transport in rat erythrocytes: rejection of the alternating conformation carrier model for sugar transport. Biochemistry 28, 4580-4594.

(101) Naftalin, R. J., and Rist, R. J. (1994) Re-examination of hexose exchanges using rat erythrocytes: evidence inconsistent with a one-site sequential exchange model, but consistent with a two-site simultaneous exchange model. Biochimica et Biophysica Acta 1191, 65-78.

(102) Regen, D. M., and Morgan, H. E. (1964) Studies of the glucose-transport system in the rabbit erythrocyte. Biochim. Biophys Acta 79, 151-166.

(103) Birnbaum, M. J., Haspel, H. C., and Rosen, O. M. (1986) Cloning and characterization of a cDNA encoding the rat brain glucose- transporter protein. Proc. Natl. Acad. Sci. USA 83, 5784-5788.

(104) Asano, T., Shibasaki, Y., Kasuga, M., Kanazawa, Y., Takaku, F., Akanuma, Y., and Oka, Y. (1988) Cloning of a rabbit brain glucose transporter cDNA and alteration ofglucose transporter mRNA during tissue development. Biochem. Biophys. Res. Commun. 154, 1204-1211.

(105) Altschul, S. F. (1991) Amino acid substitution matrices from an information theoretic perspective. J Mol Biol 219, 555-65.

(106) Cloherty, E. K., Heard, K. S., and Carruthers, A. (1996) Human erythrocyte sugar transport is incompatible with available carrier models. Biochemistry 35, 10411-10421.

(107) Diamond, D., and Carruthers, A. (1993) Metabolic control of sugar transport by derepression of cell surface glucose transporters: an insulin-independent, recruitment-independent mechanism of regulation. J. Biol. Chem. 268, 6437-6444.

(108) Blodgett, D. M., and Carruthers, A. (2004) Conventional transport assays underestimate sugar transport rates in human red cells. Blood Cells, Molecules, and Diseases 32, 401-407.

(109) Blodgett, D. M., and Carruthers, A. (2005) Quench-Flow Analysis Reveals Multiple Phases of GluT1-Mediated Sugar Transport. Biochemistry 44, 2650-60.

(110) Naftalin, R. J., and Rist, R. J. (1991) 3-O-methyl-D-glucose transport in rat red cells: effects of heavy water. Biochimica et Biophysica Acta 1064, 37-48.

(111) Naftalin, R. J., Smith, P. M., and Roselaar, S. E. (1985) Evidence for non–uniform distribution of D–glucose within human red cells during net exit and counterflow. Biochim. Biophys. Acta 820, 235–249.

(112) Heard, K. S., Fidyk, N., and Carruthers, A. (2000) ATP-dependent substrate occlusion by the human erythrocyte sugar transporter. Biochemistry 39, 3005-3014.

(113) Cloherty, E. K., Sultzman, L. A., Zottola, R. J., and Carruthers, A. (1995) Net Sugar Transport is a Multi-Step Process. Evidence for cytosolic sugar binding sites in erythrocytes. Biochemistry 34, 15395–15406.

(114) Haney, D. N., and Bunn, H. F. (1976) Glycosylation of hemoglobin in vitro: affinity labeling of hemoglobin by glucose-6-phosphate. Proc Natl Acad Sci U S A 73, 3534-8.

(115) Shapiro, R., McManus, M., Garrick, L., McDonald, M. J., and Bunn, H. F. (1979) Nonenzymatic glycosylation of human hemoglobin at multiple sites.

(116) Kumar, A., Sharma, K. K., and Pattabiraman, T. N. (1985) Nature of nonenzymatically bound hexose in hemoglobin, albumin, and crystallin. Biochem Med 34, 112-9.

(117) Gillery, P., Maquart, F. X., Gattegno, L., Randoux, A., Cornillot, P., and Borel, J. P. (1982) A glucose-containing fraction extracted from the young erythrocyte membrane is capable of transferring glucose to hemoglobin in vitro.

(118) Krishnamoorthy, R., Cahour, A., Elion, J., Hartmann, L., and Labie, D. (1983) Monosaccharides bound to hemoglobins in normal and diabetic individuals. Evidence for glucose, mannose and galactose as sugars released by methanolysis of the different hemoglobin components. Eur J Biochem 132, 345-50.

(119) Widness, J. A., Rogler, B. T., McCormick, K. L., Petzold, K. S., Susa, J. B., Schwartz, H. C., and Schwartz, R. (1980) Rapid fluctuations in glycohemoglobin (hemoglobin Alc) related to acute changes in glucose, Vol. 95.

(120) Bolli, G., Cartechini, M. G., Compagnucci, P., De, F. P., Santeusanio, F., and Brunetti, P. (1982) Kinetic behaviour of the glucose-hemoglobin labile adduct in normal and diabetic erythrocytes. Diabete Metab 8, 21-7.

(121) Hebert, D. N., and Carruthers, A. (1986) Direct evidence for ATP modulation of sugar transport in human erythrocyte ghosts. J. Biol. Chem. 261, 10093-10099.

(122) Jacquez, J. A. (1983) Modulation of glucose transport in human red blood cells by ATP. Biochim Biophys Acta 727, 367-78.

(123) Carruthers, A. (1986) Anomalous asymmetric kinetics of human red cell hexose transfer: role of cytosolic adenosine 5'-triphosphate. Biochemistry 25, 3592-3602.

(124) Carruthers, A. (1986) ATP regulation of the human red cell sugar transporter. J. Biol. Chem. 261, 11028-11037.

(125) May, J. M. (1988) Effects of ATP depletion on the mechanism of hexose transport in intact human erythrocytes. Febs Lett 241, 188-90.

(126) Cloherty, E. K., Levine, K. B., Graybill, C., and Carruthers, A. (2002) Cooperative nucleotide binding to the human erythrocyte sugar transporter. Biochemistry 41, 12639-51.

(127) Carruthers, A., and Helgerson, A. L. (1989) The human erythrocyte sugar transporter is also a nucleotide binding protein. Biochemistry 28, 8337-8346.

(128) Wheeler, T. J. (1989) ATP does not regulate the reconstituted glucose transporter. Biochemistry 28, 3413-3420.

(129) Sofue, M., Yoshimura, Y., Nishida, M., and Kawada, J. (1993) ADP modifies the function of the glucose transporter: studies with reconstituted liposomes. Biochemical Journal.

(130) Afzal, I., Cunningham, P., and Naftalin, R. J. (2002) Interactions of ATP, oestradiol, genistein and the anti-oestrogens, faslodex (ICI 182780) and tamoxifen, with the human erythrocyte glucose transporter, GLUT1. Biochem J 365, 707-19.

(131) Liu, Q., Vera, J. C., Peng, H., and Golde, D. W. (2001) The predicted atp-binding domains in the hexose transporter glut1 critically affect transporter activity. Biochemistry 40, 7874-81.

(132) Fry, D. C., Kuby, S. A., and Mildvan, A. S. (1986) ATP-binding site of adenylate kinase: Mechanistic implications of its homology with ras-encoded p21, F1-ATPase, and other nucleotide-binding proteins. Proc. Natl. Acad. Sci. U.S.A. 83, 907-911.

(133) Levine, K. B., Cloherty, E. K., Hamill, S., and Carruthers, A. (2002) Molecular determinants of sugar transport regulation by ATP. Biochemistry 41, 12629-38.

(134) Levine, K. B., Cloherty, E. K., Fidyk, N. J., and Carruthers, A. (1998) Structural and physiologic determinants of human erythrocyte sugar transport regulation by adenosine triphosphate. Biochemistry 37, 12221-32.

(135) Helgerson, A. L., Hebert, D. N., Naderi, S., and Carruthers, A. (1989) Characterization of two independent modes of action of ATP on human erythrocyte sugar transport. Biochemistry 28, 6410-6417.

(136) Bates, P. A., Kelley, L. A., MacCallum, R. M., and Sternberg, M. J. (2001) Enhancement of protein modeling by human intervention in applying the automatic programs 3D-JIGSAW and 3D-PSSM. Proteins Suppl 5, 39-46.

(137) Lambert, C., Leonard, N., De Bolle, X., and Depiereux, E. (2002) ESyPred3D: Prediction of proteins 3D structures. Bioinformatics 18, 1250-6.

(138) Jaroszewski, L., Rychlewski, L., and Godzik, A. (2000) Improving the quality of twilight-zone alignments. Protein Sci 9, 1487-96.

(139) Pawlowski, K., Jaroszewski, L., Rychlewski, L., and Godzik, A. (2000) Sensitive sequence comparison as protein function predictor. Pac Symp Biocomput, 42-53.

(140) Karplus, K., and Hu, B. (2001) Evaluation of protein multiple alignments by SAM-T99 using the BAliBASE multiple alignment test set. Bioinformatics 17, 713-20.

(141) Gough, J., Karplus, K., Hughey, R., and Chothia, C. (2001) Assignment of homology to genome sequences using a library of hidden Markov models that represent all proteins of known structure. J Mol Biol 313, 903-19.

(142) Shi, J., Blundell, T. L., and Mizuguchi, K. (2001) FUGUE: sequence-structure homology recognition using environment-specific substitution tables and structure-dependent gap penalties. J Mol Biol 310, 243-57.

(143) Jones, D. T. (1999) GenTHREADER: an efficient and reliable protein fold recognition method for genomic sequences. J Mol Biol 287, 797-815.

(144) McGuffin, L. J., and Jones, D. T. (2003) Improvement of the GenTHREADER method for genomic fold recognition. Bioinformatics 19, 874-81.

(145) Jones, D. T. (1999) Protein secondary structure prediction based on position-specific scoring matrices. J Mol Biol 292, 195-202.

(146) McGuffin, L. J., Bryson, K., and Jones, D. T. (2000) The PSIPRED protein structure prediction server. Bioinformatics 16, 404-5.

(147) Ward, J. J., McGuffin, L. J., Buxton, B. F., and Jones, D. T. (2003) Secondary structure prediction with support vector machines. Bioinformatics 19, 1650-5.

(148) Schwede, T., Kopp, J., Guex, N., and Peitsch, M. C. (2003) SWISS-MODEL: An automated protein homology-modeling server. Nucleic Acids Res 31, 3381-5.

(149) Cieslar, J., Huang, M. T., and Dobson, G. P. (1998) Tissue spaces in rat heart, liver, and skeletal muscle in vivo. Am J Physiol 275, R1530-6.

(150) Henriksson, J., and Knol, M. (2005) A single bout of exercise is followed by a prolonged decrease in the interstitial glucose concentration in skeletal muscle. Acta Physiol Scand 185, 313-20.

(151) Milici, A. J., Furie, M. B., and Carley, W. W. (1985) The formation of fenestrations and channels by capillary endothelium in vitro. Proc Natl Acad Sci U S A 82, 6181-5.

(152) Craik, J. D., Young, J. D., and Cheeseman, C. I. (1998) GLUT-1 mediation of rapid glucose transport in dolphin (Tursiops truncatus) red blood cells. Am J Physiol 274, R112-9.

(153) Honig, C. R., Feldstein, M. L., and Frierson, J. L. (1977) Capillary lengths, anastomoses, and estimated capillary transit times in skeletal muscle. Am J Physiol 233, H122-9.

(154) Regittnig, W., Ellmerer, M., Fauler, G., Sendlhofer, G., Trajanoski, Z., Leis, H. J., Schaupp, L., Wach, P., and Pieber, T. R. (2003) Assessment of transcapillary glucose exchange in human skeletal muscle and adipose tissue. Am J Physiol Endocrinol Metab 285, E241-51.

(155) Shetty, M., Loeb, J. N., and Ismail, B. F. (1992) Enhancement of glucose transport in response to inhibition of oxidative metabolism: pre- and posttranslational mechanisms. American Journal of Physiology.

(156) Weiser, M. B., Razin, M., and Stein, W. D. (1983) Kinetic tests of models for sugar transport in human erythrocytes and a comparison of fresh and cold-stored cells. Biochim Biophys Acta 727, 379-88.

(157) Monsees, T. K., Franz, M., Gebhardt, S., Winterstein, U., Schill, W. B., and Hayatpour, J. (2000) Sertoli cells as a target for reproductive hazards. Andrologia 32, 239-46.

(158) Cheung, J. Y., Regen, D. M., Schworer, M. E., Whitfield, C. F., and Morgan, H. E. (1977) Anaerobic stimulation of sugar transport in avian erythrocytes. Biochim. Biophys. Acta 470, 212-229.

(159) Simons, T. J. B. (1983) Characterization of sugar transport in the pigeon red blood cell. J. Physiol. 338, 477-500.

(160) Widdas, W. F. (1980) The asymmetry of the hexose transfer system in the human red cell membrane. Curr. Top. Memb. Transp. 14, 165-223.

(161) Jung, C. Y., Carlson, L. M., and Whaley, D. A. (1971) Glucose transport carrier activities in extensively washed human red cell ghosts. Biochim. Biophys. Acta 241, 613–627.

(162) Cloherty, E. K., Diamond, D. L., Heard, K. S., and Carruthers, A. (1996) Regulation of GLUT1-mediated sugar transport by an antiport/uniport switch mechanism. Biochemistry 35, 13231-9.

(163) Weiser, M. B., Razin, M., and Stein, W. D. (1983) Kinetic tests of models for sugar transport in human erythrocytes and a comparison of fresh and cold–stored cells. Biochim. Biophys. Acta 727, 379–388.

(164) Harrison, S. A., Buxton, J. M., Helgerson, A. L., MacDonald, R. G., Chlapowski, F. J., Carruthers, A., and Czech, M. P. (1990) Insulin action on activity and cell surface disposition of human HepG2 glucose transporters expressed in Chinese hamster ovary cells. Journal of Biological Chemistry 265, 5793-801.

(165) Hayat, M. A. (1978) Introduction to Biological Scanning Electron Microscopy, Universtiy Park Press, Balitiome, MD.

(166) Hayat, M. A. (2000) Principles and Techniques of Electron Microscopy: Biological Applications., Cambridge University Press, New York.

(167) Plagemann, P. G., and Woffendin, C. (1987) Comparison of the equilibrium exchange of nucleosides and 3-O-methylglucose in human erythrocytes and of the

effects of cytochalasin B, phloretin and dipyridamole on their transport. Biochim Biophys Acta 899, 295-301.

(168) Miller, D. M. (1971) The kinetics of selective biological transport. V. Further data on the erythrocyte–monosaccharide transport system. Biophys. J. 11, 915–923.

(169) Challiss, J. R., Taylor, L. P., and Holman, G. D. (1980) Sugar transport asymmetry in human erythrocytes--the effect of bulk haemoglobin removal and the addition of methylxanthines. Biochim Biophys Acta 602, 155-66.

(170) Garcia-Perez, A. I., Lopez-Beltran, E. A., Kluner, P., Luque, J., Ballesteros, P., and Cerdan, S. (1999) Molecular crowding and viscosity as determinants of translational diffusion of metabolites in subcellular organelles. Arch Biochem Biophys 362, 329-38.

(171) Lin, S., Yang, E., and Huestis, W. H. (1994) Relationship of phospholipid distribution to shape change in Ca(2+)- crenated and recovered human erythrocytes. Biochemistry 33, 7337-44.

(172) Hurlock, B., and Tosic, J. (1951) An organism able to metabolize 3-methylglucose and 3-methylfructose. J Gen Microbiol 5, 587-91.

(173) Narahara, H. T., and Ozand, P. (1963) Studies of tissue permeability, IX. The effect of insulin on the penetration of 3-O-methylglucose-3H in frog muscle. J. Biol. Chem. 238, 40-49.

(174) Lewis, B. E., Choytun, N., Schramm, V. L., and Bennet, A. J. (2006) Transition states for glucopyranose interconversion. J Am Chem Soc 128, 5049-58.

(175) Barnett, J. E., Holman, G. D., and Munday, K. A. (1973) Structural requirements for binding to the sugar-transport system of the human erythrocyte. Biochem J 131, 211-21.

(176) Ginsburg, H., and Stein, D. (1975) Zero-trans and infinite-cis uptake of galactose in human erythrocytes. Biochim. Biophys. Acta 382, 353-368.

(177) Faust, R. G. (1960) Monosaccharide penetration into human red blood cells by an altered diffusion mechanism. J Cell Comp Physiol 56, 103-21.

(178) Carruthers, A., and Melchior, D. L. (1985) Transport of a- and b-D-glucose by the intact human red cell. Biochemistry 24, 4244-4250.

(179) Miwa, I., Fujii, H., and Okuda, J. (1988) Asymmetric transport of D-glucose anomers across the human erythrocyte membrane. Biochem Int 16, 111-7.

(180) Bollen, M., Malaisse-Lagae, F., Malaisse, W., and Stalmans, W. (1990) The interaction of phosphorylase a with D-glucose displays alpha-stereospecificity. Biochim Biophys Acta 1038, 141-5.

(181) Eilam, Y. (1975) Two carrier models for mediated transport. II. Glucose and galactose equilibrium exchange experiments in human erythrocytes as a test for several two-carrier models. Biochim. Biophys. Acta 401, 364-369.

(182) Malaisse, W. J., and Willem, R. (2004) Anomeric specificity of D-glucose production by rat hepatocytes. Mol Cell Biochem 266, 145-50.

(183) Miwa, I., Fukatsu, H., Toyoda, Y., and Okuda, J. (1990) Anomeric preference of glucose utilization in human erythrocytes loaded with glucokinase. Biochem Biophys Res Commun 173, 201-7.

(184) Malaisse, W. J., Zhang, Y., Jijakli, H., Courtois, P., and Sener, A. (2004) Metabolism of D-glucose anomers in rat pancreatic islets exposed to equilibrated D-glucose. Horm Metab Res 36, 281-5.

(185) Malaisse, W. J., and Sener, A. (2004) Mathematical modelling of alpha- and beta-D-glucose metabolism in pancreatic islets exposed to equilibrated D-glucose. Int J Mol Med 14, 677-82.

(186) Miwa, I., Murata, T., and Okuda, J. (1991) Alpha- and beta-anomeric preference of glucose-induced insulin secretion at physiological and higher glucose concentrations, respectively. Biochem Biophys Res Commun 180, 709-15.

(187) Meglasson, M. D., Burch, P. T., Berner, D. K., Najafi, H., and Matschinsky, F. M. (1986) Identification of glucokinase as an alloxan-sensitive glucose sensor of the pancreatic beta-cell. Diabetes 35, 1163-73.

(188) Rossini, A. A., and Soeldner, J. S. (1976) Insulin release is glucose anomeric specific in the human. J Clin Invest 57, 1083-8.

(189) Zhang, Y., Courtois, P., Sener, A., and Malaisse, W. J. (2004) Anomeric specificity of D-[U-14C]glucose incorporation into glycogen in rat hemidiaphragms. Biochimie 86, 913-8.

(190) Malaisse-Lagae, F., and Malaisse, W. J. (1986) Anomeric specificity of D-glucose metabolism in rat adipocytes. Eur J Biochem 158, 663-6.

(191) Ehwald, R., Mavrina, L., and Wilken, B. (1981) Active transport and mediated diffusion of glucose and other monosaccharides in Endomyces magnusii. Folia Microbiol (Praha) 26, 388-93.

(192) Malaisse-Lagae, F., Giroix, M. H., Sener, A., and Malaisse, W. J. (1986) Temperature dependency of the anomeric specificity of yeast and bovine hexokinases. Biol Chem Hoppe Seyler 367, 411-6.

(193) Malaisse, W. J., and Malaisse-Lagae, F. (1987) Anomeric specificity of D-glucose metabolism in rat brain cells. Brain Res 419, 147-55.

(194) Nagata, Y., Nanba, T., Ando, M., Miwa, I., and Okuda, J. (1979) Anomeric preferences of D-glucose uptake and utilization by cerebral cortex slices of rats. Neurochem Res 4, 505-16.

(195) Okuda, J., Miwa, I., Sato, M., and Murata, T. (1977) Uptake of D-glucose anomers by rat retina. Experientia 33, 19-20.

(196) Okuda, J., Kawamura, M., and Didelot, S. (1987) Anomeric preference in uptake of D-glucose and of D-galactose by rat lenses. Curr Eye Res 6, 1223-6.

(197) Sakaguchi, T., Ishiguro, K., Hayashi, Y., and Hasegawa, A. (1984) Inhibition of gastric acid secretion elicited by D-glucose anomers in man. Exp Neurol 84, 231-6.

(198) Appleman, J. R., and Lienhard, G. E. (1985) Rapid kinetics of the glucose transporter from human erythrocytes. Detection and measurement of a half-turnover of the purified transporter. J. Biol. Chem. 260, 4575-8.

(199) Wheeler, T. J., and Hinkle, P. C. (1985) The glucose transporter of mammalian cells. Ann. Rev. Physiol. 47, 503–518.

(200) Bell, G. I., Kayano, T., Buse, J. B., Burant, C. F., Takeda, J., Lin, D., Fukumoto, H., and Seino, S. (1990) Molecular biology of mammalian glucose transporters. Diabetes Care 13, 198-208.

(201) Lieb, W. R., and Stein, W. D. (1971) New theory for glucose transport across membranes. Nature New Biol. 230, 108-116.

(202) Carruthers, A., Hebert, D. N., Helgerson, A. L., Tefft, R. E., Naderi, S., and Melchior, D. L. (1989) Effects of Calcium, ATP and Membrane lipids on Glucose Transporter Function. Annal. N.Y. Acad. Sci. 568, 52-67.

(203) Isbell, H. S., and Pigman, W. (1969) Mutarotation of sugars in solution. II. Catalytic processes, isotope effects, reaction mechanisms, and biochemical aspects. Adv Carbohydr Chem Biochem 24, 13-65.

(204) Baker, P. F., and Carruthers, A. (1981) Sugar transport in giant axons of Loligo. J. Physiol. (Lond.) 316, 481-502.

(205) Fujii, H., Miwa, I., and Okuda, J. (1986) Anomeric preference of glucose phosphorylation and glycolysis in human erythrocytes. Biochem Int 13, 359-65.

(206) Malaisse-Lagae, F., Sterling, I., Sener, A., and Malaisse, W. J. (1988) Anomeric specificity of D-glucose metabolism in human erythrocytes. Clin Chim Acta 172, 223-31.

(207) Malaisse-Lagae, F., and Malaisse, W. J. (1987) Anomeric specificity of D-glucose phosphorylation and oxidation in human erythrocytes. Int J Biochem 19, 733-6.

(208) Duan, Y. J., Fukatsu, H., Miwa, I., and Okuda, J. (1992) Anomeric preference of glucose utilization in rat erythrocytes. Mol Cell Biochem 112, 23-8.

(209) Kuchel, P. W., Chapman, B. E., and Potts, J. R. (1987) Glucose transport in human erythrocytes measured using 13C NMR spin transfer. FEBS Lett 219, 5-10.

(210) Potts, J. R., Hounslow, A. M., and Kuchel, P. W. (1990) Exchange of fluorinated glucose across the red-cell membrane measured by 19F-n.m.r. magnetization transfer. Biochem J 266, 925-8.

(211) Potts, J. R., and Kuchel, P. W. (1992) Anomeric preference of fluoroglucose exchange across human red-cell membranes. 19F-n.m.r. studies. Biochem J, 753-9.

(212) O'Connell, T. M., Gabel, S. A., and London, R. E. (1994) Anomeric dependence of fluorodeoxyglucose transport in human erythrocytes. Biochemistry 33, 10985-92.

(213) London, R. E., and Gabel, S. A. (1995) Fluorine-19 NMR studies of glucosyl fluoride transport in human erythrocytes. Biophys J 69, 1814-8.

(214) Appleman, J. R., and Lienhard, G. E. (1989) Kinetics of the purified glucose transporter. Direct measurement of the rates of interconversion of transporter conformers. Biochemistry 28, 8221-7.

(215) Janoshazi, A., and Solomon, A. K. (1993) Initial steps of alpha- and beta-D-glucose binding to intact red cell membrane. J Membr Biol 132, 167-78.

(216) Baker, J. O., and Himmel, M. E. (1986) Separation of Sugar Anomers by Aqueous Chromatography on Calcium- and Lead-Form Ion-Exchange Columns

Application to Anomeric Analysis of Enzyme Reaction Products. J. Chrom. 357, 161-181.

(217) Barnett, J. E., Holman, G. D., Chalkley, R. A., and Munday, K. A. (1975) Evidence for two asymmetric conformational states in the human erythrocyte sugar-transport system. Biochem J 145, 417-29.

(218) Widdas, W. F. (1972) Aspects of competitive inhibition. Biomembranes 3, 101-5.

(219) Lin, S., and Spudich, J. A. (1974) On the molecular basis of action of cytochalasin B. J Supramol Struct 2, 728-36.

(220) Cohen, C. M., Jackson, P. L., and Branton, D. (1978) Actin--membrane interactions: association of G-actin with the red cell membrane. J Supramol Struct 9, 113-24.

(221) Lux, S. E. (1979) Dissecting the red cell membrane skeleton. Nature 281, 426-9.

(222) Luna, E. J., and Hitt, A. L. (1992) Cytoskeleton--plasma membrane interactions. Science 258, 955-64.

(223) Kuhlman, P. A. (2000) Characterization of the actin filament capping state in human erythrocyte ghost and cytoskeletal preparations. Biochem J 349, 105-11.

(224) Picart, C., and Discher, D. E. (1999) Actin protofilament orientation at the erythrocyte membrane. Biophys J 77, 865-78.

(225) Schmid, M. F., Agris, J. M., Jakana, J., Matsudaira, P., and Chiu, W. (1994) Three-dimensional structure of a single filament in the Limulus acrosomal bundle: scruin binds to homologous helix-loop-beta motifs in actin. J Cell Biol 124, 341-50.

(226) Heinrich, V., Ritchie, K., Mohandas, N., and Evans, E. (2001) Elastic thickness compressibilty of the red cell membrane. Biophys J 81, 1452-63.

(227) Ursitti, J. A., Pumplin, D. W., Wade, J. B., and Bloch, R. J. (1991) Ultrastructure of the human erythrocyte cytoskeleton and its attachment to the membrane. Cell Motil Cytoskeleton 19, 227-43.

(228) Phillips, M. J., Oda, M., Yousef, I. M., and Funatsu, K. (1981) Effects of cytochalasin B on membrane-associated microfilaments in a cell-free system. J Cell Biol 91, 524-30.

(229) Vera, J. C., Castillo, G. R., and Rosen, O. M. (1991) A possible role for a mammalian facilitative hexose transporter in the development of resistance to drugs. Molecular & Cellular Biology 11, 3407-18.

(230) Zhang, J. Z., and Ismail-Beigi, F. (1998) Activation of Glut1 glucose transporter in human erythrocytes. Arch Biochem Biophys 356, 86-92.

(231) Lin, D. C., and Lin, S. (1979) Actin polymerization induced by a motility-related high-affinity cytochalasin binding complex from human erythrocyte membrane. Proc Natl Acad Sci U S A 76, 2345-9.

(232) Pinder, J. C., Weeds, A. G., and Gratzer, W. B. (1986) Study of actin filament ends in the human red cell membrane. J Mol Biol 191, 461-8.

(233) Widdas, W. F. (1954) Facilitated transfer of hexoses across the human erythrocyte membrane. J. Physiol. (Lond.) 125, 163-180.

(234) Baker, G. F., and Widdas, W. F. (1988) Parameters for 3-O-methyl glucose transport in human erythrocytes and fit of asymmetric carrier kinetics. J Physiol (Lond) 395, 57-76.

(235) Pasini, E. M., Kirkegaard, M., Mortensen, P., Lutz, H. U., Thomas, A. W., and Mann, M. (2006) In-depth analysis of the membrane and cytosolic proteome of red blood cells. Blood 108, 791-801.

(236) Harik, S. I. (1992) Changes in the glucose transporter of brain capillaries. [Review]. Canadian Journal of Physiology & Pharmacology.

(237) Alhanaty, E., and Sheetz, M. P. (1981) Control of the erythrocyte membrane shape: recovery from the effect of crenating agents. J Cell Biol 91, 884-8.

(238) van Drogen, F., and Peter, M. (2004) Revealing protein dynamics by photobleaching techniques. Methods Mol Biol 284, 287-306.

(239) van Drogen, F., and Peter, M. (2001) MAP kinase dynamics in yeast. Biol Cell 93, 63-70.

(240) Goodwin, J. S., and Kenworthy, A. K. (2005) Photobleaching approaches to investigate diffusional mobility and trafficking of Ras in living cells. Methods 37, 154-64.

(241) Judd, E. M., Comolli, L. R., Chen, J. C., Downing, K. H., Moerner, W. E., and McAdams, H. H. (2005) Distinct constrictive processes, separated in time and space, divide caulobacter inner and outer membranes. J Bacteriol 187, 6874-82.

(242) Fehr, M., Lalonde, S., Lager, I., Wolff, M. W., and Frommer, W. B. (2003) In vivo imaging of the dynamics of glucose uptake in the cytosol of COS-7 cells by fluorescent nanosensors. J Biol Chem 278, 19127-33.

(243) Taverna, R. D., and Langdon, R. G. (1973) D-glucosyl isothiocyanate, an affinity label for the glucose transport proteins of the human erythrocyte membrane. Biochem Biophys Res Commun 54, 593-9.

(244) Mullins, R. E., and Langdon, R. G. (1980) Maltosyl isothiocyanate: an affinity label for the glucose transporter of the human erythrocyte membrane. 2. Identification of the transporter. Biochemistry 19, 1205-12.

(245) Shanahan, M. F., Wadzinski, B. E., Lowndes, J. M., and Ruoho, A. E. (1985) Photoaffinity labeling of the human erythrocyte monosaccharide transporter with an aryl azide derivative of D-glucose. J Biol Chem 260, 10897-900.

(246) Sheetz, M. P. and Singer, S. J. (1974). Biological Membranes as Bilayer Couples. A Molecular Mechanism of Drug-Erythrocyte Interactions. Proc Nat Acad Sci 71, 4457-4461.

(247) Sheetz, M. P. and Singer, S. J. (1976). Equilibrium and Kinetic Effects of Drugs on the Shapes of Human Erythrocytes. J Cell Biol 70, 247-251.